Università degli Studi di Firenze - Dipartimento di Chimica

Scuola di Dottorato in Scienze

Dottorato di Ricerca in Scienze Chimiche

XXII ciclo – CHIM03 – Chimica Generale ed Inorganica

Chemical and photoinduced effects on the magnetic properties of bistable materials

Ph. D. thesis by

Giordano Poneti

Tutor:

Prof. Roberta Sessoli

Co-tutor:

Prof. Andrea Dei

Coordinator:

Prof. Gianni Cardini

Index

Chapter IV: Analysis of the relations between entropy and optically driven redox isomerism: The solid solution approach

Chapter V: X-Rays Absorption Spectroscopy for the investigation of Co-dioxolene valence tautomeric materials

List of acronyms and abbreviations

2,2'-bpy	2,2'-bipyridine
3,5-DBdiox	3,5- ditertbutyldioxolene
BM	bending magnet
Cat	catecholato
CT	charge transfer
CTH	D,L – 5,7,7,12,14,14-hexamethyl-1,4,8,11-tetraazacyclotetradecane
Diox	dioxolene ligand
ET	Electron Transfer
EXAFS	Extended X-Ray Absorption Fine Structure
ID	insertion device
IEGL	Inverse Energy Gap Law
IR	Infra-red
ISC	Intersystem Crossing
ISC	Intersystem crossing
k_B	Boltzmann constant
LIESST	Light Induced Excited Spin State Trapping
LMCT	Ligand to Metal Charge Transfer band
Mentpa	methyl derivatives of tris(2-pyridylmethyl)amine
MLCT	Metal to Ligand Charge Transfer band
OD	optical density
PBA	Prussian Blue Analogue
py	pyridine
pz	pyrazine
RT	room temperature
SC	spin crossover
SQ	semiquinonato
$T_{½}$	transition temperature
TAS	Transient Absorption Spectroscopy
TCdiox	3,4,5,6-tetrachlorodioxolene
TEY	Total Electron Yield
TIP	Temperature Independent Magnetism
tmeda	Tetramethylethylenediamine
VT	Valence Tautomerism
XANES	X-Ray Absorption Near Edge Structure
XAS	X-Ray Absorption Spectroscopy

Introduction

Molecular Magnetism is a multidisciplinary field of science straddling the interface between Chemistry and Physics. Being born as a diagnostic tool to characterise the chemical structure of paramagnetic molecules through the analysis of their magnetic properties, it has now moved to the role of developer of new systems with predetermined magnetic functionalities. This evolution is the chemical answer to a set of questions arising from the Materials' Science community. The need for systems featuring tailor-made, predetermined physical properties and the quest for them to be stored in strongly dimensionally confined environments (with density over 10^8 units cm^{-2}, found in currently used microchips) forced the materials scientific community to encompass the chemical knowledge into a real, actually working, strategy of building devices.[1,2] In this view molecules candidate as natural evolution of classic semiconductor and magnetic material based on metals and metal oxides. Coordination chemistry, in particular, is currently widely used to generate molecular materials, with optical, transport and magnetic properties being tuned by an appropriate choice of metal ions and the surrounding ligands, able to influence the final physical behaviour of the complexes, even in some cases merging the properties of the single building blocks to obtain new ones.

Particular efforts are being spent into the synthesis of molecular systems to be applied as active materials in the fields of sustainable energy development,[3] information storage[4-6] and processing at the molecular level[7,8]. In the latter two fields molecules may play the role of the traditional electrical and magnetic devices behaving as wires, rectifiers, transistors, memories and switches.[9-11] For these last issues to be undertaken, molecules must feature the coexistence of two different physical states separated by an energy barrier for the crossover from one to the other, a phenomenon known as bistability. The differences in the states involved may be related to a large set of parameters, including structural,[12] electronic[13] and magnetic features.[14]

One of the mostly investigated class of bistable molecules showing differences in the magnetic and structural features, along with the possibility to show thermal and optical driven bistability, is the Spin Crossover one. In this case some coordination complexes having a d^n (n=4–7) electronic configuration are subjected to a ligand field of comparable energy to the spin pairing one, so that a thermal, pressure as well as a pulsed magnetic field or optical stimulus can afford the population of a state with different spin multiplicity.[15,16] These classes of systems are particularly appealing for the development of working devices, since the physical features of the states with different spin multiplicity involved in the SC phenomenon are large, ranging from difference in magnetic, optical and structural properties. Moreover, the SC process has been found to take place in a huge amount of coordination systems, from mononuclear to polynuclear[17] complexes up to surface patterned coordination polymers[18] and nanoparticles.[19] For these reasons the SC systems, mainly the ones based on the octahedrically coordinated Fe^{II} ion, have been the object of

detailed investigations. In particular, the investigation of the role played by elastic interaction in the entropy driven SC process[20] and the development of the Inverse Energy Gap Law[21] has allowed to reach a control of the lifetime of the photoinduced metastable states at low temperature by means of chemical techniques, and have been used as hints for the a priori building-up of systems with predetermined physical properties.

This work concerns another class of bistable molecular materials, the so called Valence Tautomers. In this case two coexisting states differ in the charge distribution of the electronic ground state. This phenomenon has been found in a wide set of systems, as nanoparticles (cobalt ferrite nanoparticles)[22,23], polycyanometallates (Prussian blue like coordination polymers),[24] and molecular complexes with different metal ions (iron-nitroprusside, manganese, copper and cobalt-dioxolene complexes).[25,26] Valence tautomeric systems have attracted huge interest in the chemical and materials' scientific community due to their peculiar redox isomerism. In fact they provide a very simple molecular benchmark to investigate the electron transfer processes in equilibrium (and outside of it, too) between a metal ion and an organic ligand, phenomenon of paramount importance in the biochemistry of several proteins.[27] In addition to this, they candidate as advanced building blocks of nanodevices whose active material is of molecular origin, featuring the two species involved in the very different physical properties, mainly from a magnetic and optical point of view.[28-31]

The set of cobalt complexes showing redox bistability (VT) is worth of particular interest because of the differences in the magnetism of both redox species. The low temperature stable phase is characterised by a singlet spin ground state and is thus a diamagnet, while the other phase feature a non zero spin ground state. However, magnetism is not the only property of these materials to undergo changes during the valence tautomeric interconversion. Large changes in the optical absorption spectra of these systems before and after the VT equilibrium are clearly visible, in the whole radiation energy spectrum, ranging from X-Rays to IR light, due to the different population of the frontier states involved in the absorption of light. The VT process involves as well an overall change of the molecular volume, used to measure photomechanical effects on such materials.[32] In the systems investigated here the VT process features an electron transfer between the cobalt ion and the redox active organic ligand along with a change of spin state of the metal ion, thus yielding two species discussed more in detail in Chapter I.[33] The molecular origin of the process is an electron transfer occurring between an ochtaedrically coordinated Co ion and an organic ligand with two oxidation states close in energy, which may be triggered by temperature,[29,34-38] light irradiation[39-43] and magnetic fields.[44] Despite the interest the Co VT systems have arisen, the research in the field is still far from pairing the one related to SC systems. Several issues have still to be addressed, among which we mention the construction of a material showing thermal hysteresis centred at room temperature and the understanding of the parameters affecting the lifetime of the metastable state.

The work presented in this thesis deals with some of these issues and is devoted to

the investigation of the environmental effects in the optical and thermal induced VT in Co based systems. Chapter I presents a more detailed description of Co based VT systems, focusing on the building blocks of such materials, their physical requirements to show the VT phenomenon and the mechanism affording the redox equilibrium process in function of heat stimula. In Chapter II we describe a rational approach for the development of VT molecules based on the control of the redox potential of the building blocks. This synthetic strategy allowed us to obtain a new VT system, whose thermal transition in solution has been characterised from a thermodynamic point of view. In Chapter III we monitor the crystal packing effects in the solid state on the thermally and optically induced VT for two different redox bistable cores, highlighting the strong dependence of the transition temperature on the cooperativity in the lattice, on the other side being the optical bistability unaffected by the crystal surroundings. The molecular character of the optical bistability has been assessed with a more rational investigation, where the elastic interaction in the lattice have been tuned by different degrees of solid dissolution of a Co based VT complex in an inert, structurally homologous, host described in Chapter IV. Finally, we present an investigation of the structural and the electronic features of the species involved in the thermal and optical equilibrium by means of X-Ray Absorption Spectroscopy, a technique widely used in the bistable materials' community because of its capability to distinguish among several phases present in the system. We show in particular how the experimental conditions of the experiments may be tuned to use the X-Rays as probe or as pump of a molecular photoinduced state at low temperature.

References

[1] Moore, G. E. *Electronics*; **1965**, *38*, 114-117.

[2] Feynman, R. P. *Saturday Rev* **1960**, *43*, 45-47.

[3] Seland, F.; Harrington, D. A.; Tunold, R. *Electrochim. Acta* **2006**, *52*, 773-779.

[4] Manriquez, J. M.; Yee G. T. ; McLean, R. S.; Epstein, A. J.; Miller, J. S. *Science* **1991**, *252*, 1415.

[5] Ferlay, S.; Mallah, T.; Ouahes, R.; Veillet, P.; Verdaguer, M. *Nature* **1995**, *378*, 701-703.

[6] Muller, A.; Kogerler, P.; Dress, A. W. M. *Coord. Chem. Rev.* **2001**, *222*, 193-218.

[7] Leuenberger, M. N.; Loss, D. *Nature* **2001**, *410*, 789-793.

[8] Bogani, L.; Wernsdorfer, W. *Nature Mater.* **2008**, *7*, 179-186.

[9] Joachim, C.; Gimzewski, J. K.; Aviram, A. *Nature* **2000**, *408*, 541-548.

[10] Chen, J.; Reed, M. A.; Rawlett, A. M.; Tour, J. M. *Science* **1999**, *286*, 1550-1552.

[11] Balzani, V.; Credi, A.; Venturi, M. *Chem., Eur. J.* **2002**, *8*, 5524-5532.

[12] Naumov, I. I.; Bellaiche, L.; Fu, H. X. *Nature* **2004**, *432*, 737-740.

[13] Caironi, M.; Natali, D.; Sampietro, M.; Bertarelli, C.; Bianco, A.; Dundulachi, A.; Canesi, E.; Zerbi, G. *Appl. Phys. Lett.* **2006**, *89*.

[14] Gatteschi, D.; Sessoli, R.; Villain, J. *Molecular Nanomagnets*, Oxford University Press: Oxford, 2006.

[15] Gutlich, P.; Hauser, A.; Spiering, H. *Angew. Chem., Int. Ed. Engl.* **1994**, *33*, 2024-2054.

[16] Bousseksou, A.; Negre, N.; Goiran, M.; Salmon, L.; Tuchagues, J. P.; Boillot, M. L.; Boukheddaden, K.; Varret, F. *Eur. Phys. J. B* **2000**, *13*, 451-456.

[17] Garcia, Y.; Niel, V.; Munoz, M. C.; Real, J. A. *Spin Crossover in 1d, 2d and 3d Polymeric Fe(II) Networks* in *Spin Crossover in Transition Metal Compounds I*; Gütlich, P.; Goodwin, H. A., 2004; Vol. 233, pp 229-257.

[18] Molnar, G.; Cobo, S.; Real, J. A.; Carcenac, F.; Daran, E.; Vien, C.; Bousseksou, A. *Adv. Mater.* **2007**, *19*, 2163-2167.

[19] Larionova, J.; Salmon, L.; Guarl, Y.; Tokarev, A.; Molvinger, K.; Molnar, G.; Bousseksou, A. *Angew. Chem. Int. Ed.* **2008**, *47*, 8236-8240.

[20] Spiering, H. *Elastic Interaction in Spin Crossover Compounds* in *Spin Crossover in Transition Metal Compounds III*; Gütlich, P.; Goodwin, H. A., Eds.; Springer: Berlin, 2004; Vol. 235, pp 171-195.

[21] Hauser, A. *Light-Induced Spin Crossover and the High-Spin -> Low-Spin Relaxation* in *Spin Crossover in Transition Metal Compounds II*; Gütlich, P.; Goodwin, H. A., Eds.; Springer: Berlin, 2004; Vol. 234, pp 155-198 .

[22] Imaz, I.; Maspoch, D.; Rodriguez-Blanco, C.; Perez-Falcon, J. M.; Campo, J.; Ruiz-Molina, D. *Angew. Chem. Int. Ed.* **2008**, *47*, 1857-1860.

[23] Giri, A. K.; Kirkpatrick, E. M.; Moongkhamklang, P.; Majetich, S. A.; Harris, V. G. *Appl. Phys. Lett.* **2002**, *80*, 2341-2343.

[24] Goujon, A.; Varret, F.; Escax, V.; Bleuzen, A.; Verdaguer, M. *Polyhedron* **2001**, *20*1339-1345.

[25] Hendrickson, D. N.; Pierpont, C. G. *Top. Curr. Chem.* **2004**, *234*, 63-95.

[26] Pierpont, C. G. *Coord. Chem. Rev.* **2001**, *219*, 415-433.

[27] Moser, C. C.; Keske, J. M.; Warncke, K.; Farid, R. S.; Dutton, P. L. *Nature* **1992**, *355*, 796-802.

[28] Gutlich, P.; Dei, A. *Angew. Chem. Int. Ed.* **1997**, *36*, 2734-2736.

[29] Sato, O.; Cui, A. L.; Matsuda, R.; Tao, J.; Hayami, S. *Acc. Chem. Res.* **2007**, *40*, 361-369.

[30] Cui, A.; Takahashi, K.; Fujishima, A.; Sato, O. *J. Photochem. Photobiol., A* **2004**, *167*,

69-73.

[31] Shultz, D. A. *Valence tautomerism in dioxolene complexes of cobalt* in *Magnetism: Molecules to Materials II*; Miller, J. S.; Drillon, M., Eds.; 2001; pp 281-306.

[32] Jung, O. S.; Pierpont, C. G. *J. Am. Chem. Soc.* **1994**, *116*, 2229-2230.

[33] Adams, D. M.; Dei, A.; Rheingold, A. L.; Hendrickson, D. N. *Abs. Pap. Am. Chem. Soc.* **1994**, *207*, 390.

[34] Jung, O. S.; Jo, D. H.; Lee, Y. A.; Conklin, B. J.; Pierpont, C. G. *Inorg. Chem.* **1997**, *36* , 19-24.

[35] Dei, A.; Gatteschi, D.; Sangregorio, C.; Sorace, L. *Acc. Chem. Res.* **2004**, *37*, 827-835.

[36] Roux, C.; Adams, D. M.; Itie, J. P.; Polian, A.; Hendrickson, D. N.; Verdaguer, M. *Inorg. Chem.* **1996**, *35*, 2846-2852.

[37] Caneschi, A.; Dei, A.; De Biani, F. F.; Gutlich, P.; Ksenofontov, V.; Levchenko, G.; Hoefer, A.; Renz, F. *Chem., Eur. J.* **2001**, *7*, 3926-3930.

[38] Li, B.; Tao, J.; Sun, H. L.; Sato, O.; Huang, R. B.; Zheng, L. S. *Chem. Commun.* **2008**, 2269-2271.

[39] Sato, O.; Hayami, S.; Gu, Z. Z.; Seki, K.; Nakajima, R.; Fujishima, A. *Chem. Lett.* **2001**, 874-875.

[40] Sato, O.; Hayami, S.; Gu, Z. Z.; Takahashi, K.; Nakajima, R.; Fujishima, A. *Chem. Phys. Lett.* **2002**, *355*, 169-174.

[41] Neuwahl, F. V. R.; Righini, R.; Dei, A. *Chem. Phys. Lett.* **2002**, *352*, 408-414.

[42] Beni, A.; Carbonera, C.; Dei, A.; Letard, J. F.; Righini, R.; Sangregorio, C.; Sorace, L. *J. Braz. Chem. Soc.* **2006**, *17*, 1522-1533.

[43] Carbonera, C.; Dei, A.; Letard, J. F.; Sangregorio, C.; Sorace, L. *Angew. Chem. Int. Ed.* **2004**, *43*, 3136-3138.

[44] Markevtsev I. N. ; Monakhov M. P. ; Platonov V. V.; Mischenko A. S.; Zvezdin A. K. ; Bubnov M. P. ; Abakumov G. A.; Cherkasov V. K. *J. Magn. Magn. Mater.* **2006**, *300*, 407-410.

Chapter I

The valence tautomeric interconversion

In this chapter we introduce the main issues about VT in Co – o-dioxolene complexes, introducing the reader to the concepts the presented research work is related to. We start by stressing the physical requirements of a molecule to be capable to afford redox isomerism (coexistence of close-lying molecular electronic levels featuring a low degree of covalence), showing how these conditions are fulfilled in the case of the building blocks of the molecules this thesis is about (the Co ion, the o-dioxolene redox active ligands as well as the N-donor ancillary ligands), as well as a brief overview of the commonly encountered ones in the scientific literature. We also describe, by using a simplified molecular orbitals approach, the electronic states involved in the VT process, pointing out the differences in their physical properties. Finally, a detailed discussion of the mechanisms of thermally and optically induced VT, along with the physical parameters governing the lifetimes of the photoinduced metastable states, will be given.

1.1 The building blocks of the system

In chemical terminology tautomerism is a structural rearrangement of the chemical bonds of a determined system (*e.g.*: an isomerism) due to an intramolecular chemical reaction. It has been studied so far in organic chemistry in the case of ketones, amides and amines, mostly. However, several classes of tautomerism can be identified according to the nature of the states involved in the equilibrium process. In particular, if these states differ only in the electronic configuration of the frontier orbitals of the system, being unchanged the topology of the molecular bonds, the process is called valence tautomerism. Valence tautomers are a very large class of bistable materials, ranging from molecules (dioxolene complexes of cobalt,[1-3] copper,[4] manganese[5], chromium[6], rhodium[1] as well as iron – nitroprusside complexes[7]) to nanoparticles (cobalt-ferrite nanoparticles)[8] and coordination polymers (Prussian Blue Analogues)[9]. For brevity purposes we will review here only the VT equilibrium in the cobalt-dioxolene complexes, being the subject of this thesis' work.

It is implied in the above reported definition that valence tautomeric transitions are characterised by an electron transfer occurring within the framework of one molecule. Such a situation is not straightforward to be achieved, but we can state, as a rule of thumb, a general recipe for a system to show valence tautomeric equilibrium, consisting in three requirements:

- the molecular subsystems exchanging electrons must have frontier electronic orbitals closely lying in energy. If these orbitals' energies differ too much an irreversible redox reaction is likely to occur instead of a thermodynamic equilibrium. In particular, this difference should be of the order of k_BT, *i.e.* the thermal energy at room temperature. On the contrary thermal decomposition of the compound may take place instead of electron transfer.

- The degree of electronic coupling between the centres should be small. To say it according to Robin and Day classification of mixed-valence species, [10] molecules showing valence tautomerism must be classified as belonging to class II.

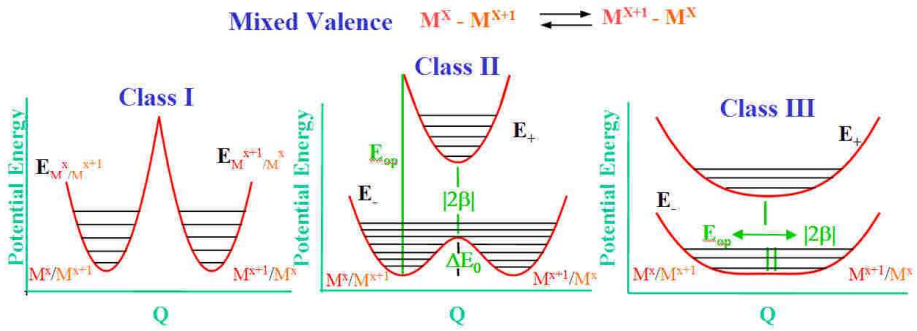

Figure 1.1: Robin and Day classification of bistable electronic systems.

The figure helps in rationalising the different degrees of electronic delocalisation occurring in mixed valence species. These species are characterised by the coexistence, in the same structural framework, of ions in different oxidation states (indicated in Figure 1.1 as M^X/M^{X+1}). In the picture the energies of the system is described by considering the dependence of the energies of the vibrational functions of the M ions on the reaction coordinate Q. In Class I materials the potential wells of the M^X and M^{X+1} ions are separated by a high energy barrier preventing them to mix. This leads to a strictly defined electronic structure of the whole system, which cannot be switched, the different ions behaving independently one from the other. On the opposite side, Class III materials feature a zero energy barrier for electronic states mixing, corresponding to a situation where the M ions share completely the electron, thus being indistinguishable. It is clear that the interest of such compounds for applicative purposes is zero, since their valence cannot be switched by any external perturbation. The intermediate situation (Class II materials) looks appealing, since the electron is localised on a single centre, leading to a well defined chemical and physical picture of the molecule, but can be moved by properly acting on the system, which can be now considered as electronically bistable. The same picture holds when dealing about distinct centres sharing one electron, as found in VT systems.

- The different charge configurations involved in the redox isomerism must involve a different population of the antibonding orbitals of the redox isomers. As will be shown later on in sections 1.3 and 1.4, this is the main physical reason for the thermodynamic as well as optical bistability of VT species.

All of these issues are taken into account when dealing about cobalt-dioxolene molecules. In this situation the active redox centres giving rise to the VT behaviour are:

The Cobalt cation. This ion has different valences of accessible energy and chemical stability: +2 and +3. The 0, +1 and +4 oxidation states are out of the energies taking part into the valence tautomeric equilibrium.

The dioxolene ligand. The ortho-quinone systems feature several chemical properties making them attractive for the development of bistable molecular materials. Firstly, they are characterized by three available and chemically stable oxidation states: 0 (quinones); -1 (semiquinones) and -2 (catechols) as shown in Figure 1.2. Due to their particularly rich redox chemistry, the quinones family is also found in proteins involved in electron transfer.

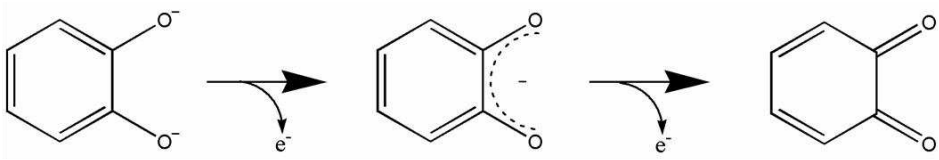

Catecholate S = 0 | Semiquinonate S=1/2 | Quinone S = 0

Figure 1.2: different oxidation states of the dioxolene ligands, along with their spin ground state.

These molecules in all their three oxidation states are able to efficiently bind metal ions ranging from the first transition row up to lanthanides.[11] However the most stable complexes are made out of the charged states of *o*-dioxolenes, semiquinonate and catecholate, and their number overwhelms the one involving the ligand in its quinone neutral form, whose complexes are less stable than the ones involving the ligand in lower oxidation states. For this reason the M-Q complexes won't be dealt about in the context of this thesis (for a review about M-Q complexes *cfr.* ref. 12). The oxidation state of the organic ligand in a complex is mainly determined by the redox potential of the coordinated metal ion. A quick glance at the electronic ground states of the metal - *o*-dioxolene complexes can be taken looking at Figure 1.3.

Figure 1.3 shows how the redox potential for M^{IV}/M^{III} and M^{III}/M^{II} redox pairs monotonically increases with the atomic number of the metal ion. For comparison it is also reported the potential of the SQ/Cat redox pair, while the Q/SQ isn't shown for the above mentioned reason. For low Zs the SQ/Cat redox potential is higher than the ones related to the metal ions: in this case the M-dioxolene complexes are characterised as semiquinonate adducts of metals in their high oxidation state (as in the case of Ti^{IV} and V^{IV}). On the opposite side, for heavier first row *3d* elements the catecholate oxidation state is the most stable one, along with lower oxidation numbers of the metal ions (Ni^{II}, for example). To our aims particular attention deserve the crossing points highlighted in blue areas in Figure 1.3. In this region (related to Cr, Mn, Fe and Co atoms) the redox potentials

of the metal ions match the one of the organic ligand, and the first condition of the recipe to obtain electronically bistable materials is fulfilled.

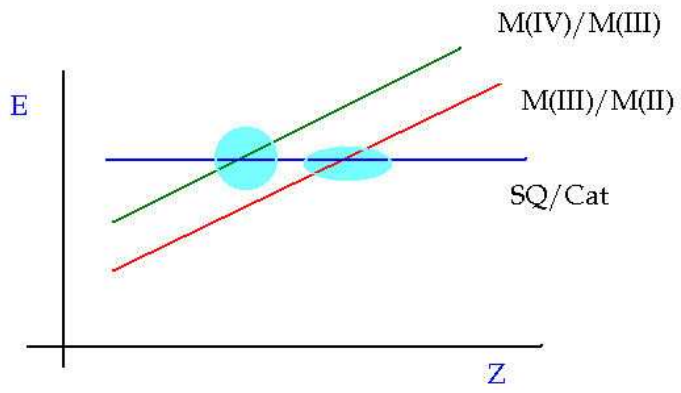

Figure 1.3: Trend of M^{IV}/M^{III} and M^{III}/M^{II} redox potential for a 3d metal ion in function of the atomic number of the ion.

O-dioxolene ligands are able to accomplish the other conditions for the development of Cobalt based redox isomeric species. In fact, contrarily to what found for Co complexes with diamines or 1,2-dithiolenes they provide complexes with low character of covalence of the Co-O bonds and well defined charge structures, that can be investigated by means of magnetic, spectroscopic and structural techniques. Experimental evidences of class II behaviour, according to Robin and Day classification, can be found considering that it has been possible to investigate the magnetic exchange among radicals in $M^{III}(SQ)_3$ systems, confirming the intramolecular charge localisation. Moreover the ligand charge transfer optical bands, found in the IR region for $M^{IV}(SQ)_2Cat$ systems, suggest a nonzero degree of orbital mixing among the different oxidation states of the ligand.[11] Another interesting feature of this class of redox active ligands is the tunability of their reduction potential in function of the substituents on their carbon ring, increasing their synthetic ability to afford VT systems. The large set of *o*-dioxolenes has allowed to investigate the magnetic exchange mechanism in *3d* metals adducts, clarifying the role of σ- and π-kind metal orbitals as well as the one of SQ-SQ superexchange in determining the spin ground state of the complex[13,14]. They were revealed to be able to tune the conversion features of VT systems leading also to the achievement of a thermal hysteresis cycle in a polymeric Co-dioxolene adduct[15].

The ancillary ligand. Contrarily to what found in the tris-quinone complexes of V^{III}, Cr^{III} and Fe^{III}, featuring monomeric octahedral $M^{III}(SQ)_3$ type complexes, in the case of Co the oxidative addition of 1.5 equivalents of 3,5-ditert-butyl-benzoquinone to $Co_2(CO)_{10}$ affords a tetrameric species uncapable to show VT.[16] The only two possible stoichiometries for Co-dioxolene based VT systems are thus the 1:1 and 1:2, respectively. Despite this

difference, the chemical and physical behaviour of 1:1 and 1:2 Co:dioxolene complexes look very similar, because only one among the two dioxolenes is able to share an electron with the metal ion, the other staying on like mononegative, semiquinonate form.

A direct consequence of this is the necessity to complete the first coordination sphere of the Co ion to satisfy an octahedral geometry. This is accomplished by some ancillary ligands, whose name is related to their indirect role in the redox isomeric conversion. Such ligands are usually mono, bi or tetradentate organic ligand featuring N-donor atoms, and are known since a long time to form stable adducts with Co ion in both +2 and +3 oxidation states. In Figure 1.4 are shown some of the commonly used ancillary ligands for the development of VT materials.

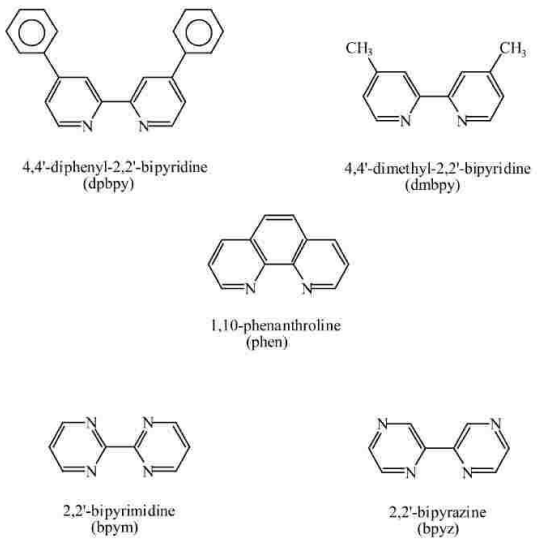

Figure 1.4. Most widely employed N-donor ancillary ligands for the development of molecular VT.

Despite these ligands do not take direct part into the redox isomerism of cobalt-dioxolene complexes, they play a double role in it: first and foremost they afford a crystal field of the correct strength in order to have spin crossover of the metal ion, which will be shown to be the thermodynamic driver of the process on one side, secondly they are able to tune its redox properties, as will be discussed in section 1.3.

1.2 Orbital description of Redox Isomers in Cobalt-dioxolene complexes

In order to understand the electronic properties of Co – dioxolene based valence tautomers we present a description based on symmetry considerations and the molecular orbital theory of their frontier orbitals. In Figure 1.5 is shown the energy pattern of Co – dioxolene systems, along with the frontier orbitals (HOMOs and LUMOs) of the redox active moieties of the molecule.[17]

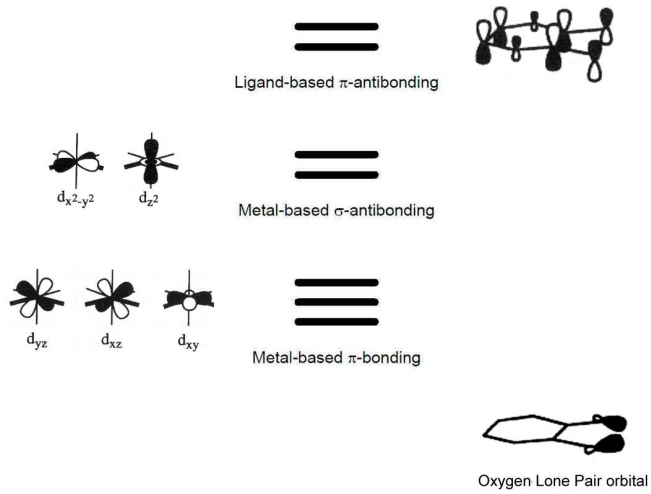

Figure 1.5: Energy pattern of the frontier molecular orbitals of Co-dioxolene systems.

The Co *3d* frontier orbitals, shown on the left, are split by the presence of an octahedral ligand field into a t_{2g} set, made of the *xy*, *xz* and *yz* orbitals, and an e_g set, constituted by the x^2-y^2 and z^2 ones, lying higher in energy. The molecular orbitals belonging to the organic moiety able to interact with the metal ion ones are shown on the right.[18] The lower in energy is mainly characterized by the *p* orbitals of the lone electronic pairs of the oxygens, able to overlap with the metal e_g orbitals in a σ fashion, giving rise to a metal centred, feebly destabilised σ* set of molecular orbitals, antibonding in character. Higher in energy stays the π* molecular orbital, capable to give rise to a π-type of interaction with the t_{2g} metal orbitals. Such an overlap stabilises a π-type of molecular orbital, mainly constituted by the metal t_{2g} orbitals and a very high-lying, unoccupied, π* ligand centred one.

The three molecular orbitals of interest in the description of the electronic features of the different redox isomers undergoing VT are shown in the central part of Figure 1.5. These electronic functions are able to describe the different redox isomers as well as the mechanism of thermally and optically triggered VT. First, they can account for the

occurrence of electronic bistability in Co-dioxolene systems. It is possible, in fact, to re-consider the requirements shown in paragraph 1.1 from a molecular orbital view. The interacting moieties feature indeed frontier orbitals lying close in energy, being the HOMO of organic system in between the *3d* Co orbitals split by an octahedral field. Moreover, the feeble orbital mixing between the two partners accounts for, on one side, a well localised charge structure, allowing a process of redox isomerism, accomplished by an electron transfer; on the other gives rise to the spin crossover phenomenon being the e_g-based built molecular orbital antibonding in character, thus lowering the crystal field on the Co ion when populated. With this energy picture in mind, we focus hereon on the description of the redox isomers taking part into the valence tautomeric interconversion.

The VT interconversion in Co-dioxolene systems may be seen as an electron transfer process between the metal and the dioxolene redox centres, joint to a change of spin state of the former, schematised in Equation 1.1

$$ls - Co^{III} - Cat \rightleftarrows hs - Co^{II} - SQ \tag{1.1}$$

where we call Cat and SQ the dinegative, catecholate and the mononegative, semiquinonate, forms of the *o*-dioxolene ligand, respectively. A schematic picture of the redox isomers from a molecular orbital point of view is shown in Figure 1.6

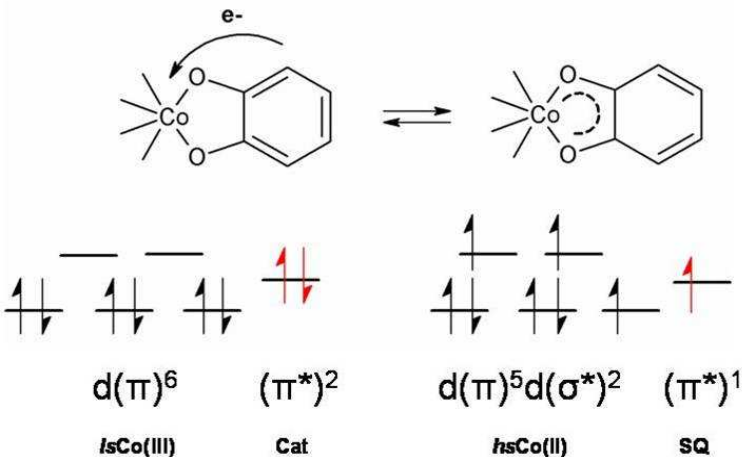

Figure 1.6: Schematic picture of the frontier orbitals' population of the two redox isomers involved in the VT of cobalt-dioxolene complexes.

The low temperature electronic isomer is shown in the left side of Fig. 1.6. It features the Co ion in the +3 valence state and in the low spin configuration, bound to the dioxolene ligand in its catecholate, dinegative, form. In this case the π bonding molecular orbital, mainly arising from the t_{2g} metal set of orbitals and thus labelled, according to the

nature of the electronic interaction, $d(\pi)^6$, meaning that the *d* set is involved in a π-type of chemical bond and six-fold occupied, is fully populated. On the other side, the π* molecular orbital, now almost completely localised on the semiquinonato moiety, is doubly occupied. Since the lowest lying electronic levels of the molecule are fully occupied, this is the quantum-mechanical electronic ground state of the Co-dioxolene molecular systems and, as such, is the stable form predominating at low temperature. For the same reason in this electronic state the molecule is diamagnetic.

Under the appropriate physical stimula, the mostly investigated being heat[19-25], pressure[26-28], light irradiation[15,29-34] and magnetic field[35] the interconversion process described by Eq. 1.1 may occur, related to a flow of one electron from the organic ligand π*-type orbital to the π set located on the metal ion and its change of spin state. This leads to the population of the *d*(σ)*, metal centred, antibonding molecular orbitals, affording huge changes in the physical properties of the system, described in the following.

Magnetic properties: in the VT transition the molecule changes its spin ground state, thus featuring huge differences in its magnetic properties. The description of the magnetism of the two states depends on the stoichiometry of the system, distinguishing between 1:1 and 1:2 Co:dioxolene systems. In the former case the redox active molecule is made of a Co ion, a bidentate *o*-dioxolene ligand and a tetrapodal N-donating ancillary ligand. The low temperature ground state can thus be formulated as in Eq. 1, *ls*-Co^{III} – Cat, and features an S=0 ground spin state. On the other side of the equilibrium the system feature an S=3/2 coupled to an unpaired electron located onto the organic moiety (S=1/2), thus stabilising an S=1 or S=2 spin state, depending on the sign of the magnetic exchange interaction. In the second case the system is constituted by a Co ion, two *o*-dioxolene ligands and a bidentate N-donating ancillary ligand. In this case the low temperature state features an S=1/2 spin ground state, while at high temperature an S=1/2 or an S=5/2 is the spin ground state. It must be stressed that dealing with spin quantum numbers about systems containing the high spin Co^{II} ion may look inappropriate, due to its high orbital contribution to its magnetic moment. However, since the spin coordinates are the significant parameters controlling the physics of VT interconversion, leaving the orbital contribution just the side role of determining the amount of magnetisation of the system, and since the quantitative determination of such a contribution is still an open challenge in the scientific literature about VT material, we will neglect here the orbital contribution and we'll deal only about the spin issues related to the magnetic properties of Co:dioxolene materials. For a review covering the aspects of orbital magnetism of *hs*-Co^{II} in octahedral coordinative environments *cfr.* ref. 36.

From these considerations it is straightforward that M-SQ complexes showing a low degree of orbital contribution to the magnetism can be used as testing grounds to attempt a theoretical investigation of their intramolecular exchange coupling. In particular, DFT methods using different functionals have been proved to reproduce very well both sign and amplitude of the experimentally determined coupling constants for Cr^{III}[18] and Ni^{II}[37] complexes of semiquinonate ligands. The investigation of these two systems allowed

to address the role of the different set of molecular orbitals of these systems in the exchange mechanism. In fact in the Cr^{III} ion, with its [Ar]$3d^3$ electronic shell, the unpaired electrons responsible for the exchange interaction are located in the π bonding molecular orbitals, mainly arising from the t_{2g} set, and experience a high overlap with the π* SOMO of the organic moiety, as can be seen from Figure 1.7.

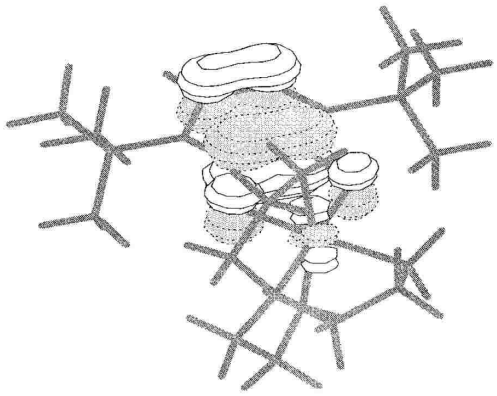

Figure 1.7: HOMO of the Cr-(tren)(3,6-DTBSQ) complex, as resulting from DFT calculations using the U-BLYP/6-311G** functional. The plot highlights the overlap between the d_{yz} metal orbital and the p_z one located on the oxygen atom of the ligand.

This kind of magnetic interaction leads to very strongly antiferromagnetic couplings, estimated to be of the order of 1000 cm^{-1}. Such an interpretation has been corroborated by investigations of d^3 (Cr^{III})[38], d^4 (Mn^{III})[39] and d^5 metal ions (Fe^{III}, Mn^{II})[40] coordinated to semiquinonate ligands.

On the opposite side, the effect on magnetic coupling of the overlap of the e_g-deriving set of molecular orbitals with the π* dioxolene ones has been checked as well. Such goal has been achieved investigating an [Ar]$3d^8$ transition metal (Ni^{II}) bound to a *o*-dioxolene ligand. Both magnetometry and DFT investigations, this last one using a broken symmetry approach, suggested a very strong ferromagnetic interaction, estimated to be active at room temperature as well.[37] The magnetic orbitals for 9,10-dioxophenanthrenesemiquinonato adduct of a nickel(II) are pictorially shown in Fig. 1.8. As can be seen, the SOMOs belonging to the Ni^{II} and organic radical moieties are orthogonal one to each other (in idealised C_{2v} symmetry they span a_1 and b_2 irreducible representations, respectively), thus supporting the experimental evidences, according to the recipes of Kahn.[41]

Figure 1.8: *Left and centre*: SOMOs of the Ni^{II} moiety. *Right*: SOMO of the semiquinonato ligand.

The above mentioned reasons make the determination of the magnetic exchange constant in Co:dioxolene systems rather challenging. In particular, the orbital contribution to the magnetism hinders the experimental determination of the spin ground state at low temperature, the *hs*-Co^{II} ion very strongly deviating from a Curie behaviour, as can be seen having a glance at Figure 1.9.

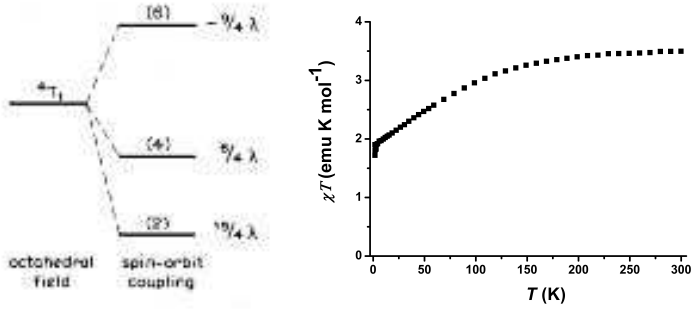

Figure 1.9. *Left*: Splitting of the electronic levels of the *hs*-Co^{II} ion in octahedral symmetry due to spin-orbit coupling, as taken from ref. 36. Levels' degeneracies are shown in parentheses. *Right*. Temperature dependence of the χT product for an octahedral *hs*-Co^{II} complex showing its deviations from Curie behaviour.

From a quick glance at Fig. 1.9 and considering a spin-orbit coupling parameter of about -180 cm^{-1} we estimate an energy separation between the ground state doublet with the first excited quartet state of about 300 cm^{-1}. However, the distorted octahedral first coordination sphere of Co^{II} in dioxolene molecular systems reduces this value down to about 100 cm^{-1}. This interaction is enough to hinder the quantitative determination of the exchange coupling between Co and SQ ligand, which is expected to be lower in energy. The onset of orbital contributions to the magnetism thus prevents the application of a spin Hamiltonian treatment of the low-temperature $\chi_M T$ data and so the attribution of deviations from the Curie law as due to magnetic coupling. Up to now the crystal field and orbital effect to the magnetisation of Co:dioxolene systems has been estimated using the diamagnetic analogue technique, in which the $\chi_M T$ of a Co:SQ system, incapable of giving

VT and thus keeping the same charge distribution over the whole range of temperatures investigated, is compared to another one of a *hs*-Co^{II} ion bound to a diamagnetic analogue of the paramagnetic semiquinonate ligand, yielding a very similar coordination environments around the metal ion. Such approach revealed a dominant antiferromagnetic exchange interaction between the magnetic partners.[42] This finding has been supported by DFT calculations, revealing a predominance of the antiferromagnetic interaction over the ferromagnetic one in systems where the magnetic orbitals aren't perfectly orthogonal. This result is not trivial, since the orbitals involved in the magnetism of Co:dioxolene systems are both σ and π in nature.

Optical properties: The difference in the electronic configurations of the two isomers involved in VT yields is reflected in UV-Vis absorption spectra. In Figure 1.10 are shown the electronic spectra of a 1 : 1 Co : *o*-dioxolene system in two different redox states[43].

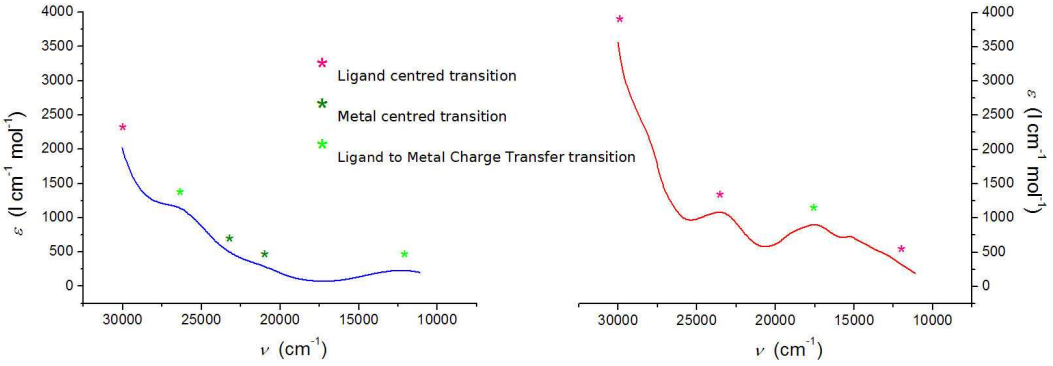

Figure 1.10: UV-Vis absorption spectra of Co : *o*-dioxolene 1 : 1 systems in *ls*-Co^{III}-Cat (*left*) and *hs*-Co^{II}-SQ (*right*) charge distributions.

The above spectra can be rationalised considering three active contributors to the absorption of light: the metal ion, the redox active dioxolene ligand and charge transfer levels involving both centres. Particularly useful for a proper assignment of the bands is the energy diagram of the electronic states of the catecholate (*left*) and semiquinonate (*right*) ligands, shown in Figure 1.11.[44]

While only two transitions for the catecholate can be seen, falling in the UV region of the spectrum (31700 and 35000 cm^{-1}) and related to the population of the first two excited states from the HOMO level ($3b_1$), the semiquinonato species features in addition three more bands located in the visible region of the spectrum (10000 – 13000 cm^{-1}), due to the transition from inner levels to the SOMO, generated by the removal of one electron from the HOMO.

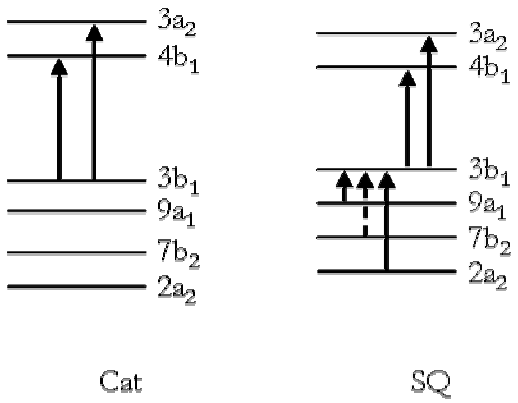

Figure 1.11: Energy diagram of the electronic states of catecholate (*left*) and semiquinonate (*right*) forms of *o*-dioxolene ligands in M : dioxolene 1 : 1 complexes, as arising from an extended Hückel calculation.

In the *ls*-Co^{III} – Cat redox isomer (left side of Fig. 1.10) the high energy, near UV, spectral region is dominated by a very intense band, located above 30000 cm^{-1}. This absorption has been assigned to the population of the first two excited states from the HOMO level ($3b_1$) of the dioxolene ligand, shown in the left side of Figure 1.11, by means of an extended Hückel calculation. Lowering the energy it is possible to find the expected band due to the presence of octahedral *ls*-Co^{III} ion, located at 23200 cm^{-1} and related to the transitions between the HOMO $^1A_{1g}$ to the $^1T_{1g}$ level. Finally, comparison among spectra of different semiquinonate adducts of Co^{III} revealed a shift of the energies of the bands located at 26200 and 12100 cm^{-1}, suggesting their Ligand to Metal Charge Transfer character. These bands will be shown to be the pump of the metastable state at low temperature.

Concerning the *hs*-Co^{II} – SQ redox isomer (right side of Fig. 1.10), the contribution of *d-d* transitions in its absorption spectrum is negligible. In the UV region of the spectra are found, in analogy with the previous case, the SOMO-LUMO transitions of the dioxolene ligand. In addition to these, its monoelectronic oxidation gives rise to three different bands located in the visible region of the spectrum (10000 – 13000 cm^{-1}), due to the transition from inner levels up to the SOMO, which are distinctive of semiquinonate type of ligands. The broadening of these bands is supposed to be due to a vibrational structure involving the C-O stretching. The unresolved pattern of bands in the 15000 – 19000 cm^{-1} spectral range is attributed to Metal to Ligand Charge Transfer processes, involving the *d* orbitals of the metal ion and the singly occupied π^* orbital of the ligand.

1.3 Thermal induced Valence Tautomeric Equilibrium

In this paragraph we describe the temperature dependence of the valence tautomeric equilibrium expressed by Eq. 1.1, which can be understood considering the energy pattern of the frontier molecular orbitals for the two isomers involved in the equilibrium, *ls*-Co^{III} – Cat and *hs*-Co^{II} – SQ, shown in Figure 1.6. From a quantum-mechanical point of view the *ls*-Co^{III} – Cat redox isomer is the ground state of the system for all the temperatures, since it features a complete population of the lowest lying molecular orbitals. The significant stabilisation of this electronic configuration is due to the enthalpy of formation of the Co-O_{diox} bonds.

Heating the system the VT transition takes place, consisting in an intramolecular electron transfer along with a spin state change of the Co ion. This process leads to the population of the e_g molecular orbitals, which are antibonding in nature, and thus to an increasing of the Co-O_{diox} bonds lengths during the transition. This phenomenon can be pictorially described using a double well energy diagram, in which the energy of the vibrational levels of the two electronic states are plotted *vs.* the reaction coordinate, assumed to be the Co-O bond totally symmetric metal – ligand breathing mode, shown in Figure 1.12.

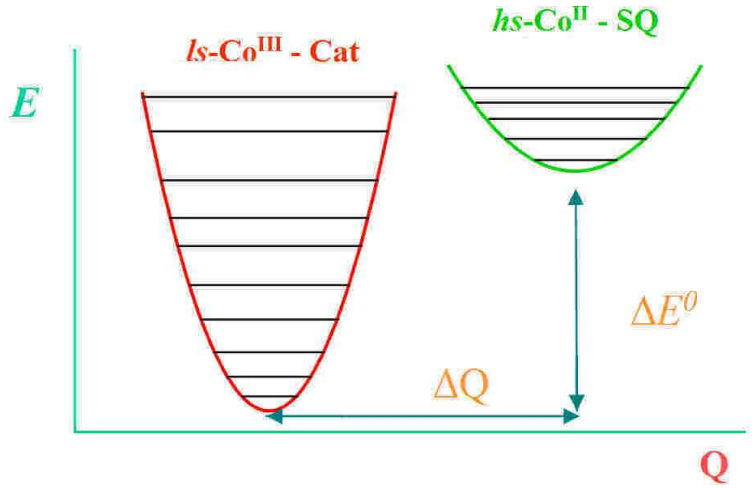

Figure 1.12: Schematic picture of the potential energy surfaces describing the *ls*-Co^{III} – Cat (*left*) and *hs*-Co^{II} – SQ (*right*) redox states at low temperatures.

Since the increase of the metal-ligand bond lengths (usually passing from 0.18 Å for *ls*-Co^{III} – Cat to 0.21 Å for *hs*-Co^{II} – SQ) is responsible for a positive ΔH of the VT equilibrium, the thermodynamic driving force of the process can be found in an entropy gain. The positive contributions to $\Delta S_{HT\text{-}LT}$ are of electronic and vibrational nature:

$$\Delta S_{HT} - \Delta S_{LT} = \Delta S_{electr} + \Delta S_{vib} > 0 \qquad (1.2)$$

The first contribution is due to the electronic degeneracy of the different isomers, resulting as the product of the orbital and spin degeneracies. In the low temperature phase a $(t_{2g})^6(e_g)^0(\pi^*)^2$ electronic configuration yields a $^1A_{1g}$ electronic ground state, with only one electronic distribution available. On the other hand the high temperature state features the metal in a $^4T_{2g}$ and the $(\pi^*)^1$ states (*cfr.* right side of Fig. 1.12), featuring thus an overall electronic degeneracy of 12. The expected energy stabilisation can be evaluated using the Boltzmann formula as

$$\Delta S_{electr} = R \ln \frac{g_{HT}}{g_{LT}} = 20.6 \text{ J K}^{-1} \text{ mol}^{-1}. \quad (1.3)$$

This value represents an upper limit, since it must be considered that not all these levels are populated at the transition temperature, and the removal of the $^4T_{2g}$ degeneracy due to the strong spin-orbit coupling of the *hs*-Co^{II} ion may lower this limit up to 5 J K^{-1} mol^{-1}.

The main term for the positive entropy change accompanying VT equilibria is however arising from the lowering of the vibrational frequencies and the increased density of vibrational states of the high temperature phase with respect to the low temperature one, due to the change in metal-ligand bond strength, as highlighted by the $\Delta r = 0.18$ Å in the Co-O bonds. The frequencies of vibrations of the different states have been characterised by means of Raman spectroscopy to be about 450 cm^{-1} in the *ls*-Co^{III} – Cat form and 350 cm^{-1} in the *hs*-Co^{II} – SQ one[45]. The vibrational contribution to the entropy of the transition can then be calculated according to

$$\Delta S_{vib} = R \ln \left[\frac{\prod_{HT} (1 - e^{(-\frac{Z_{HT}}{k_B T})})}{\prod_{LT} (1 - e^{(-\frac{Z_{LT}}{k_B T})})} \right] \quad (1.4)$$

where Z is the vibrational partition function of the high or low temperature state[17].

Holding these considerations the VT equilibrium in solution can then be described using the thermodynamic approach for regular solutions, according to Eq. (1.5):

$$\Delta G = \Delta H - T\Delta S \quad (1.5)$$

Moreover, considering the relation

$$\Delta G = -RT \ln K_{eq} \quad (1.6)$$

we can derive an expression to describe the entropy driven valence tautomeric interconversion:

$$[hs\text{-}Co^{II}\text{–}SQ] = \frac{1}{e^{\left(-\frac{\Delta H}{RT}+\frac{\Delta S}{R}\right)}+1} \tag{1.7}$$

Eq. 1.6 points out the thermodynamic character of the entropy driven VT, which can be assumed to be an equilibrium population of the vibrational states belonging to the two electronic phases according to Boltzmann statistics. In addition it lets us quantitatively describe the VT equilibrium in solution and in solid state for non interacting interconverting centres, and its behaviour is shown in Figure 1.13, where $\Delta H/R$= 900 K and $\Delta S/R$ = 7.

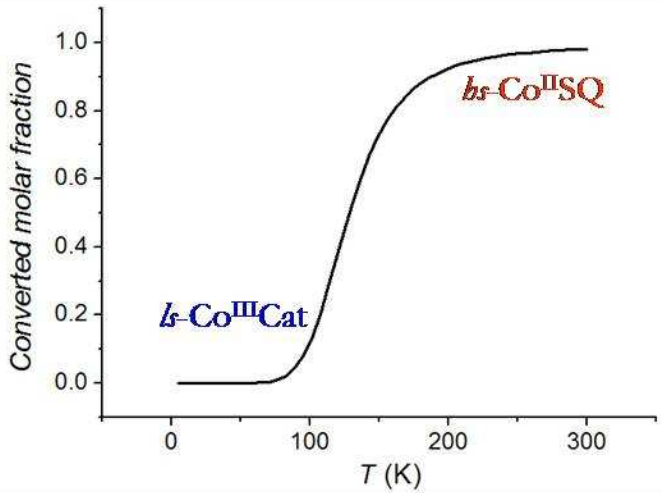

Figure 1.13: Profile of an entropy driven valence tautomeric conversion process calculated using Eq. 1.7 with the parameters reported in the text.

As expected, in the low temperature region a complete population of the *ls*-Co^{III} – Cat is found while heating the system the *hs*-Co^{II} – SQ becomes the thermodynamically stable state and the system is completely converted.

The effects of variations of the thermodynamic parameters characterising the VT process can be understood considering the analytical expression for the transition temperature ($T_{½}$, defined as the temperature featuring an equimolar amount of interconverting species). This can be extrapolated considering that $T_{½}$ is the temperature where the equilibrium described by Eq. 1.5 is reached, thus vanishing the ΔG of the process:

$$T_{½} = \frac{\Delta H}{\Delta S} \tag{1.8}$$

As expected, a decrease in ΔH as well as an increase in ΔS stabilise the high temperature form, lowering the $T_{½}$ value.

So far we have dealt about non interacting interconverting centres, a situation found for solution or diluted crystalline environments. In the solid state, however, the physical description of the entropy driven VT is more complicate because of intermolecular and molecule-lattice interactions. The first can be taken into account by using a model, developed by Slichter and Drickamer in the seventies to consider the pressure driven spin crossover and redox chemistry of Fe ions in the solid state.[46] In this model the interactions among interconverting centres is described as an additional term to the total Free Gibbs energy of the system:

$$\Delta G = \Delta H - T\Delta S + \Gamma x(1-x) \tag{1.9}$$

From the relation $d\ln K / dT^{-1} = -\Delta H$ the correction to the enthalpy variation of the process in function of the degree of interaction can be obtained:

$$\Delta H_{eff} = \frac{\Delta H}{1 - \Gamma / 2k_B T} \tag{1.10}$$

This elegant description highlights the transition properties in the solid state, where the molecules undergoing transition usually interact because of elastic strains induced in the lattice. If $0<\Gamma<2k_BT$, the interaction among centres in the same electronic state stabilises the system. The transition is no more gradual but features a cooperativity, raising the $T_{½}$ and making the transition profile more steep. If $\Gamma>2k_BT$ value, a bistability occurs and the system shows thermal hysteresis of the entropy driven transition. The negative Γ case is not taken into consideration since its physical requirements are harder to be matched for the majority of bistable systems.

On the other hand, the role of molecule-lattice interactions in determining the VT transition profiles are very far from being quantitatively elucidated. VT equilibria have in fact revealed to be very sensitive to this interactions, showing significant shift of the $T_{½}$ upon changes in crystallisation solvent[1,21,47,48] and counteranion[26]. Even more subtle effects have been reported to be exerted by a change of the isotopic distribution of the crystallisation solvent in determining the relative stability of the two isomers[49]. As a safe general conclusion we can state anyway that the sterical hindrance around the converting molecular centre appears to be crucial in determining the possibility of molecules to expand during the VT transition.

1.4 Photoinduced Valence Tautomeric interconversion

The photophysics of metal complexes is a very wide field of investigation in Inorganic Chemistry. In the 30000 cm^{-1} (330 nm) – 10500 cm^{-1} (950 nm) energy (wavelength) range, the one spanned by the conventional electronic absorption spectroscopy, occur the transitions involving the frontier orbitals of the metal complexes. In case of low degree of covalence of the M-L bonds we can address the character of the phenomenon according to the molecular constituents is related to: the metal ion, the ligand, or both (transitions trespassing the first coordination sphere's context, like metal – counter ion or intermolecular charge transfers, will be skipped here not being object of this thesis' work). While the metal and ligand centred transitions involve orbitals located on a single molecular constituent, the absorption of light of a charge transfer band excite an electron from a ligand (metal) centred molecular orbital to a metal (ligand) centred one, promoting a transient change of the charge distribution in the molecular framework. This phenomenon is found in a large set of complexes featuring closely spaced electronic states, as Co:dioxolene systems. In this case, by pumping the system on its CT band, it is possible to populate the excited electronic state, which in both the redox isomeric species corresponds to trigger the VT transition.[50] The peculiarity of bistable systems, however, is the ability to retain in time the population of the excited electronic states, thus behaving as a molecular switch or a optically addressable binary component of a quantum computer.

In the following we will introduce the concepts of light population of metastable states along with the optical bistability of VT systems.

1.4.1 High temperature optical bistability of Co:dioxolene systems

The investigation of optically induced valence tautomeric interconversion in solution at room temperature is not straightforward because of the kinetics of the interconverting phases falling in the picosecond time domain. For this reason the optically induced VT in solution at room temperature has been monitored with Transient Absorption Spectroscopy (TAS), where a laser pulse is used to promote the transition to a transient species in solution. The spectral features of the photoinduced transient phase can then be analysed at a fixed pump-probe delay time, thus affording the transient absorption spectra, or, at a fixed wavelength, in function of the pump-probe delay time, thus providing information about the time dependence of the photoinduction. In this way it has been possible to analyse the detailed mechanism of interconversion of a 1:1 Co:dioxolene adduct in solution, pictorially reported in Figure 1.14.

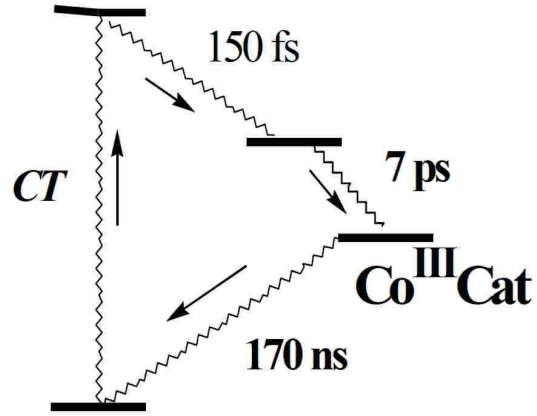

Figure 1.14. Jablonsky diagram of the states involved in the photoinduced VT interconversion of a 1:1 Co:dioxolene adduct at RT.

The diagram clarifies the details of photo-triggered VT interconversion in solution at RT for a *hs*-$Co^{II}(Me_4Cyclam)DBSQ^+$ cation, incapable to afford entropy driven VT in the 2-300 K range and taken as a reference species, featuring a well defined temperature independent electronic structure (namely a triplet ground spin state), for the behaviour of others Co:dioxolene 1:1 complexes. The process involves four different steps.

1. After the excitation pulse on the MLCT band, the system goes into an excited vibronic level of an excited electronic state. The assignment of the charge transfer state is tentative, however DFT calculations showed an energy accessible *ls*-Co^{II} – SQ level,[51] which is compatible with the observed kinetics.

2. A vibronic transition to the vibrational ground state of the excited state is suggested by the femtosecond timescale of the second process.

3. A subsequent ISC relaxation is then found, yielding a state whose transient spectrum points out its *ls*-Co^{III} – Cat character. The ISC process is favoured by the spin-orbit coupling of the Co ion, able to mix the wavefunctions belonging to the different electronic configurations of the system.

4. The reverse VT conversion step, taking the system back in its initial electronic state, is much slower than the previous ones, consisting in a spin-forbidden transition coupled to an intramolecular charge transfer. This physical behaviour can be rationalised taking into account an energy barrier to the relaxation, related to the difference of spin configuration of the interconverting electronic states.

The presence of an activation barrier for the relaxation can be important to visualize these molecules as systems showing optical bistability, and therefore it has been investigated for several classes of bistable materials, Fe^{II} SC and Co-based VT complexes. The wide range of complexes investigated allowed to connect the photophysical properties of these systems to their electronic and nuclear structures in both electronic states. The theory currently employed to describe the low temperature photoinduction of excited electronic states in bistable materials will be shown in the next paragraph.

1.4.2 Low temperature optical induction – the LIESST effect in Co:dioxolene systems

The low temperature optical population of the metastable electronic state in Co:dioxolene systems has been firstly reported by the Japanese group of Prof. Sato in 2001.[34] Pushed by what previously found for another class of VT systems, even if non molecular – the Prussian Blue analogues, a coordination polymer made out of a Fe – CN – Co cubic network, whose valence may be switched from *ls*-Fe^{III} – CN – *ls*-Co^{II} to *ls*-Fe^{II} – CN – *ls*-Co^{II} by optical irradiation in the solid state at cryogenic temperatures[52] – they irradiated the complex Co(tmeda)(3,5-DBCat)(3,5-DBSQ) on its LMCT band at low temperature in the solid state. The results, monitored by magnetometry and IR spectroscopy, pointed out an about 50 % of photoconverted fraction, which can be reversibly erased warming the system at 60 K.

The possibility to follow the change of electronic state by means of magnetometry suggests a very slow relaxation regime of the metastable photoinduced phase at cryogenic temperatures. This finding, named, in analogy with the SC literature, LIESST effect, aroused a wide interest in the inorganic chemistry and materials' science scientific communities, due to the possibility to use Co based VT systems as building block of new, molecular based, optical technology.[21] The rationalisation of the kinetics of decay in this set of molecules turned out to be mandatory: from a synthetic point of view chemists felt the need to increase the critical temperature of relaxation of the photoinduced phase; on the other side, unveiling the secrets of how to pump the excite states of the systems as well as to probe them by optical means could make the addressability of these systems closer.

The up to now employed theoretical approach to deal with optical bistability in VT systems has been developed by Jortner and coworkers in 1980 for the treatment of spin crossover between two electronic states with different nuclear structural configurations. It has been widely employed to describe the kinetics of conversion of photoinduced metastable excited states in solution and in the solid state for spin crossover and valence tautomeric systems.[30,31,43,50,53,55] Despite the obvious differences in the phenomenology of conversion for SC and VT complexes, the theory fits well to both families of bistable materials. In fact the physical reasons for the presence of an activation

barrier to the state crossover in both classes is related to a different spin configuration in the converting states, being the electron transfer much faster than the spin conversion in VT materials.[29] According to this treatment, the relaxation between two different electronic states can be considered as a multiphonon non adiabatic tunnelling process, depicted in Figure 1.15. In this picture the system, trapped at low temperature in the metastable *hs*-Co^{II} – SQ state after the photoinduction, has two different pathways of relaxation to the electronic *ls*-Co^{III} – Cat state: a purely electronic one, involving the direct coupling between the two electronic states involving a first (or higher ordered) spin-orbit interaction or a vibrational one, where the decay is activated by the overlap of the vibrational functions belonging to different potential wells. The role of the medium the systems is dipped in (solvent for solutions or crystal lattice for the solid state) is of paramount importance for this model: it is in fact considered as a source of low energy phonons (whose energy is in the 50 – 100 cm^{-1} range) providing the continuum of energy states able to absorb the optical energy released by the excited system during the relaxation process.

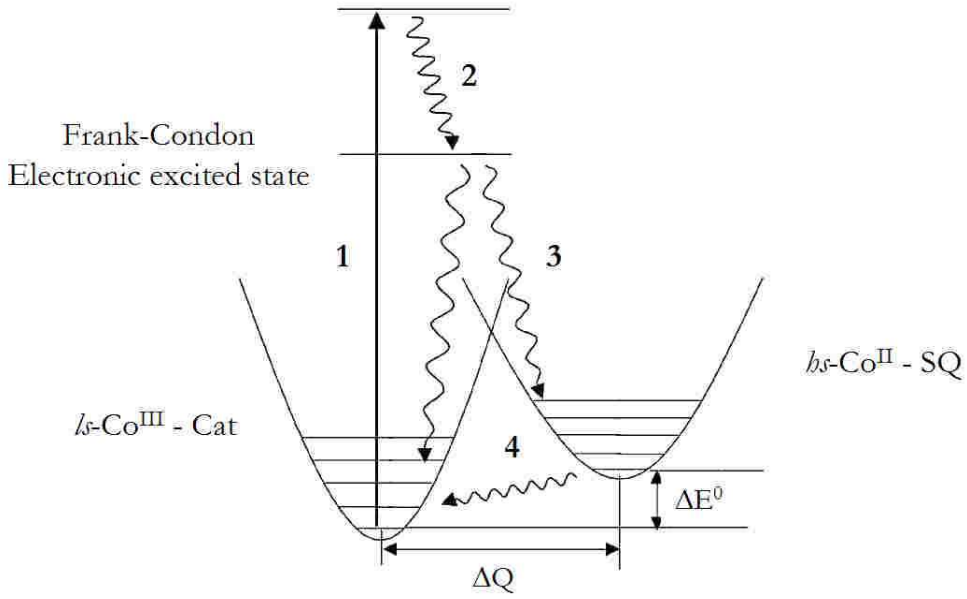

Figure 1.15. The electronic features of the states involved in the LIESST effect of VT complexes.

The model considers the conversion between the states as purely quantomechanic, being due to the mixing of vibrational functions belonging to different electronic states, and as such ruled by the Fermi Golden Rule, expressed in Equation 1.11

$$k = \frac{1}{\hbar\omega} g_f |V|^2 G \qquad (1.11)$$

where $\hbar\omega$ is the energy of the active vibrational mode of the system, g_f is the degeneracy of the final state, V is the factor related to the spin-orbit coupling between the different electronic states involved in the process and G is the thermally averaged Franck-Condon factor, describing the vibrational effect on the electronic transition rate. The treatment involves some approximations to let the math easier. Firstly, the vibration modes of the different states are supposed to have the same frequency and force constant. Moreover, the solvent contribution to the entropy change of the conversion is supposed to be small and introduced as a parameter. The two important factor in determining the relaxation rate are thus the spin-orbit coupling of the two electronic states, accounted for by V, and the coupling of the vibrational functions belonging to the ground and excited states, expressed by G. Let's have a brief overview of these latter two objects.

V: This term represent a pure quantomechanic relaxation path for the system, brought in by the spin-orbit coupling effect:

$$V = \langle \Psi_i | H_{SO} | \Psi_f \rangle \tag{1.12}$$

where $|\Psi_j\rangle = |\Psi_j^0\rangle + \sum_h \frac{\langle \Psi_j^0 | H_{SO} | \Psi_h \rangle}{(E_m - E_j)} |\Psi_h\rangle$ are the pure electronic functions corrected at the first order for the higher states mixing due to spin-orbit coupling. In the cases dealt within this work, we face a relaxation from a *hs*-Co^{II} – SQ electronic state to a *ls*-Co^{III} – Cat one. In such a context $|\Psi_i\rangle$ is a molecular orbital mainly due to the metal centred σ^* (e_g) molecular orbital and the $|\Psi_f\rangle$ is the ligand centred π^* orbital. Moreover, considering that the electronic states involved in the relaxation process feature different spin molteplicities, the expected value of the V factor for the *hs*-Co^{II} – SQ → *ls*-Co^{III} – Cat relaxation process arise from second order spin-orbit coupling matrix elements and is quite small.

G: Fermi's Golden Rule points out another active mechanism in the relaxation of electronically bistable systems, due to the coupling of the vibrational functions belonging to the different electronic states. This relaxation mechanism is usually accounted for by the G parameter, whose explicit expression is given in Eq. 1.13.

$$G(T) = \frac{\sum_{i,k} \langle \chi_k | \chi_i \rangle e^{-\frac{\hbar\omega_i}{k_B T}}}{\sum_i e^{-\frac{\hbar\omega_i}{k_B T}}} \tag{1.13}$$

Here the $|\chi\rangle$ functions are the vibrational states belonging to the different electronic isomers. Considering vibrational modes with the same force constant and frequency,

energy conservation requires that, i - k = n with $n = I\frac{\Delta E^0}{\hbar\omega}$ (I integer) is the sum of the vibrational quanta lying between the fundamental vibrational states belonging to the different electronic isomers. Being a measure of the vertical displacement of the two electronic wells reported in Fig. 1.12, it has thus been called the Zero Point Energy Difference. We will show later on the effect of this parameter on the relaxation rate k.

An important property of the G term is the explicit consideration of the temperature into the expression of k through the Boltzmann dependence of the population of the different vibrational states. From Figure 1.16 is possible to see qualitatively the increase of the mixing of functions (the shaded area of the graph is proportional to the Franck-Condon overlap integral $\langle\chi_k|\chi_i\rangle$) increasing the temperature (thus populating vibrational states higher in energy). At high temperatures k shows an Arrhenius type dependence on the temperature:

$$k = k_0 e^{-\frac{\Delta E_a}{k_B T}} \tag{1.14}$$

Such a mechanism is typical of the presence of an activation barrier. The presence of this hindrance to the relaxation, which can be appreciated looking at Figure 1.15, is related to the orthogonality of the electronic function describing the *hs*-Co^{II} – SQ and *ls*-Co^{III} – Cat states. It must be stressed that the rate determining step of the back VT process is due to the orthogonality of the electronic functions describing the *hs*-Co^{II} – SQ to *hs*-Co^{II} – SQ state and to the change of molecular spin involved in the process. The rates of the intramolecular electron transfer usually fall into the picosecond time domain, thus fully justifying the adopted model firstly developed for spin crossover materials, not withstanding the electron transfer issue.

According to this picture the relaxation time is supposed to diverge lowering the temperature. However, one of the main outcomes of the Jortner theory for the multiphonon relaxation of excited electronic states is the ability to consider a finite, nonzero, rate constant for T approaching 0. This can be easily seen considering the limiting value for G with with $T \rightarrow 0$. In this case only the fundamental vibration of the excited electronic state will be active and k becomes:

$$k = \frac{1}{\hbar\omega} g_f |V|^2 |\langle\chi_n|\chi_0\rangle|^2 \tag{1.15}$$

Under the above mentioned approximations it is possible to relate the relaxation rate of the excited state with the structural parameters of the system, according to the Eq. 1.16:

$$|\langle\chi_n|\chi_0\rangle|^2 = \frac{S^n e^{-S}}{n!} \tag{1.16}$$

where S is the Huang-Rhys factor

$$S = \frac{f \Delta Q^2}{2\hbar\omega} \tag{1.17}$$

and ΔQ is the difference in reaction coordinate between the electronic states, due to the nuclear displacement induced by the change in electronic configuration of the system, and f is the force constant of the active vibration of frequency ω. The theory is thus able to account for an Arrhenius dependence of the relaxation time at high temperatures, while a finite relaxation time is found in the low temperature, pure quantum activated, relaxation regime.

1.4.2.1 Parameters governing the metastable lifetime at cryogenic temperatures

In the previous paragraph the theory for nonadiabatic multiphonon relaxation in electronic bistable systems has been discussed, pointing out its ability to account for different relaxation regimes of the photoinduced metastable states at low temperature. Another key point justifying the wide use of the Jortner theory in the analysis of optically bistable systems at low and room temperature is indeed its capability to provide a direct connection between the metastable lifetimes and the structural and thermodynamic parameters governing the VT transition.[54] From a chemical point of view, the two most important quantities to play with in order to tune the relaxation time of the photoinduced metastable phases are the change in reaction coordinate following the optical transition, ΔQ, and the reduced energy gap, $\frac{\Delta E^0}{\hbar\omega}$.

The **Huang-Rhys factor** measures the overall change in reaction coordinate between the two electronic states of the systems. Since in the bistable systems investigated up to now the main nuclear displacement is due to the change of metal-ligand's donor atoms bond lengths, we can estimate the effect of ΔQ on k by measuring the relaxation rate for systems showing different variation of coordination lengths before and after the photoexcitation. Figure 1.16 pictorially shows the dependence of the $|\langle\chi_n|\chi_0\rangle|^2$ Franck-Condon overlap term between the lowest vibrational state of the excited electronic well with the electronic ground state for different SC materials.[55] The overlap, reported in figure as a shaded area, increases for small nuclear displacements, moving from Fe^{II} (where Δr, the difference in average first coordination sphere lengths, is 0.2 Å and S spans the 40/50 range) to Fe^{III} (featuring Δr of 0.13/0.16 Å and S of 25/30) and Co^{II} (0.09/0.12 Å and S ranging from 15 to 20). It follows from Eqs. 1.15 and 1.16 that an increase in the nuclear displacement following the electronic excitation should reflect in a decrease of the

relaxation rate of the metastable photoinduced state. The Figure 1.16 reports the effect of the ΔQ on the kinetics of the decay.

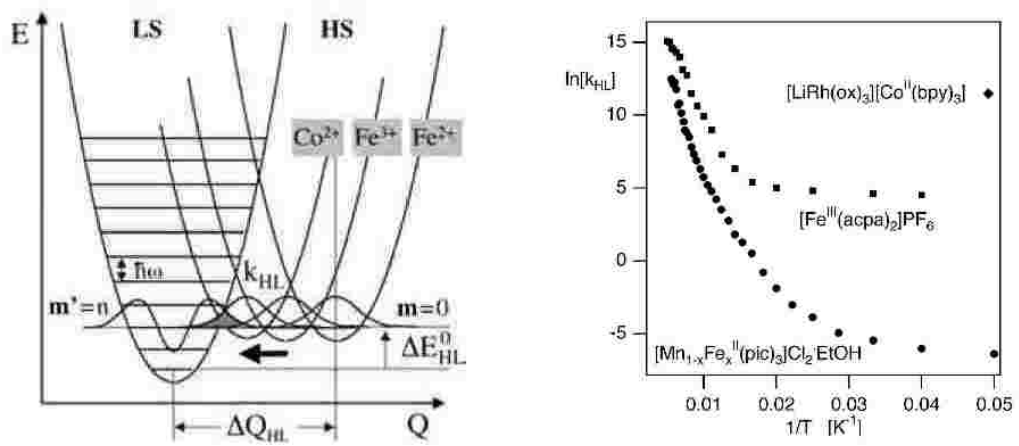

Figure 1.16. *Left*: Schematic picture of the overlap of the vibrational functions for different ΔQ values, corresponding to different Fe^{II}, Fe^{III} and Co^{II} SC materials. *Right*: Arrhenius plots of the relaxation of different SC materials featuring Fe^{II}, Fe^{III} and Co^{II} as switching ion.

The experimental support for the mentioned ΔQ effect on the kinetics of relaxation in SC materials is reported in the right side of Figure 1.16, showing the Arrhenius plots for three different compounds, containing Fe^{II}, Fe^{III} and Co^{II} as active metal centres for the SC behaviour.[55] In order to pick out the effect of coordination length differences and to neglect thermodynamic contributions to the change in relaxation rate (discussed in detail in the following paragraph) the materials have been chosen to feature similar $T_{½}$. In this way it is reasonable to expect similar energy difference between the electronic potential wells at low temperatures (*vide infra*). The results show that the relaxation times in the quantum activated tunnelling regions for the Fe^{III} and the Co^{II} compounds are 4 and 7 orders of magnitude faster than the one found for the Fe^{II} SC materials.

Particularly appealing for the chemical and physical control of the properties of optical bistability in bistable systems is the role of the **Reduced Energy Gap**, $\frac{\Delta E^0}{\hbar\omega}$. This quantity corresponds to the difference in energy between the lowest lying vibrational levels belonging to the different electronic states at low temperature, and can be tuned acting on a huge set of parameters: chemical substitution of the constituent of the system, as discussed in paragraph 1.1, controlling the vibrational coupling of the bistable molecules with the crystalline environment, or applying a pressure.[56] The latter two physical

approaches for the tuning of ΔE^0 rely on the difference in molecular volume of the two electronic states involved in the optically induced conversion. The crystal lattice is in fact usually considered as an overall pressure stimulus on the interconverting centres, as will be shown in Chapter 5. Since the high temperature stable form features an increased molecular volume due to the population of molecular orbitals, which are antibonding in character (arising from the e_g set of the octahedrically coordinated metal ion), an increased pressure is supposed to stabilise the low spin form. This behaviour can be rationalised considering the free energy of the system increased by the work term $p\Delta V$ due to pressure:

$$\Delta E(p) = \Delta E(0) + p\Delta V \tag{1.18}$$

where ΔV is the volume difference between the initial and final electronic states. Pictorially, this means to raise up the excited electronic well with respect to the ground state one.

The effect of increased pressure on the relaxation of a Fe^{II} SC system has been investigated by Hauser and is in perfect agreement with the theory of Jortner, revealing a linear increase of the relaxation rate with increased pressure up to 1 kbar.

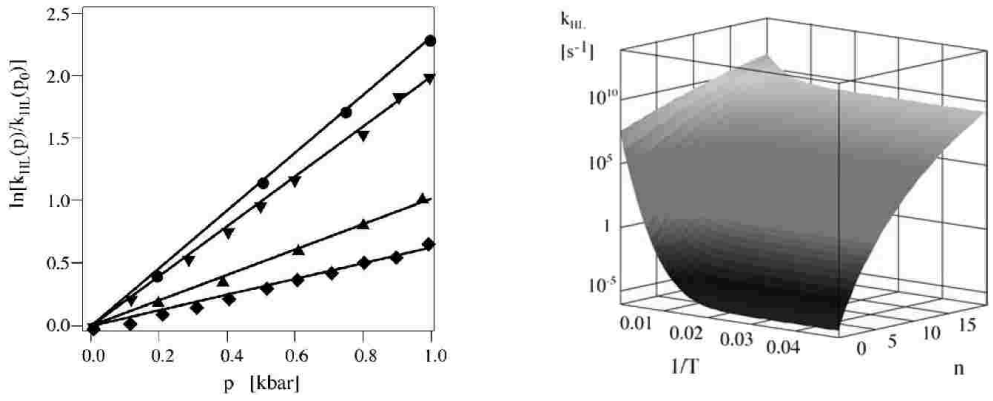

Figure 1.17. *Left*: Linear increase of the normalised pressure induced relaxation rate of the metastable photoinduced high spin states for a series of four Fe^{II} SC compounds. *Right*: Calculated dependence of the relaxation constant in function of temperature and reduced energy gap.

This effect can be easily seen from the right side of Fig. 1.17, where the relaxation rate constant k is plotted against he inverse of temperature and the reduced energy gap. The plot has been calculated from Eq. 1.11, considering the parameters typical of Fe^{II} SC complexes. The temperature dependence of k has already been discussed. At low temperatures, where the thermally activated, classic relaxation regime is not active, for small values of the reduced energy gap n the tunnelling rate constant increases exponentially with n. For higher values of n of the complex, the relaxation rate faces less

dramatic effects and follows the bell shape behaviour of the Marcus theory,[57] with a maximum value as *n* approaches S.

The physical parameters reported above are not, however, the only factors to be taken into account for the rationalisation of the metastable states' lifetimes. They are, however, the mostly easily controllable ones from the point of view of a rational development of molecular systems with predetermined physical properties using the bottom up approach of chemical building block assembling. We should not forget the effect of several other terms. Firstly, different ligands may reduce the spin-orbit coupling governing the V electronic coupling matrix,[53] which is usually supposed to be independent of the coordination environment. Moreover, a drawback of the theory of adiabatic multiphonon relaxation is the underestimation of the solvent reorganisation entropy, considered to be small with respect to the electronic entropy term involved in the transition. This assumption can be accepted for spin crossover interconversions, while this could not be the case for coulombic, longer ranged, electrostatic interactions characterising different charge distribution's isomers. Another aspect to be considered in the discussion of the lifetimes of metastable states is the vibrational coupling of the molecule with the environment, which may lead to significant deviations from Eq. 1.11, which has been developed for electronic states switching in solution environment.

1.4.2.2 The Inverse Energy Gap Law

In the previous sections we have shown how the interconversion processes occurring in bistable materials can be treated with a quantomechanic approach arising from the Fermi Golden Rule applied in the limit of strong vibronic coupling of electronic excited states. The theory allowed the rationalisation of the kinetic details of an equilibrium process in solution (the thermodynamic, entropy driven, SC or VT equilibrium) as well as the kinetics of an out-of-equilibrium interconversion (decay of a metastable state) in terms of the same parameters (the difference in reaction coordinate ΔQ and in energy $\frac{\Delta E^0}{\hbar\omega}$ of the two states involved in both processes). Following the syllogism suggested by the above mentioned paradigm, a connection between the entropy driven and the optically induced processes can be figured out: if both processes rely on the same parameters, they are expected not to be independent one from the other. In particular, it could be reasonable to expect that a stability of the high temperature phase in the temperature domain may come along with a correspondent stability in the domain of time, both of them relying in fact on vibrations. The first one to put on a solid and quantitative basis this idea has been Prof. Hauser, analysing a great set of data related to the transition temperature and low temperature metastable state's lifetimes for different Fe^{II} based SC complexes, all of them featuring a $Fe\text{-}N_6$ first coordination sphere. The validity of the comparison among the

physical properties of these different materials holds because all the parameters appearing in the Jortner theory are kept fixed into this huge family: the electronic degeneracy of the states involved, the active molecular vibrations in determining the relaxation, and the Huang-Rhys factor. The free parameters to be changed in this analysis are thus the relaxation rate k, the reduced energy gap $\frac{\Delta E^0}{\hbar\omega}$ and the transition temperature $T_{½}$. The results have been plotted in Figure 1.18.

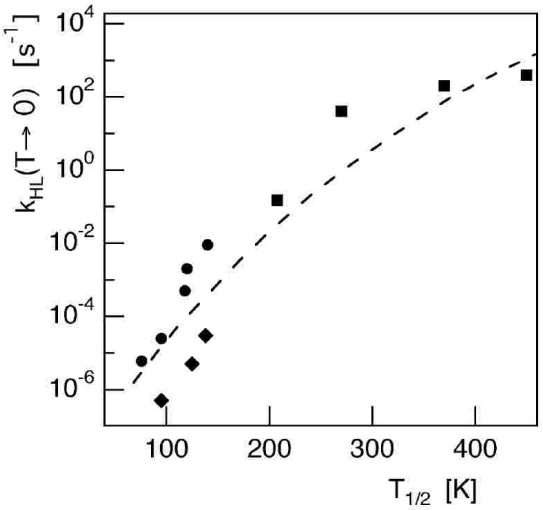

Figure 1.18. Dependence of the relaxation rate of the photoinduced metastable state at low temperature on the transition temperature for a series of Fe^{II} SC complexes featuring an Fe-N_6 first coordination sphere. The dotted line is the fitting function described in the text.

Figure 1.18 points out a close dependence of the relaxation constant k on the $T_{½}$ for a series of Fe^{II} SC systems. The validity of the relation is corroborated by the domain of the Cartesian axes: the relaxation rates in fact span ten orders of magnitude, while the transition temperatures are present in a 300 K interval.

The observed behaviour can be rationalised relating the thermodynamic expression of the transition temperature (Eq. 1.8) with the definition of the reduced energy gap ($\frac{\Delta E^0}{\hbar\omega}$). If we neglect the temperature dependence of the enthalpy change involved in the process, we are able to connect the Gibbs Free Energy variation going on with the equilibrium process ($\Delta G = \Delta H - T\Delta S$) with the zero point energy difference at low temperature between the electronic states, deriving the desired relation:

$$n = \frac{\Delta E^0}{\hbar\omega} = \frac{T_{1/2}\Delta S}{\hbar\omega} \tag{1.19}$$

This equation fits the data reported in Fig. 1.18 considering the same values of the fixed parameters ΔS and $\hbar\omega$. Moreover, it nicely follows the expected trend of the relaxation times for increasing n, previously shown in Fig. 1.17. In this case, in fact, the limit of strong vibronic ($S >> n$) coupling seems to be overcome and the exponential increase of k on increasing n lacks; however the beginning of a bell-like shape occurs, expected to peak for n matching S. This trend can be rationalised considering the effect of the reduced energy gap variation on the relaxation rate constant k and the transition temperature $T_{½}$. From the kinetic point of view, we have shown in paragraph 1.4.1.1 how an increase in n leads to an increase of k, mainly because of an enhanced overlap of the vibrational functions belonging to the different electronic states. These purely quantomechanic pictures can be extended to the thermodynamic case of entropy driven equilibrium, where the Gibbs free energy of the system is lowered by the quantity $T\Delta S$. In this case n can be seen as the limiting value for $\Delta G(T \rightarrow 0)$, ΔH(0 K). If we suppose the enthalpy variation of the equilibrium process to be independent of temperature, we can state that an increase in n is reflected in an increase of $T_{½}$.

The theory reproduces very well the experimental data in a very wide domain. It must be stressed, however, that the treatment is not yet able to consider systems in their neat solid state, but deals with interconverting centres in highly diluted environments, like solutions or highly diluted mixed crystals. In the solid state the role of elastic interactions with the environment has been revealed to strongly affect the $T_{½}$ for SC[58] and VT[1] systems. The more striking report of cooperative effects on the entropy and optically induced VT interconversion in a Co:dioxolene coordination polymer has been claimed by Dei *et al.* showing how the 1 D character of cooperative elastic interactions may give rise to an enhanced cooperativity and increase of the relaxation time at cryogenic temperature.[15]

1.4.2.3 The *T*(LIESST) parameter

The aforementioned treatments gained great attention in the scientific community of bistable materials for their ability to clarify the role of the electronic and structural parameters on the relaxation rate of metastable states on a strikingly wide set of systems. However, the Arrhenius plots reported in the previous paragraphs are affected by an experimental inconvenient: the time they require to be experimentally accessible is very often exceeding by far the majority of laboratories' resources, due to the high set of isotherm measurements in function of time to define one point in the plot. Moreover, for very slowly relaxing systems, the determination of the relaxation time in cryogenic conditions requires the operator to quit the measurement before the system has relaxed to $1/e$ times the value of the metastable fraction at the beginning of the relaxation (we remind

that, by definition, τ is the time required by the system to relax to $1/e$ of its starting value of metastable fraction). This problem has been elegantly solved using AC based methods in the case of dielectrics, superconducting and magnetic materials.[59] The method relies on a phase dependent measurement of a physical quantity induced by a sinusoidal, time dependent, field. Measuring in function of the frequency of the applied field is thus possible to investigate the dynamics of the systems for different decades of time quite easily. However, this experimental issue represents still an open problem for the field of this bistable electronic materials.

For these reasons Létard and coworkers developed a quicker experimental method to measure the kinetics of relaxation of SC materials.[60] Their approach consists in pumping the system at low, fixed, temperature (10 K) up to the photostationary limit, switch the excitation source off and then heating the system with a closely controlled rate (0.3 K min^{-1}) until it relaxes back to the ground state. The temperature of the relaxation has been called *T*(LIESST) and is related to the relaxation time of the system, since the temperature variation triggering the relaxation depends on time. From 1999 *T*(LIESST) of about sixty SC materials have been measured, highlighting a phenomenological linear dependence on the transition temperatures of the systems in analogy with the Hauser's Inverse Energy Gap Law (*cfr.* Figure 1.19),

$$T(LIESST) = T_0 - 0.3T_{1/2} \tag{1.20}$$

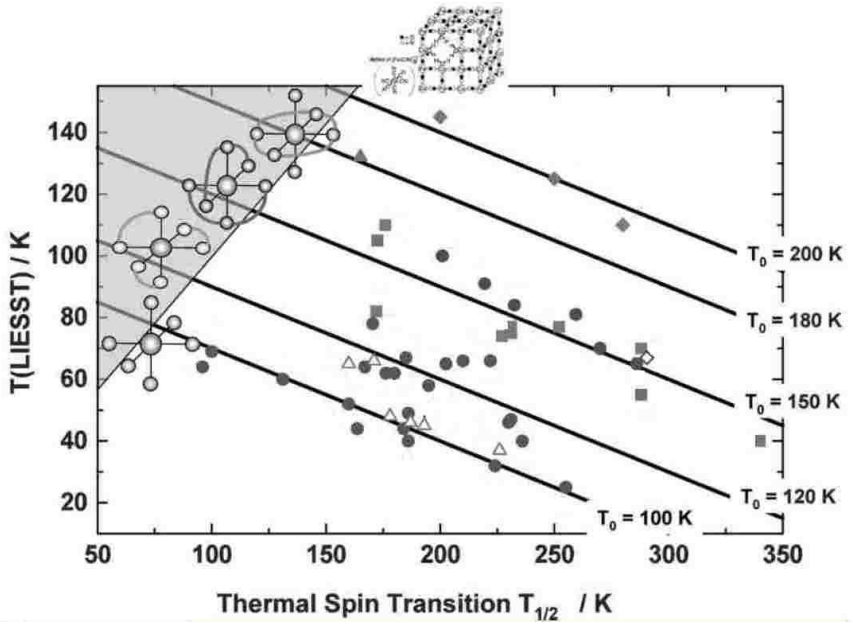

Figure 1.19. *T*(LIESST) dependence on $T_{1/2}$ for different structural families of spin crossover compounds. The grey zone corresponds to the unphysical situation where *T*(LIESST) is lower than $T_{1/2}$.

The authors found also a dependence of the T_0 parameter on the geometry of coordination of the first sphere of donor atoms around the bistable metal ion.

The great advantage of this experimental treatment relies indeed in the shortening of the measurements time with respect to standard kinetics characterisation. In this case is in fact possible in few hours point out the potential of a material to retain the optically written information. However, the approach aroused some doubts as well in the scientific community. As the same author pointed out, an about 20 K shift in the *T*(LIESST) value for the same compound can be measured by varying the temperature scan rate from 1 to 0.05 K min^{-1}.[61] Moreover, the exponential dependence of the relaxation time on temperature in the high temperature regime may be easily source of uncertainty on the *T*(LIESST) value, and a very careful and reproducible sample preparation protocol should be theorised as well, in order to take into account time dependent thermalisation effects.

References

[1] Hendrickson, D. N.; Pierpont, C. G. *Top. Curr. Chem.* **2004**, *234*, 63-95.

[2] Adams, D. M.; Dei, A.; Rheingold, A.; Hendrickson, D. N. *J. Am. Chem. Soc.* **1993**, *115*, 8221.

[3] Adams, D. M.; Dei, A.; Rheingold, A. L.; Hendrickson, D. N. *Angew. Chem., Int. Ed. Engl.* **1993**, *32*, 880-882.

[4] Pierpont, C. G. *Coord. Chem. Rev.* **2001**, *219*, 415-433.

[5] Caneschi, A.; Dei, A. *Angew. Chem. Int. Ed. Engl.* **1998**, *37*, 3005.

[6] Pierpont, C. G. *Inorg. Chem.* **2001**, *40*, 5727-5728.

[7] Carducci, M.; Pressprich, M.; Coppens, P. *J. Am. Chem. Soc.* **1997**, *119*, 2669-2678.

[8] Giri, A. K.; Kirkpatrick, E. M.; Moongkhamklang, P.; Majetich, S. A.; Harris, V. G. *Appl. Phys. Lett.* **2002**, *80*, 2341-2343.

[9] Bleuzen, A.; Lomenech, C.; Escax, V.; Villain, F.; Varret, F.; Moulin, C. C. D.; Verdaguer, M. *J. Am. Chem. Soc.* **2000**, *122*, 6648-6652.

[10] Robin, M. B.; Day, P. *Adv. Inorg. Chem. Radiochem* **1967**, *10*, 247-422.

[11] Pierpont, C. G.; Lange, C. W. *Progr. Inorg. Chem.* **1994**, *41*, 331.

[12] Rogez, G.; Riviere, E.; Mallah, T. *C. R. Chimie* **2003**, *6*, 283-290.

[13] Perekhodtsev, G. D.; Lebedev, Y. S. *J. Struct. Chem.* **1997**, *38*, 41-46.

[14] Perekhodtsev, G. D.; Lebedev, Y. S. *J. Struct. Chem.* **1997**, *38*, 884-889.

[15] Beni, A.; Dei, A.; Shultz, D. A.; Sorace, L. *Chem. Phys. Lett.* **2006**, *428*, 400-404.

[16] Buchanan, R. M.; Fitzgerald, B. J.; Pierpont, C. G. *Inorg. Chem.* **1979**, *18*, 3439.

[17] Shultz, D. A. *Magnetism: Molecules to Materials II* in Wiley and Sons: New York, 2001; pp 281-306.

[18] Rodriguez, J. H.; Wheeler, D. E.; Mccusker, J. K. *J. Am. Chem. Soc.* **1998**, *120*, 12051-12068.

[19] Buchanan, R. M.; Pierpont, C. G. *J. Am. Chem. Soc* **1980**, *102*, 4951-4957.

[20] Adams, D. M.; Dei, A.; Rheingold, A. L.; Hendrickson, D. N. *J. Am. Chem. Soc.* **1993**, *115*, 8221-8229.

[21] Dei, A.; Gatteschi, D.; Sangregorio, C.; Sorace, L. *Acc. Chem. Res.* **2004**, *37*, 827-835.

[22] Sato, O.; Cui, A. L.; Matsuda, R.; Tao, J.; Hayami, S. *Acc. Chem. Res.* **2007**, *40*, 361-369.

[23] Jung, O. S.; Jo, D. H.; Lee, Y. A.; Conklin, B. J.; Pierpont, C. G. *Inorg. Chem.* **1997**, *36*, 19-24.

[24] Dei, A.; Feis, A.; Poneti, G.; Sorace, L. *Inorg. Chim. Acta* **2008**, *361*, 3842-3846.

[25] Jung, O. S.; Pierpont, C. G. *Inorg. Chem.* **1994**, *33*, 2227-2235.

[26] Caneschi, A.; Dei, A.; De Biani, F. F.; Gutlich, P.; Ksenofontov, V.; Levchenko, G.; Hoefer, A.; Renz, F. *Chem., Eur. J.* **2001**, *7*, 3926-3930.

[27] Li, B.; Tao, J.; Sun, H. L.; Sato, O.; Huang, R. B.; Zheng, L. S. *Chem. Commun.* **2008**, 2269-2271.

[28] Roux, C.; Adams, D. M.; Itie, J. P.; Polian, A.; Hendrickson, D. N.; Verdaguer, M. *Inorg. Chem.* **1996**, *35*, 2846-2852.

[29] Neuwahl, F. V. R.; Righini, R.; Dei, A. *Chem. Phys. Lett.* **2002**, *352*, 408-414.

[30] Beni, A.; Dei, A.; Rizzitano, M.; Sorace, L. *Chem. Commun.* **2007**, 2160-2162.

[31] Beni, A.; Carbonera, C.; Dei, A.; Letard, J. F.; Righini, R.; Sangregorio, C.; Sorace, L. *J. Braz. Chem. Soc.* **2006**, *17*, 1522-1533.

[32] Carbonera, C.; Dei, A.; Letard, J. F.; Sangregorio, C.; Sorace, L. *Angew. Chem. Int. Ed.* **2004**, *43*, 3136-3138.

[33] Sato, O.; Hayami, S.; Gu, Z. Z.; Takahashi, K.; Nakajima, R.; Fujishima, A. *Chem. Phys. Lett.* **2002**, *355*, 169-174.

[34] Sato, O.; Hayami, S.; Gu, Z. Z.; Seki, K.; Nakajima, R.; Fujishima, A. *Chem. Lett.* **2001**, 874-875.

[35] Markevtsev I. N. ; Monakhov M. P. ; Platonov V. V.; Mischenko A. S.; Zvezdin A. K. ; Bubnov M. P. ; Abakumov G. A.; Cherkasov V. K. *J. Magn. Magn. Mater.* **2006**, *300*, 407-410.

[36] Carlin, R. D. L. *Magnetochemistry*; Springer-Verlag: Berlin, 1986.

[37] Bencini, A.; Carbonera, C.; Dei, A.; Vaz, M. G. F. *Dalton Trans.* **2003**, 1701-1706.

[38] Benelli, C.; Dei, A.; Gatteschi, D.; Güdel, H. U.; Pardi, L. *Inorg. Chem.* **1989**, *28*, 3089-3091.

[39] Kessel, S. L.; Emberson, R. M.; Debrunner, P. G.; Hendrickson, D. N. *Inorg. Chem.* **1980**, *19*, 1170-1178.

[40] Tuchagues, P. M.; Hendrickson, D. N. *Inorg. Chem.* **1983**, *22*, 2545-2552.

[41] Kahn, O. *Molecular Magnetism*; VCH: Weinheim, 1993.

[42] Bencini, A.; Beni, A.; Costantino, F.; Dei, A.; Gatteschi, D.; Sorace, L. *Dalton Trans.* **2006**, 722-729.

[43] Beni, A.; Dei, A.; Laschi, S.; Rizzitano, M.; Sorace, L. *Chem., Eur. J.* **2008**, *14*, 1804-1813.

[44] Benelli, C.; Dei, A.; Gatteschi, D.; Pardi, L. *Inorg. Chim. Acta* **1989**, *163*, 99.

[45] Buhks, E. ; Bixon, M.; Jortner, J. *J. Phys. Chem.* **1981**, *85* , 3763.

[46] Slichter, C. P.; Drickamer, H. G. *J. Chem. Phys.* **1972**, *56*, 2142-2160.

[47] Cui, A.; Takahashi, K.; Fujishima, A.; Sato, O. *J. Photochem. Photobiol., A* **2004**, *167*, 69-73.

[48] Evangelio, E.; Rodriguez-Blanco, C.; Coppel, Y.; Hendrickson, D. N.; Sutter, J. P.; Campo, J.; Ruiz-Molina, D. *Solid State Sci.* **2009**, *11*, 793-800.

[49] Cador, O.; Dei, A.; Sangregorio, C. *Chem. Commun.* **2004**, 652-653.

[50] Adams, D. M.; Hendrickson, D. N. *J. Am. Chem. Soc.* **1996**, *118*, 11515.

[51] Carbonera, Chiara *PhD Thesis* .

[52] Sato, O.; Iyoda, A.; Fujishima, K.; Hashimoto, K. *Science* **1996**, *272*, 704-705.

[53] Gentili, P. L.; Bussotti, L.; Righini, R.; Beni, A.; Bogani, L.; Dei, A. *Chem. Phys.* **2005**, *314*, 9-17.

[54] Adams, D. M.; Hendrickson, D. N. *J. Am. Chem. Soc.* **1996**, *118*, 11515-11528.

[55] Hauser, A. *Light-Induced Spin Crossover and the High-Spin -> Low-Spin Relaxation* in *Spin Crossover in Transition Metal Compounds II*; Gütlich, P.; Goodwin, H. A., Springer: Berlin, 2004; Vol. 234, pp 155-198.

[56] Jeftic, J.; Hauser, A. *Chem. Phys. Lett.* **1996**, *248*, 458-463.

[57] Marcus, R. A. *Angew. Chem., Int. Ed. Engl.* **1993**, *32*, 1111-1121.

[58] Spiering, H. *Elastic Interaction in Spin Crossover Compounds* in *Spin Crossover in Transition Metal Compounds III*; Gütlich, P.; Goodwin, H. A., Springer: Berlin, 2004; Vol. 235, pp 171-195.

[59] Gatteschi, D.; Sessoli, R.; Villain, J. *Molecular Nanomagnets*; Oxford University Press: Oxford, UK, 2006.

[60] Letard, J. F.; Capes, L.; Chastanet, G.; Moliner, N.; Letard, S.; Real, J. A.; Kahn, O. *Chem. Phys. Lett.* **1999**, *313*, 115-120.

[61] Letard, J. F. *J. Mater. Chem.* **2006**, *16*, 2550-2559.

Chapter II

Thermodynamics of the valence tautomeric equilibrium in 1:1 Co:dioxolene systems

This chapter is devoted to the evaluation of the thermodynamic parameters governing the VT equilibrium of cobalt – ortho-dioxolene complexes with 1 : 1 stoichiometry. The quantitative addressing of the factors controlling the relative stability of the two redox isomers has in fact several consequences on their chemical and physical behaviour. First, they give information about the energies involved in the VT process, thus providing hints for its real mechanisms. On the other hand a controlled shift of the energy of one redox species with respect to the other can lead to the stabilisation of different charge configurations and thus to the development of new bistable VT systems. For these reasons we provide hereafter a description of the charge distributions in function of the dielectric properties of different solvents and the temperature for a compound belonging to the simplest class of systems featuring electronic bistability, the 1:1 Co : o-dioxolene complexes.

2.1 Thermodynamic approach for the development of new Co-dioxolene valence tautomers

One of the aim of this thesis work has dealt with the synthesis of new redox bistable molecular materials. The task is not trivial, since very often the charge distribution in a molecular framework is very well defined and can't be switched in the energy ranges assuring the chemical stability of the systems. To shed light on the physical properties an inorganic synthon should posses in order to afford bistable molecular materials a three points recipe has been shown in Paragraph 1.1. The thermodynamic approach we are presenting in this chapter is a straightforward consequence of those three rules.

The underlying idea is to control the energy differences between the states shown in Eq. 2.1 with a rational chemical tuning of the Gibbs free energies of the reactants.

$$ls - Co^{III}(L) - Cat \rightleftarrows hs - Co^{II}(L) - SQ \qquad (2.1)$$

In Eq. 2.1 is shown a VT equilibrium for the 1:1 Co:dioxolene class of complexes.[1] In this case the active building blocks sharing one electron are the Co ion and an organic ligand. The ligand L is an ancillary ligand completing the first coordination sphere of the transition metal ion. In Figure 2.1.1 is shown a schematic picture of the free energies of the redox isomers taking part to the VT process in Eq. 2.1.

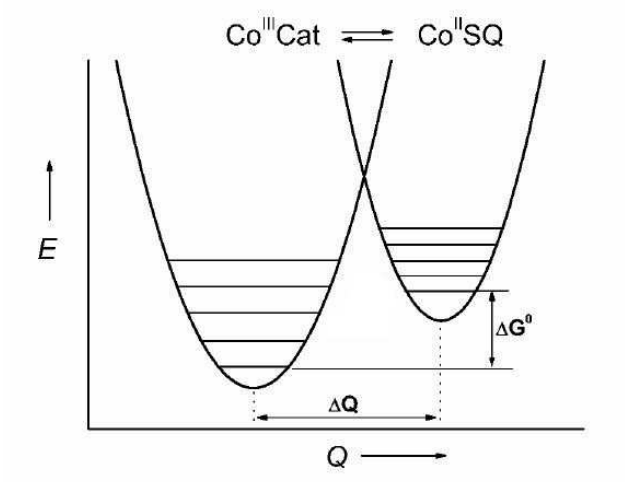

Figure 2.1: Potential-energy wells for the VT interconversion process shown in Eq. 2.1.

In order to tune the electronic properties of the resulting Co(L)diox adduct it is possible to act on each of the building blocks of the system. Appropriate choices of the structural and electronic features of the building blocks will provide chemically driven modifications in the sign and in the absolute value of the ΔG^0 energy difference (pictorially shown in Fig. 2.1) In this way rational modifications of the VT equilibrium can be obtained, according to Eq. 1.7.
The link between the thermodynamics of the isolated bricks of the system can be understood looking at Figure 2.2.

Figure 2.2 is a more general schematisation of the simple VT equilibrium, involving an intramolecular electron transfer process, and points out the three redox processes involved in the thermodynamic cycle related to the Valence Tautomeric equilibrium of a general M-L monocationic system.

1. Metal centred oxidation.
2. Ligand centred oxidation.
3. Valence Tautomeric equilibrium.

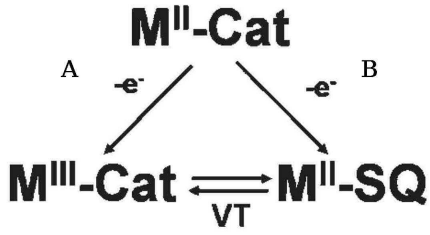

Figure 2.2: Thermodynamic cycle of the states arising from monoelectronic oxidation of the M-L system.

Since the overall energy variation in a thermodynamical cycle is zero, Figure 2.2 affords a direct connection between the Gibbs free energies of electron transfer (*i.e.* the redox potentials, named $\Delta G_{M^+ \to M}$ and $\Delta G_{L^+ \to L}$) and the one involved in the VT equilibrium (ΔG_{VT}) That can be mathematically expressed as

$$\Delta G_{VT} = \Delta G_{M^+ \to M} - \Delta G_{L^+ \to L} \tag{2.2}$$

The control over the parameters on the right side of Eq. 2.2 affords the tuning of the VT behaviour. This tuning arises from a very delicate balance of the redox potentials of the metal and the dioxolene ligand moieties, which can be expressed according to an equilibrium population of the electronic states

$$K_{VT} = \frac{[hsCo^{II} - SQ]}{[lsCo^{III} - Cat]} = e^{-\frac{\Delta G_{VT}}{k_B T}} \quad (2.3)$$

The main advantage of this method relies in the fact that it allows to estimate the charge distribution in a Co(diox) adduct just by measuring the difference in the redox potentials of its electronic active moieties. It must be stressed that the experimental evaluation of both metal and ligand centred redox processes cannot be directly taken out with a single measure, since only the one of the two reactions will occur in the system under the applied voltage. This drawback can actually be overcome considering the low degree of covalence of the Co-diox bonds, providing a complex featuring molecular moieties which are redox independent one from the other, thus allowing the measure of the "hidden" redox potential by analysis of structurally related systems.

In order to describe the rational tuning of the VT properties provided by this thermodynamic approach we will skip the analysis of network and polymeric structures of Co based VT systems.[2,3] In this compounds, in fact, the vibrational coupling with the crystalline environment may have consequences unexpected on the basis of our above mentioned strategy. Thus, for neglecting electronic delocalisation as well as intermolecular cooperativity on determining the properties of the systems we will focus our attention on the simplest class of these materials, the zero-dimensional mononuclear one, which can be considered as a testing ground for the evaluation of the thermodynamic approach exposed. In the next paragraphs we will review the tuning of the $\Delta G_{M^+ \rightarrow M}$ through an appropriate choice of the ancillary ligand and of the $\Delta G_{L^+ \rightarrow L}$ through the use of different substituents on the dioxolene ring and their consequences on the VT properties of Co:dioxolene systems.

2.1.1 The role of the organic *o*-dioxolene ligand

Ortho-Dioxolene ligands are appealing synthons to build supramolecular architectures using the metal-radical approach. They afford stable radicalic oxidation states, are chemically versatile and their redox properties can be tuned acting on their structure, in particular on the substituents on their benzene ring.[4,5] However, the experimental determination of the redox potential related to the ligand monoreduction process, SQ → Cat (Equilibrium B in Fig. 2.2) is not always possible to be carried out. In fact, between the two A and B processes, only the one characterised by a lower energy will take place in solution. To overcome this complication, we can estimate the redox potential of the SQ → Cat reduction process analysing properly chosen metal-dioxolene complexes in which process A is not taking place. This approximation relies on the fact that the redox properties of these bidentate ligands do not vary changing the molecular framework they are involved in, while they will depend only on their ionic charge density. According to this approximation, a metal ion bound to a

dioxolene is thus considered to exert an applied and constant electric bias on the orbital energies of the latter, thus simply shifting the energies of its electronic levels.[1]

A successful example of these features can be seen in the *a priori* determination of the charge distribution in a two structurally related [Co(CTH)diox]·PF_6 molecules, the diox ligands to be chosen between the 3,5-DBdiox and the TCdiox. The redox properties of the building blocks of the system are shown in Table 2.1.[6]

	[Co(CTH)]$^{3+}$	3,5-DBSQ	TCSQ
E^0_{red} [a,b]	-0.69	-0.6	0.0
$E^0_{red}(Co) - E^0_{red}(diox)$ [a]		-0.09	-0.69

[a] The reported vales are in V. [b] values are referred to the Standard Calomelane Electrod.

Table 2.1: Reduction potentials of the building block of the [Co(CTH)diox]·PF_6 system, measured by cyclic voltammetry in acetonitrile solution.[6]

Table 2.1 points out the differences in the reduction potentials of the different building blocks of the molecular system. In particular was found that the introduction of electron-withdrawing groups on the dioxolene ring increase the redox potential of the monoelectronic reduction process SQ → Cat. So, in the case of the TCdiox dioxolene ligand, the variation of the Free Gibbs Energy of the reaction can be calculated to be -0.69 eV. Putting this value into Eq. 2.3 it is possible to see that the resulting molecular adduct will stay in the *ls*-Co^{III} – Cat state in all the range of temperatures.

The replacement of the chlorines with two *tert*-buthyl groups lowers the reduction potential of the dioxolene moiety, and the ΔG_{VT} as well, now being -0.09 eV. This value is comparable to the thermal energy at room temperature, and so the [Co(CTH)3,5-DBdiox]·PF_6 molecule is able to exhibit VT.

The validity of this approach allowed as well to investigate the energies of the ligand-to-metal charge transfer (LMCT) transitions in some Fe^{III}– Cat complexes.[7]

2.1.2 The role of the ancillary ligand

The redox properties of the Co centre can be modulated acting on its ancillary ligand, tuning its electronic and structural features.[6,8] Hereafter we provide the description of two different strategies in the framework of the metal-radical approach.

2.1.2.1 Chemical tuning of the electronic features of the ancillary ligand

The founding idea of this method can be understood considering the symmetry of the frontier molecular orbitals of a general Co:dioxolene system, reported in Figure 1.5. As can be seen, the t_{2g} metal orbitals are non bonding and have a π symmetry. As widely known, these orbitals can interact with a ligand centred empty π^* orbital, thus stabilising the bonding energy of the complex with a mechanism of back donation of electrons.[9] Tuning the energy of the π^* orbital of the ancillary ligand is possible to decrease the energy difference with the lower lying t_{2g} set. In this way the 10Dq energy separation of the metal ion frontier orbitals can be tuned, thus influencing the temperature of the spin crossover process following the electron transfer involved in VT. It must be noted that this ligand induced energy lowering is enough to increase the energy separation among the t_{2g} and the e_g orbitals, while keeping the spin crossover features of a valence tautomeric system still available. With this approach it has been possible to shift the $T_{½}$ of a series of $Co(N\text{-}N)(diox)_2$ structurally related complexes from 300 K up to 190 K.[10,11]

2.1.2.2 Chemical tuning of the structural features of the ancillary ligand

In this case the charge distribution of a Co:dioxolene adduct is tuned thanks to steric means. It is in fact very well known that VT interconversion involves isomers with very different structural features, and an overall increase of the molecular volume is found passing from the low temperature *ls*-Co^{III} – Cat species to the *hs*-Co^{II} – SQ one, whose antibonding e_g based molecular orbitals have been populated by the electron transfer and the spin crossover of the Co ion. As a natural consequence of the Le Chatelier principle, the system with higher steric hindrance will spontaneously favour the small isomer. It must be stressed that this physical effect is reflected, as usual, in the redox potentials of the molecular building blocks and can thus be evaluated by means of simple cyclic voltammetry.

An example of this strategy for the *a priori* determination of the charge distribution in VT systems. In fact the steric hindrance induced by the successive introduction of methyl groups into 6-position of pyridine moieties of the ancillary ligand tpa (tris(2-pyridylmethyl)amine) was indeed found to modulate the redox properties of the metal acceptor in a series of cobalt complexes of general formula $Co(Me_ntpa)(diox)PF_6$ (n = 0,1,2,3).[12,13] On its turn, this determines the charge distribution of the metal-dioxolene moiety in function of temperature. In particular the zero and monomethylated derivatives are present in the 5-300 K temperature range in the *ls*-Co^{III} – Cat charge distribution where the *hs*-Co^{II} – Cat redox isomer can be stabilised using the threefold methyl-substituted tpa ligand. The Me_2tpa ligand containing species, on the other side, shows an entropy driven VT process.

2.2 The [Co(Me$_3$TPA)TCdiox]PF$_6$ system

From the two above mentioned ways to shift the ΔG_{VT} value is possible to see the opposite effect of the ancillary Me$_3$tpa ligand and the TCdiox one in determining the electronic ground state of Co:dioxolene systems. The Co(Me$_3$tpa)(TCCat)PF$_6$ complex in acetonitrile solution featured a quasi reversible one electron redox process at – 0.4 V *vs* ferrocenium/ferrocene couple.[12] Compared to the redox potential of the SQ → Cat reduction of the dioxolene ligand[14] it has been possible to determine for the Co(Me$_3$tpa)TCdiox·PF$_6$ molecule the ΔG_{VT} of 17(1) kJ mol^{-1} in acetonitrile, compatible with an entropy driven VT in the room temperature range.
For these reasons we investigated the entropy driven VT in the solid state and in solutions for the Co(Me$_3$tpa)TCdiox·PF$_6$ complex.[†]

2.2.1 Crystallographic analysis

The general features of the molecular structure of [Co(Me$_3$TPA)TCdiox]PF$_6$, obtained by refinement of X-ray crystallographic data, are in agreement with previously reported 1:1 Co:dioxolene adducts with tpa derivatives as ancillary ligands.[12] The moiety Co(Me$_3$TPA)(TCCat), of which a Diamond view is shown in Figure 2.3, is monopositively charged, the electric neutrality of the crystal being assured by one PF$_6$ unit.

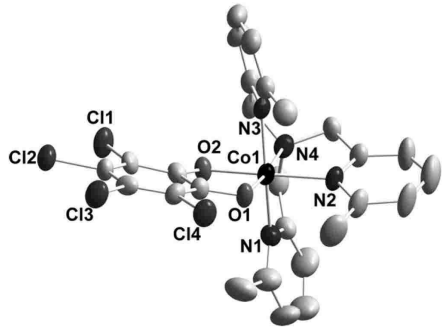

Figure 2.3: Diamond view of the cationic moiety of [Co(Me$_3$TPA)TCdiox]PF$_6$. Hydrogen atoms are omitted for clarity sake.

[†] Me$_3$tpa ligand was prepared by using a general one step procedure, according to that recently reported for tpa[12]. The complex Co(Me$_3$tpa)(TCCat) was obtained by mixing equimolar amounts of cobalt(II) chloride, Me$_3$tpa ligand and tetrachlorocatechol in methanol in the presence of triethylamine. The yellow compound was filtered, dried in oven at 50° C and then suspended in acetone. Upon addition of a stoichiometric amount of silver nitrate in the minimum quantity of water, a brown solution was obtained. The addition of an aqueous solution of potassium hexafluorophosphate yielded [Co(Me$_3$tpa)(TCCat)]PF6, as grey-brown powder, which was filtered and then recrystallised from acetone/diethyl ether or dichloromethane/hexane. Crystals suitable for X-ray analysis were obtained from a ethanol solution using dichloromethane as precipitating agent.

The cobalt ion is six-coordinated in a *cis*-distorted pseudo-octahedral coordination and the tripodal ligand Me_3TPA adopts a folded conformation around the metal ion, with the dioxolene ligand acting as bidentate. The values of the metal-donor bond lengths strongly indicates that at room temperature K the molecule is in the Co^{III}-Cat charge distribution. Indeed, Co-N bond distances vary between 1.95 and 2.01 Å, whereas Co-O ones amount to 1.88 and 1.89 Å. This result is confirmed by the analysis of the C1-C2 (1.41 Å) and C-O (1.31 Å) bond lengths of the dioxolene ligand, which give strong indication of the system being in the catecholato form. We provide the structural and refinement information about this system in Table 2.2.

Empirical formula	$Co(C_6O_2Cl_4)(C_{21}N_4H_{24})(PF_6)\cdot CH_2Cl_2$
Formula weight	867.13
Temperature	295(2) K
Wavelength	0.71069 Å
Crystal system	Monoclinic
Space group	C 2/c
Unit cell dimensions	a = 25.621(4) Å α= 90°.
	b = 17.765(4) Å β= 114.694(11)°.
	c = 17.773(3) Å γ = 90°.
Volume	7350(2) $Å^3$
Z	8
Density (calculated)	1.567 Mg/m^3
Absorption coefficient	1.01 mm^{-1}
F(000)	3488
Crystal size	0.44 x 0.41 x 0.05 mm^3
θ range for data collection	3.77 to 28.9°.
Index ranges	$-32\leq h\leq 33$, $-22\leq k\leq 23$, $-23\leq l\leq 23$
Reflections collected	25561
Independent reflections	8347 [R(int) = 0.0401]
Completeness to θ = 25°	99.2 %
Absorption correction	Semi-empirical from equivalents
Max. and min. transmission	0.951 and 0.615
Refinement method	Full-matrix least-squares on F^2
Data / restraints / parameters	8347 / 0 / 436
Goodness-of-fit on F^2	1.039

Table 2.1. Crystal data and structure refinement for $[Co(Me_3TPA)TCdiox]PF_6$.

2.2.2 Solid state conversion features

The VT interconversion may be followed using magnetometric means, since the change of the orbital population of the frontier orbitals belonging to the different isomers leads to very different magnetic properties of the two species.
The temperature dependence of $\chi_M T$ product is shown in Figure 2.4.

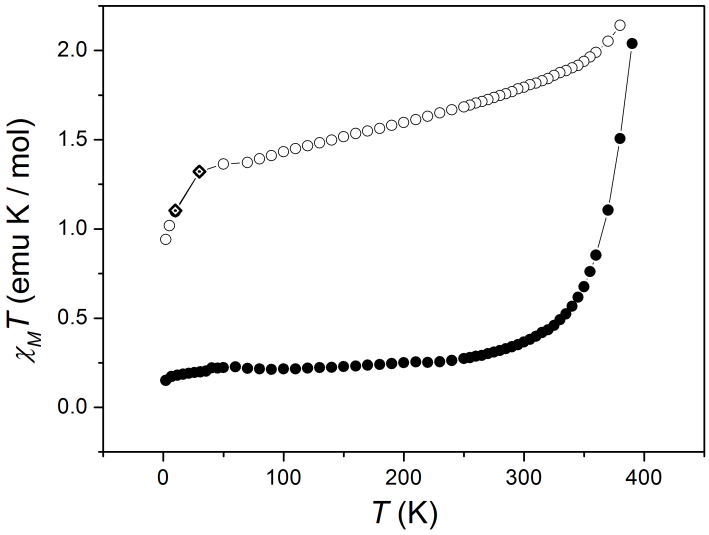

Figure 2.4: Temperature dependence of $\chi_M T$ product of $Co(Me_3tpa)(TCCat)PF_6$ in the 2-300 K temperature range and 1 T applied magnetic field. First heating branch: full circles; cooling branch: empty circles; second heating branch: empty lozenges. Lines are guides to the eye.

In agreement with the diamagnetic electronic configuration of the *ls*-Co^{III} – Cat species, the $\chi_M T$ value in the 5 – 275 K range is 0.25 emuK mol^{-1}, the contribution being due to the TIP of the Co^{III} ion and to a unavoidable presence of a *hs*-Co^{II} – Cat unreacted fraction (estimated to be less than the 5% in comparison with a reference compound, stable in the *hs*-Co^{II} – SQ state for all temperatures).

However, warming the system above 280 K an increase of the $\chi_M T$ product occurs. This behaviour is typical for thermally induced valence tautomeric interconversion, which leads to the progressive formation of Co^{II}-SQ species. The *hs*-Co^{II} – SQ state features values of the $\chi_M T$ product ranging from 2.6 to 3.1 emu $Kmol^{-1}$, due to the presence of the uncoupled *hs*-Co^{II} ion and the radical semiquinonate ligand. From these data we can estimate the transition temperature of the entropy driven VT transition in the solid state for this system, defined as the temperature at which the two species are present in equimolar amount should be around 390 K. However, on increasing temperature above 360 K a very steep increase in $\chi_M T$ is observed which we

attribute to thermally induced polymerization of the sample. Since repeated temperature cycles revealed a non thermal reproducibility of the $\chi_M T$ values, we attributed the high temperature phenomenon as result of the formation of 2,3-hexachloro-oxanthrenequinone, a product of the nucleophilic reaction between two dioxolene ligands, often observed like condensation product,[15] with subsequent sample degradation.

2.2.3 Solvent dependence of the charge distribution

As stated above, previous studies on *3d* metal complexes formed by the tetrachlorodioxolene in both catecholato or semiquinonato oxidation states have shown that these compounds are unstable in solution.[15 37] In particular, these reactions are slow at room temperature, but cannot be neglected at higher temperatures. This precludes the possibility of carrying out temperature dependent spectroscopic studies in a temperature range above 300 K.

For this reason we performed a study of the charge distribution of a 1:1 Co:dioxolene complex in function of the dielectric properties of a series of four solvents.

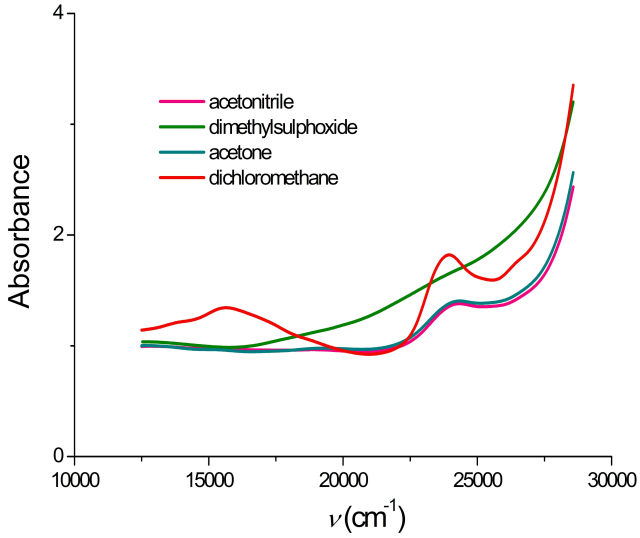

Figure 2.5: Electronic spectra of $Co^{III}(Me_3tpa)(TCCat)PF_6$ in different solvents at room temperature.

Figure 2.5 shows the electronic spectra of the system in four different solvents at RT. The solvent with higher dielectric constant chosen is the dimethylsulphoxide (green line). Its solution spectrum consists in two weak bands occurring in the near infrared and violet regions of the spectrum were reasonably assigned to the symmetry

forbidden LMCT transitions involving both the π*(HOMO) and the highest energy π molecular orbitals of the ligand, respectively, and the empty e_g (σ* in character) orbital of the metal ion.[31] The band at 19200 cm^{-1} is assigned to the internal *d-d* transition ($^1A_1 \rightarrow {}^1T_1$ in O_h symmetry), typical of the cobalt(III) six-coordinate chromophores.[16] The second expected *d-d* transition, $^1A_1 \rightarrow {}^1T_2$ in O_h, cannot be clearly detected being obscured by the LMCT transition in the violet region. The analysis revealed a Co^{III}-Cat charge distribution at RT, in agreement with its higly polar character, able to effectively stabilise the electronic configuration with higher electric dipole moment. Lowering the polarity of the solvent we found that acetonitrile and acetone show similar features.

On further increasing of the apolar character of the medium the electronic spectrum changes. In fact a dichloromethane solution of $[Co(Me_3TPA)TCdiox]PF_6$ shows absorption bands occurring 13750 and 23900 cm^{-1} that can be attributed, as discussed in paragraph 1.2, to ligand's internal transitions.[17] Therefore the other bands we observe are presumably charge transfer in origin, since *d-d* transitions in pseudo-octahedral cobalt(II) chromophores are very weak. The transitions occurring at 15600 and 17300 cm^{-1} are assigned to MLCT transitions in agreement with the higher oxidizing power of the TCSQ anion with respect to the DBSQ one.[8,12] The bands associated to these transitions are broad and relatively weak (ε about 950 $M^{-1}cm^{-1}$). We suggest that these transitions might involve an electron transfer between the *d* metal orbital and the π* SOMO of the TCSQ ligand. The more intense transition occurring in the violet region of the spectrum are more difficult to assign because of the overlap with the internal transition of the ligand.

The different charge distribution observed in low donor solvents with respect to that observed in high donor ones is obviously due to different solvation free energy changes associated to the equilibrium

$$Co^{III}(Me_3tpa)(TCCat)^+ \rightarrow Co^{II}(Me_3tpa)(TCSQ)^+ \qquad (2.4)$$

in the different solvents. Temperature dependent cyclic voltammetry experiments suggested that similar equilibria are controlled by the enthalpy changes, the high donor solvents stabilising the Co^{III}-Cat species with respect to the Co^{II}-SQ one. As a comparison, for the $Fe(CTH)(diox)^+$ chromophore the contribution due to the different solvation enthalpies between 1,2-dicloroethane and acetonitrile was calculated of the order of 5 kJ mol^{-1}.[7] The solvation entropy changes did not seem to substantially affect the equilibrium (< 1 kJ mol^{-1} at room temperature).

2.4 Evaluation of the thermodynamic parameters of the entropy VT process in solution

Since the spectral features of the dichloromethane solution of $Co(Me_3tpa)(TCCat)PF_6$ are consistent with a mixture of the two redox isomers, being the high temperature stable one in strong excess, we carried on a temperature

investigation of the electronic spectra. It must be reminded that temperatures higher than 300 K cannot be studied for this system, since they are know to induce a degradation of the sample trough a polymerisation.
However temperature dependent electronic spectra in dichloromethane carried out in the 200 – 300 K range showed the existence of spectral changes consistent with the existence of VT entropy driven equilibrium as shown in Figure 2.6. The reversible character of an equilibrium involving two species is further supported by the presence of two isosbestic points.

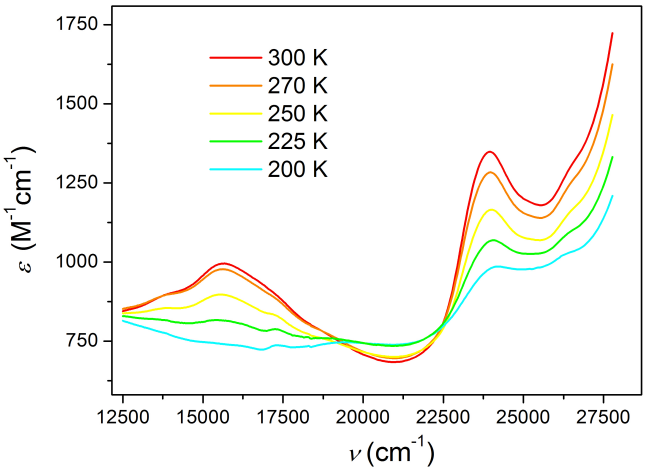

Figure 2.6: Temperature dependence of the UV–Vis absorption spectra of a dichloromethane solution of Co(Me$_3$tpa)(TCCat)PF$_6$ in the 200–300 K range.

It is possible to use the intensity of peak occurring at 23900 cm^{-1} to investigate the temperature dependence of the VT process and quantitavely estimate its thermodynamic parameters, yielding the points presented in Figure 2.7.

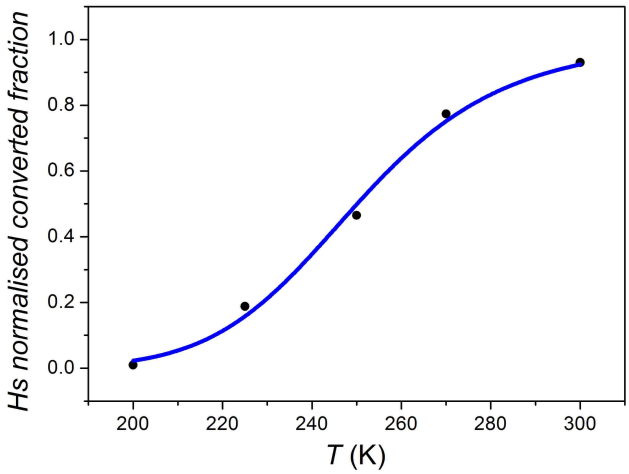

Figure 2.7: variation of the fraction of Co^{II}-SQ species as a function of temperature, obtained by the intensity of the 23900 cm^{-1} peak and corresponding best-fit curve, according to the model described in the text.

The observed spectral data were fitted using the regular solution model described in paragraph 1.3,[18] taking into account that in the temperature range investigated just an incomplete conversion occurs (at 200 K we have 1 % of high spin Co(II) species, while at 300 K 7 % of Co(III) form is present), according to Eq. 2.5.

$$[hs\text{-}Co^{II}\text{–SQ}] = \frac{1}{e^{\left(-\frac{\Delta H}{RT}+\frac{\Delta S}{R}\right)}+1} \qquad (2.5)$$

The thermodynamic quantities calculated were ΔH = 31.2 kJ mol^{-1} and ΔS = 125 J $K^{-1}mol^{-1}$ (R^2 = 0.99), in agreement with the entropy driven character of equilibrium of Eq. 2.2. Since the expected electronic contribution to the entropy change between the two redox isomers is calculated, according to the Boltzmann statistical definition of entropy, to be of the order of 10 - 15 J $(Kmol)^{-1}$, the high value of the entropy change should be attributed to the change in the vibrational entropy contributions characterising the two redox isomers. The here reported data are the first ones concerned with this dioxolene ligand and, what it is more important, with the most simple system undergoing valence tautomeric interconversion, and substantially agree with previously reported investigation for $Co(L)(diox)_2$ systems.[19-25]

The presence of two isosbestic points in the spectra reveals, in agreement with other cobalt systems undergoing valence tautomeric equilibria, no evidence of the formation of a low-spin Co^{II}-semiquinonato species, although subpicosecond transient absorption spectroscopy studies evidence the existence of a further species in the relaxation process of optically induced metastable state.[26]

References

[1] Bencini, A.; Caneschi, A.; Carbonera, C.; Dei, A.; Gatteschi, D.; Righini, R.; Sangregorio, C.; Van Slageren, J. *J. Mol. Struct.* **2003**, *656*, 141-154.

[2] Bodnar, S. H.; Caneschi, A.; Dei, A.; Shultz, D. A.; Sorace, L. *Chem. Commun.* **2001**, 2150-2151.

[3] Jung, O. S.; Pierpont, C. G. *J. Am. Chem. Soc.* **1994**, *116*, 2229-2230.

[4] Pierpont, C. G. *Coord. Chem. Rev.* **2001**, *219*, 415-433.

[5] Dei, A.; Gatteschi, D.; Sangregorio, C.; Sorace, L. *Acc. Chem. Res.* **2004**, *37*, 827-835.

[6] Benelli, C.; Dei, A.; Gatteschi, D.; Pardi, L. *Inorg. Chim. Acta* **1989**, *163*, 99.

[7] Dei, A. *Inorg. Chem.* **1993**, *32*, 5730-5733.

[8] Caneschi, A.; Dei, A.; Gatteschi, D.; Tangoulis, V. *Inorg. Chem.* **2002**, *41*, 3508-3512.

[9] Albright, T. A.; Burdett, J. K.; Whangbo, M.-H. *Orbital Interactions in Chemistry;* Wiley & sons: New York, 1985.

[10] Adams, D. M.; Dei, A.; Rheingold, A. L.; Hendrickson, D. N. *Angew. Chem., Int. Ed. Engl.* **1993**, *32*, 880-882.

[11] Adams, D. M.; Dei, A.; Rheingold, A. L.; Hendrickson, D. N. *J. Am. Chem. Soc.* **1993**, *115*, 8221-8229.

[12] Beni, A.; Dei, A.; Laschi, S.; Rizzitano, M.; Sorace, L. *Chem., Eur. J.* **2008**, *14*, 1804-1813.

[13] Nagao, H.; Komeda, N.; Mukaida, M.; Suzuki, M.; Tanaka, K. *Inorg. Chem.* **1996**, *35*, 6809-6815.

[14] Dei, A. *Inorg. Chem.* **1993**, *32*, 5730-5733.

[15] Kessel, S. L.; Emberson, R. M.; Debrunner, P. G.; Hendrickson, D. N. *Inorg. Chem.* **1980**, *19*, 1170-1178.

[16] Lever, A. B. P.; Solomon, E. I. *Ligand Field Theory and the Properties of Transition Metal Complexes* in *Inorganic Electronic Structure and Spectroscopy, Vol. I*; Lever, A. B. P.; Solomon, E. I., Eds.; Wiley Interscience: New York, 1999; pp 1-91.

[17] Benelli, C.; Dei, A.; Gatteschi, D.; Güdel, H. U.; Pardi, L. *Inorg. Chem.* **1989**, *28*, 3089.

[18] Slichter, C. P.; Drickamer, H. G. *J. Chem. Phys.* **1972**, *56*, 2142-2160.

[19] Shultz, D. A. *Valence tautomerism in dioxolene complexes of cobalt* in *Magnetism: Molecules to Materials II*; Miller, J. S.; Drillon, M., Eds.; Wiley-VCH: Weinheim, 2001; pp 281-306.

[20] Adams, D. M.; Hendrickson, D. N. *J. Am. Chem. Soc.* **1996**, *118*, 11515-11528.

[21] Jung, O. S.; Pierpont, C. G. *Inorg. Chem.* **1994**, *33*, 2227-2235.

[22] Adams, D. M.; Dei, A.; Rheingold, A.; Hendrickson, D. N. *J. Am. Chem. Soc.* **1993**, *115*, 8221-8229.

[23] Pierpont, C. G.; Jung, O. S. *Inorg. Chem.* **1995**, *34*, 4281-4283.

[24] Caneschi, A.; Cornia, A.; Dei, A. *Inorg. Chem.* **1998** , *37*, 3419.

[25] Gentili, P. L.; Bussotti, L.; Righini, R.; Beni, A.; Bogani, L.; Dei, A. *Chem. Phys.* **2005**, *314*, 9-17.

[26] Neuwahl, F. V. R.; Righini, R.; Dei, A. *Chem. Phys. Lett.* **2002**, *352*, 408-414.

Chapter III

Crystal packing effects on the entropy and optically driven Valence Tautomerism

The thermodynamic approach for the development of new 1:1 Co:dioxolene based Valence Tautomeric materials shown in Chapter II provided a rational synthetic strategy for the synthesis of several bistable molecules. In the following we present the investigation of the crystal packing effects on the entropy driven and the optical induced valence tautomeric interconverison for one of these, the Co(Me_2TPA)DBdiox·PF_6 system. The replacement of the crystallisation solvent lead to an increase of the molecular volume in the solid state which strongly influenced the thermal profile of the valence tautomeric equilibrium and the yield of photoconversion at cryogenic temperatures, indicating the system as an ideal candidate for investigation of physical properties of the photoinduced states in confined environments. The analysis of the time evolution of the metastable state at different temperatures pointed out the unexpected failure of the quantum mechanical treatments used up to now by the bistable molecular materials community for the rationalisation of the connection between the stability of the thermal and optical induced hs-Co^{II} – SQ phase. These results have been corroborated by the investigation of another Co:dioxolene complex with 1:2 stoichiometry.

3.1 Crystal packing effects on the valence tautomerism in a 1:1 Co:dioxolene system

Co:dioxolene 1:1 materials are molecular systems quite easily to be handled both from a chemical point of view, due to their stability in the solid state, and from a physical one, being their physical properties able to be tuned not just acting on the electroactive moieties of the systems, but also on the molecular components not taking part directly into the electron transfer process. We already stressed in Chapter I the role of the ancillary ligand in determining the entropy driven conversion features. However, several other structural factors may be used to tune the physical behaviour of these systems, like the coordination solvent and the counter-anion (this option is unavailable for 1:2 Co:dioxolene complexes). Since the free energy of the ET process is known to strongly depend on the vibronic coupling with the environment,[1-4] we decided to investigate the dependence of the VT interconversion features on the crystal packing in the solid state, with the aim of controlling the conversion properties of VT materials. Hereafter we will show the results obtained for the tuning of the entropy and optically driven VT interconversion of two different Co:dioxolene systems.

3.1.1 The Co(Me_2TPA)DBdiox·PF_6 system

In Chapter II we presented the thermodynamic approach for the development of new Co-based bistable molecular materials, showing how this rational chemical strategy lead to the predetermination of the expected charge distribution of a series of cobalt-dioxolene complexes of formula [Co(Me_ntpa)(diox)](PF_6) with respect to the difference between the redox potentials of the metal acceptor and of the coordinated dioxolene ligand.[5, 6]

The most interesting complex of the [Co(Me_ntpa)(diox)](PF_6) family can be seen in the Co(Me_2TPA)DBdiox·PF_6 system (**1**·ethanol), whose molecular structure is reported in Figure 3.1.[†]

[†] The complex was obtained according to literature methods.[5] Methanol solutions containing cobalt(II) chloride and the ligand in 180 1:1 ratio were mixed with a solution of the appropriate catecholate and triethylamine (1:2.5 ratio) in the same solvent under inert atmosphere. The metal(II) - catecholato complexes were oxidised with atmospheric dioxygen and the resulting products were precipitated by adding an aqueous solution of KPF_6.

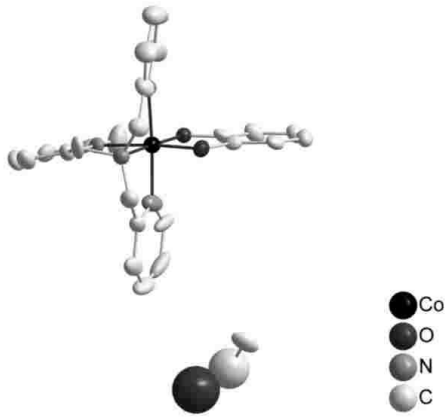

Figure 3.1. Molecular structure of the **1**·ethanol, showing the presence of the ethanol molecule of crystallisation, as adapted from 6. *Tert*-butyl groups have been omitted for clarity.

In this case, the energy difference involved in the VT equilibrium was found to be of the order of k_BT at room temperature, and thus the system showed an incipient VT entropy driven interconversion at about 300 K (*cfr.* Figure 3.3). We chose this system, deeply characterised in literature by means of cyclic voltammetry and magnetometry, as a solid starting point of our investigation of solid state's effects on the entropy and optically induced VT interconversion features.

Our approach for the modulation of the VT features by means of solid state techniques firstly foresaw a change of crystallisation solvent. The solvent chosen has been toluene, due to its higher sterical hindrance with respect to ethanol, suggesting huge effects on the vibrational coupling among tautomers in the crystal lattice.

3.1.2 Temperature dependent crystallographic analysis

Recrystallisation of **1**·ethanol from a toluene solution under reduced pressure yielded the compound **1**·toluene, whose structure, taken at 160 K, is presented in Figure 3.2.

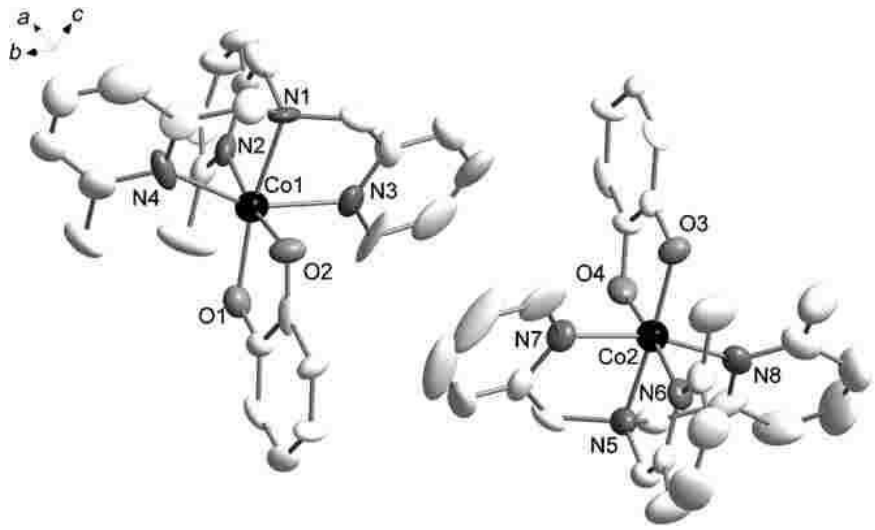

Figure 3.2. View of the two crystallographically independent cationic units of **1**·toluene. Selected bond lengths (in Å): Co1-O1 1.873(11), Co1-O2 1.898(12), Co2-O4 1.869(11), Co2-O3 1.880(11) at 100 K; Co1-O1 1.986(12), Co1-O2 2.037(12), Co2-O3 1.883(12), Co2-O4 1.884(12) at 160 K.

The first coordination sphere has the usual configuration reported for all the $[Co(L)diox]^+$ (where L is a tetradentate, N-donating, ligand) complexes reported to date:

- the Co ion is six-coordinate in a distorted octahedral first coordination sphere;
- the tetraazamacrocyle adopts a folded *cis*-configuration;
- the DBdiox ligand occupies the two remaining positions.

At this temperature the asymmetric unit of **1**·toluene consists of two different molecules, suggesting their inequivalence in the lattice. It must be stressed that a only a partial refinement of the data could be obtained. The reason for the poor refinement[7] should be ascribed to the occurrence of a third phase, most probably a fraction of the Co^{II}-SQ phase nucleating at low temperatures. This could explain the presence of intense *h0l* reflections which should be extinct due to the glide plane of the space group $P2_{1/c}$. A refinement in the lower symmetry group $P2_1$ did not lead to an improvement of the quality, in agreement with the E-statistics of SIR-97,[8] which clearly indicate that the structure is centrosymmetric. The probable presence of another phase is also suggested by different reflections, at the end of the refinement, featuring high F_o and low F_c. The presence of this phase can be due to the probable

formation of spin-like domains.[9] The solution of X-Ray structures at room temperature failed, due to the poor diffractive power of the crystals.

The temperature dependence of the bond lengths allowed a first determination of the charge distributions of the system in function of the temperature. This method of investigating the entropy driven VT process is strictly related to the Class II behaviour of these systems according to Robin and Day classification,[10] previously mentioned in paragraph 1.1. In particular, at 100 K the bond lengths characterising both cobalt ions indicate the same charge distribution (*ls*-Co^{III}-Cat), whereas at 160 K they agree with the two molecules being in two different charge distributions, Co^{II}-SQ (Co1) and Co^{III}-Cat (Co2) (see caption to figure 2).

An interesting structural modification induced by the replacement of an ethanol molecule with a toluene one is a substantial increase of the lattice volume per molecule. In the ethanolate case was found, at 150 K, a molecular volume of 474(9) Å^3 while, in the case of toluene solvate, an increase occur even at lower temperature (100 K), affording a 482(9) Å^3 value. As will be shown later on in the chapter, this change will strongly affect the VT conversion properties of **1**·toluene.

3.1.3 Magnetometric analysis

The VT interconversion in the solid state may be followed using magnetometric means, since the change of the orbital population of the frontier orbitals belonging to the different isomers leads to very different magnetic properties of the two species.

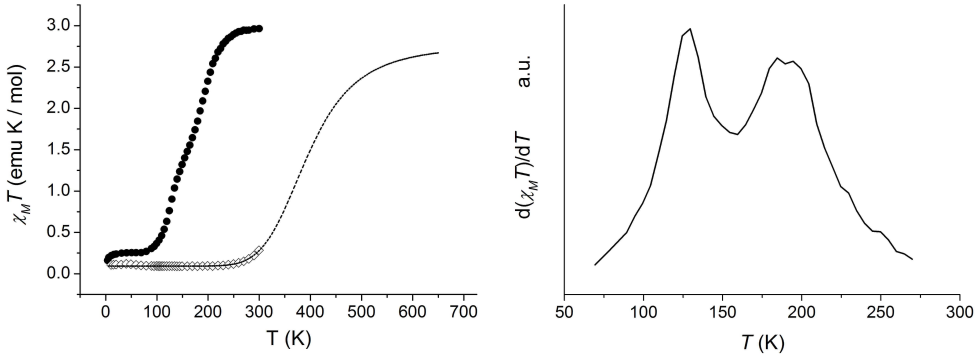

Figure 3.3. *Left:* Temperature dependence of the $\chi_M T$ product of **1**·toluene (full circles) and **1**·ethanol (empty squares, adapted from 6). The dotted line is a simulation of the transition profile of the ethanol solvate calculated with the equation 1.7 discussed in the text. *Right:* Temperature dependence of the first derivative of the $\chi_M T$

product of **1**·toluene against temperature, highlighting the double stepped transition profile.

The temperature dependence of the $\chi_M T$ product of **1**·toluene is shown in Figure 3.3. At low temperature the $\chi_M T$ value (0.25 emu K mol^{-1}) is consistent with a Co^{III}-Cat charge distribution, the residual paramagnetism being attributable to the TIP of Co^{III} and to an unavoidable presence of *hs*- Co^{II}. Around 100 K $\chi_M T$ value starts to rise, indicating the occurrence of a thermally induced valence tautomeric process which results, above 270 K, in Co^{II}-SQ charge distribution. The observed value ($\chi_M T$ = 2.96 emu K mol^{-1}) at 300 K is indeed in agreement with what expected for the sum of the two contribution of uncoupled Co^{II} (2.6 < $\chi_M T$ < 3.1 emu K mol^{-1}) and a radical species ($\chi_M T$ = 0.375 emu K mol^{-1}) as well as with previous reports.[11]

The plot highlights an intriguing and hitherto unreported feature for valence tautomeric interconversion processes: the transformation between the two redox isomers takes place in two separated steps, at 125 K and 185 K, respectively, with a plateau centred at 155 K, where 50% of conversion occurs, as discussed by means of crystallographic analysis in paragraph 3.2.1. The phenomenon is highlighted in the right panel of Fig. 3.3, where the two peaks in the first derivative of the $\chi_M T$ product *vs.* temperature are shown. The two-step character of the conversion is related to the above mentioned presence of two non-equivalent Co:dioxolene molecules in the crystal lattice, whereas the absence of thermal hysteresis for both steps indicates a low degree of cooperativity.

The main consequence of crystal packing changes following the replacement of the crystallisation solvent is the downward shift of the transition temperature of about 200 K with respect to the ethanol solvate, confirming the major role of the intermolecular interaction and crystal packing in determining the relative stability of the different charge distributions in valence tautomeric complexes.[5,6] As a rude comparison, the transition temperature of the ethanol solvate has been estimated fitting its $\chi_M T$ *vs* T plot according to a Regular Solution model, as developed by Slichter and Drickamer,[12] assuming a negligible cooperativity between interconverting centres in the solid state. The curve shown is the result of the fitting procedure based on Eq. 1.7, featuring a ΔH of 26.8 kcal mol^{-1} and a ΔS of 67.7 kcal K^{-1}mol^{-1}.

Co:dioxolene VT entropy driven transitions have shown previously to be strongly dependent on the vibrational coupling with the crystalline environments.[13,14] Even very subtle chemical substitutions may afford important properties changes, as found in the case of a tetraaza macrocyclic complex of cobalt with 1,10-phenantrenesemiquinonate ion, [Co(CTH)(Phendiox)]PF_6, where isotopic distribution in the crystallisation solvent lead to increased cooperativity along with a thermal hysteresis in the entropy driven transition profile.[3] Bearing these considerations in mind, we investigated by magnetometry the VT equilibrium for a sample of **1**·toluene

recrystallised from d_8-toluene. The comparison of the temperature dependence of the $\chi_M T$ product for both species is shown in Figure 3.4.

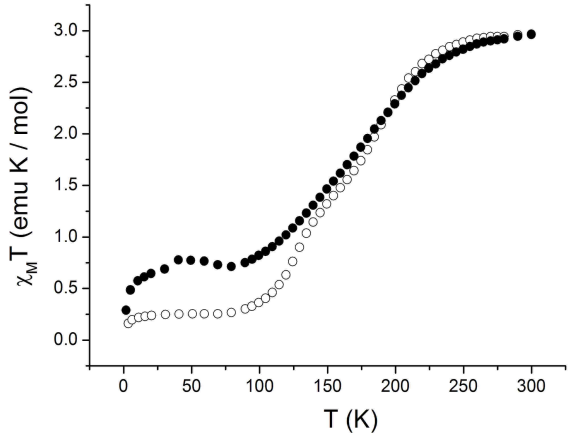

Figure 3.4. Comparison between the VT equilibria in the solid stated exhibited by the toluenate (empty circles) and the d_8-toluenate (full circles) solvates of **1**.

In the present case, however, no dependence is found on the isotopic replacement of the crystallisation solvent. The overall broadening of the transition profile may be safely due to a different degree of crystallisation of the sample. We attributed this finding to the lower cooperativity shown by **1**·toluene with respect to [Co(CTH)(Phendiox)]PF_6, as can be seen comparing the ΔT range for the entropy driven transition to complete.

3.1.4 Solid state effects on the photomagnetic properties

3.1.4.1 Optical induction of Valence Tautomerism

The effect of the lattice – softening effect induced by the toluene is also evident in the variation of the photomagnetic properties of the system. When irradiated at 904 nm and 9 K (power of ca. 1 mW/cm^{-2}), the system evolves to the metastable high spin state, according to the valence tautomeric interconversion, Co^{III}-Cat → Co^{II}-SQ. Taking as reference the 9 K $\chi_M T$ value of $[Co(Me_3tpa)DBSQ]^+$,[6] the steady state conversion has been estimated in 85 % of the total molar amount of cobalt after irradiation. Such a high percentage of conversion, compared to the one measured for the ethanol solvate,[5,6] may be attributed to the increase of the lattice volume per molecule (483 Å^3 at 100 K for **1**·toluene *vs* 475 Å^3 at 150 K for **1**·ethanol). This may

account by itself for the improved conversion capabilities of the cation, by reducing the lattice pressure on it.

3.1.4.2 Metastable states' lifetimes

The dynamics of the relaxation of the photoinduced high spin metastable state has been monitored for different temperatures. The results obtained, normalized to the photoinduced fraction γ (Figure 3.5.) at the beginning of the decay, were fitted using a stretched exponential law:

$$\gamma(t) = \gamma(0)e^{-(\frac{t}{\tau})^{\beta}} \tag{3.1}$$

where the β parameter takes into account the time evolving crystal forces acting on a single reference molecule during the relaxation, due to the different molecular volumes of the high and low spin species, and τ is the relaxation time of the system at the temperature T.[15-18] This procedure gave for the lowest temperature a relaxation time of 1.18(±0.02) x 10^6 s (R^2 = 0.997) which should be compared with 4.5(±0.1) x 10^5 s obtained for the ethanolato derivative.[5]

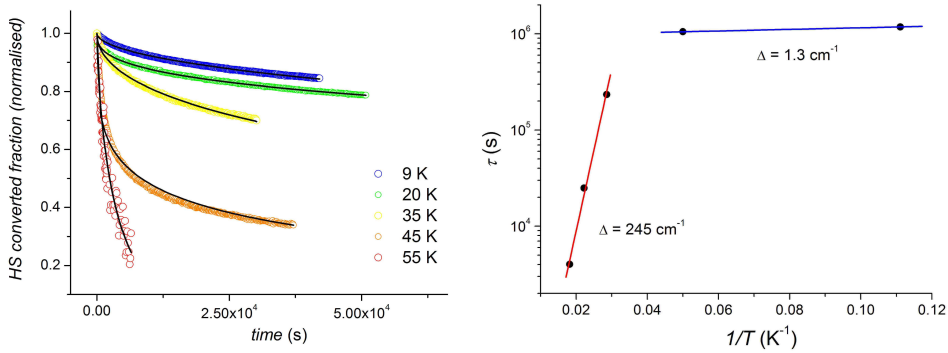

Figure 3.5. *Left*: Relaxation of the photoinduced fraction of **1**·toluene in the dark at 9K (blue circles), 20 K (green), 35 K (yellow), 45 K (orange), 55 K (red) and best fits (continuous black lines) using the stretched exponential law with parameters reported in the text. The converted fraction is normalized at **1**·toluene when t=0. *Right*: The corresponding Arrhenius plot is reported, with two different regimes clearly distinguishable (dotted line for low temperature and continuous one for high temperature). The best fit lines are obtained using the parameters reported in the text.

Two distinct dependences of τ with temperature were observed (right panel of Figure 3.5): in the high temperature range (30 - 55 K) an Arrhenius behaviour

($\tau(T) = \tau_0 e^{\frac{\Delta E}{k_B T}}$, being τ_0 the pre-exponential factor and ΔE the energy barrier) with an energy barrier of 269(±27) cm^{-1} and a pre-exponential factor of 4 (±1) s was obtained (R^2 = 0.997). The activation energy of the thermally induced relaxation well agrees with a mechanism involving the total-symmetric vibrational breathing mode of the Co-O bond, expected to be about 300 cm^{-1}. The comparison with previous results for **1**·ethanol (ΔE = 242 cm-1, τ_0 = 4.5 s)[5] confirms the single molecule nature of the LIESST phenomenon.[19,20] On the other side, the low temperature (9-20 K) behaviour of the relaxation time exhibits a very weak dependence on temperature., in agreement with the multiphonon adiabatic relaxation theory,[21] discussed in paragraph 1.3.1. A best fitting procedure with the Arrhenius relation gave ΔE = 1.3 cm^{-1} and τ_0 = 9.5 x 10^5 s, in agreement with a temperature independent tunnelling of the system from the metastable high spin state to the low spin stable one at low temperature.

3.1.4.3 *T*(LIESST) analysis

The *T*(LIESST) parameter was created with the aim of defining a standard and simple procedure allowing a rapid comparison of the light induced properties of different materials as well as to identify a parameter affecting the decay of the photo-induced state, and it is measured taking the temperature value of the downward peak of the first derivative of the $\chi_M T$ product after irradiation heating the material at a rate of 0.3 K min^{-1}, starting from 10 K after having switched off the pumping laser source at the photostationary limit. Figure 3.6 reports the *T*(LIESST) curve for **1**·toluene, showing a relaxation temperature of 53.9 K, as can be seen from the first derivative of the plot *vs* temperature.

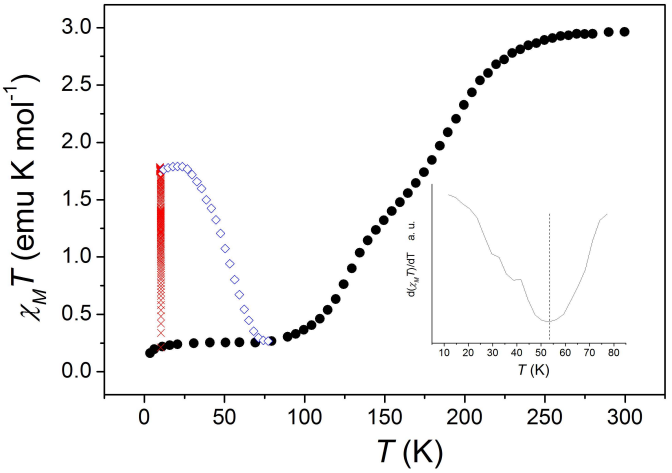

Figure 3.6. Temperature evolution of the $\chi_M T$ product of **1**·toluene without (full black circles) and after (open blue circles) irradiation on its LMCT band. *Inset:* first derivative of the $\chi_M T$ product after irradiation, showing the TLIESST value.

After switching off the light and increasing the temperature, the $\chi_M T$ recovered the pristine value around T=80 K. These data suggests that the decay process does not occur in two well defined steps, in contrast with the entropy driven one.

3.1.4.4 The Reverse LIESST effect

Another important feature of this system is the possibility of enhancing the rate of the relaxation process of the photoinduced metastabile high spin state by irradiating it on its MLCT band, located in the red region of the visible spectrum. This process, called Reverse LIESST effect, discovered almost twenty years ago for spin crossover compounds by Hauser,[22] took 16 years to be observed for a 1 : 2 Co : dioxolene based valence tautomer.[23] Its importance for technological use of these compounds is clear, making them light triggered bistable switches or data storage media. Here we report it for the first time in a 1 : 1 Co : dioxolene species undergoing valence tautomerism.

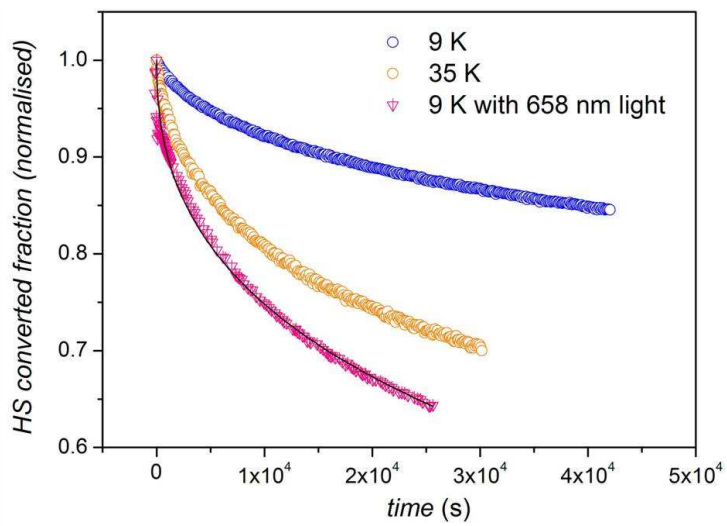

Figure 3.7. Comparison between the relaxation of the photoinduced fraction of **1**·toluene at 9 K in the dark (blue circles) and under irradiation at 658 nm (pink triangles) and at 35 K in the dark (orange circles). The black solid line is the stretched exponential fit whose parameters are reported in the text.

As shown in Fig. 3.7, when the *hs*-Co^{II} - SQ state is irradiated at 9 K with a 658 nm laser diode, its relaxation is much faster than in the dark. A stretched exponential fit gave a relaxation time of 1.58(±0.04) x 10^5 s (R^2 = 0.993) indicating that irradiation increases the relaxation rate of one order of magnitude (τ_{dark}(9 K) = 1.18 x 10^6 s). The possibility of this being a thermal effect is ruled out by considering that the observed rate under irradiation at 9 K (power of ca. 1 mW/cm^2) is faster than that in the dark at 35 K (Figure 4) and for the 9 K irradiation with different wavelengths (532 and 405 nm) using the same power on the sample. The reversibility of the process has been checked as well, assuring no degradation of the sample during several cycles of irradiation and relaxation.

The above presented results point out the effect of the change of crystallisation solvent on the temperature and light dependence of the valence tautomeric behaviour of a 1:1 Co–dioxolene compound, showing a new way to tune its magnetic properties. In particular, the different dependence on the chemical surroundings of the thermal and light induced valence tautomeric transition paves the way for the development of new molecular magnetic materials whose properties may be controlled by chemical techniques.

3.2 Crystal packing effects on the valence tautomerism in a 1:2 Co:dioxolene system

The results obtained in the investigation of 1:1 Co:dioxolene based bistable molecular materials led us to carry on a similar study for a more complex system, featuring 1:2 stoichiometry, in collaboration with the group of Dr. Colette Boskovic at the University of Melbourne, Australia.

3.2.1 The $Co(3,5\text{-}DBdiox)_2(py)_2$ system

1:2 Co:dioxolene systems have been the first molecules so far to feature an equilibrium population of states differing in the charge distribution, both in solution and in the solid state. The first report of VT behaviour in cobalt complexes from 1980 in fact describes a VT transition between the pair of redox isomers of the [Co(3,5-DBdiox)$_2$(2,2'-bpy)]. Most of the VT bis(o-dioxolene)cobalt complexes that have been reported since the original [Co^{III}(3,5-DBCat)(3,5-DBSQ)(2,2'-bpy)] species have been obtained by replacing the 2,2'-bpy ligand with other bidentate N-N donor ancillary ligands. Such complexes are constrained to adopt a *cis* arrangement of the N donor atoms.

A *trans* arrangement of the N donor atoms may be achieved by employing monodentate rather than bidentate N-donor ancillary ligands. However, there are only a few reports of VT bis(o-dioxolene)cobalt complexes with a *trans* arrangement of the N-donor ligands. Two of these concern mononuclear complexes: [Co^{III}(3,5-DBCat)(3,5-DBSQ)(tati)$_2$], where tati is trithanolaminetriisonicotinate,[24] and [Co(C$_n$Opy)$_2$(3,6-DBCat)(3,6-DBSQ)] where C$_n$Opy is (3,5-dialkoxy(C$_n$H$_{2n+1}$O$^-$; n = 9, 12 and 17) pyridine, 3,6-DBCatH$_2$ is 3,6-di-tert-butyl-catechol and 3,6-DBSQH = 3,6-di-tert-butyl-semiquinone.[25] A couple of one dimensional polymeric complexes [Co^{III}(3,6-DBCat)(3,6-DBSQ)(pz)]$_n$ and [Co^{III}(3,5-DBCat)(3,5-DBSQ)(4,4'-bpy)]$_n$, where pz is pyrazine, and 4,4'-bpy is 4,4'-bipyridine have also been reported.[26,27] All of these complexes exhibit VT transitions in the solid state, with the peculiar case of [Co(C$_n$Opy)$_2$(3,6-DBCat)(3,6-DBSQ)] which simultaneously undergoes melting of the crystalline phase.

Herein we report the analysis of a deceptively simple bis(o-dioxolene)cobalt complex, with two monodentate pyridine ancillary ligands in a trans conformation, the $Co(3,5\text{-}DBdiox)_2(py)_2$ system, **2**. Two different solvates of **2** have been obtained, **2**·0.5py and **2**·MeCN. The results obtained emphasise the important role that solvation and packing effects may play in controlling VT transitions in the solid state. highlighted in the previous part of the chapter.

3.2.2 Temperature dependent crystallographic analysis

The neutral complex **2**·0.5py crystallizes from pyridine/hexane in the monoclinic space group $P_{21/c}$. Data collected at 130 K revealed that the asymmetric unit contains one half of each of two crystallographically independent complex molecules (Fig. 3.8) and half a pyridine solvate molecule. Each independent molecule displays C_i point symmetry. At 130 K, the Co-O and Co-N bond distances for both molecules are in the ranges 1.881(3)-1.898(3) and 1.956(3)-1.958(3) Å, respectively, revealing the presence of Co^{III} centres in both molecules. The C-O and ring (O)C-C(O) bond distances can be, on the other hand, be considered diagnostic of the oxidation state of *o*-dioxolene ligands, due to the low degree of covalence of the adduct. Catecholate C-O distances are typically in the range 1.33-1.39 Å and semiquinonate distances are in the range 1.27-1.32 Å, while ring (O)C-C(O) distances are in the ranges 1.36-1.43 Å and 1.44-1.48 Å for catecholates and semiquinonates, respectively.[28-31] The C-O and (O)C-C(O) bond lengths for both independent molecules of **2**·0.5py were found to span the 1.322(5)-1.338(5) and 1.423(6)-1.425(6) Å ranges, respectively. The observed distances lie between the values typical for semiquinonate and catecholate ligands, consistent with disorder of the 3,5-DBSQ$^-$ and 3,5-DBCat^{2-} redox states of the ligand over the two *o*-dioxolene positions for both independent molecules, leading to a center of inversion at each of the metal centers. These data thus indicate that at 130 K all of the bond lengths are consistent with a formulation of [Co^{III}(3,5-DBCat)(3,5-DBSQ)$(py)_2$] for both independent molecules.

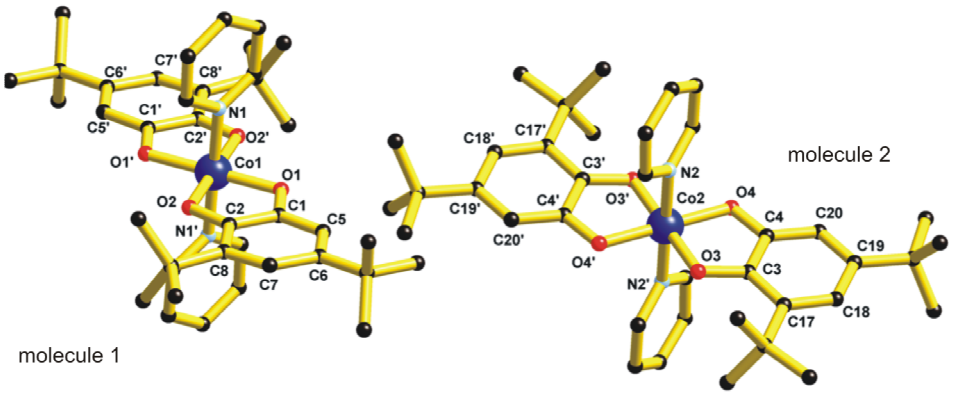

Figure 3.8. Structural representation of the two independent molecules of **2**·0.5py.

The crystallographic data collected at 295 K for **2**•0.5py revealed a significant change in the bond distances associated with molecule 1, but little difference in those for molecule 2. The Co-O and Co-N distances in molecule 1 increased by *ca.* 0.15 Å to

2.010(3)-2.042(4) Å and 2.118(5) Å, respectively. In contrast the Co-O/N bond distances of molecule 2 remained similar to the values obtained at 130 K.

The observed results are consistent with Co^{II} and Co^{III} valencies for molecules 1 and 2, respectively. The longer Co-O/N bonds in molecule 1 result from population of the antibonding e_g orbitals for the high spin Co(II) center. A small decrease in the C-O distances to 1.295(6)-1.306(6) Å at 298 K is also evident for molecule 1, which is accompanied by a small increase in the ring (O)C-C(O) bond to 1.444(7) Å. This is consistent with 3,5-DBSQ$^-$ oxidation state for both *o*-dioxolene positions in molecule 1 at this temperature. These results suggest that at 295 K, molecule 1 has undergone a VT transition to a *hs*-Co^{II}-(3,5-DBSQ)$_2$(py)$_2$ tautomer, while molecule 2 remains as the *ls*-Co^{III}-(3,5-DBCat)(3,5-DBSQ)(py)$_2$ tautomer. In contrast, the equivalent distances for molecule 2 display no significant variation from the values determined at 130 K.

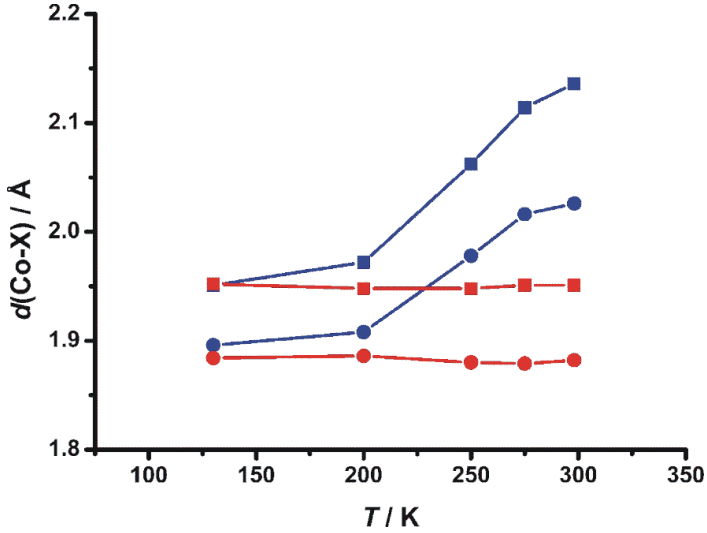

Figure 3.9. Plot of Co-O (circles) and Co-N (squares) bond lengths *vs* temperature for molecule 1 (blue) and molecule 2 (red) in **2**·0.5py.

The lengthening of the Co-O/N bonds occurs gradually and can be monitored by varying the temperature at which the data are collected, as reported in Figure 3.9. At 130 K, the corresponding Co-O/N bond distances of the two molecules are similar. At 200 K, the bond distances for molecule 1 start to increase, while those of the other molecule remain unchanged. A dramatic increase in the distances is evident at 250 K and continues until an apparent levelling off occurs around room temperature. Overall an increase in cell volume of ca. 4 % occurs between 130 and 295 K.

An analysis of the interactions among the molecules in the crystal lattice can be considered as an example of the role the lattice packing effect on determining the VT properties of molecular systems and help to understand the non equivalent nature of the molecule 1 and 2.

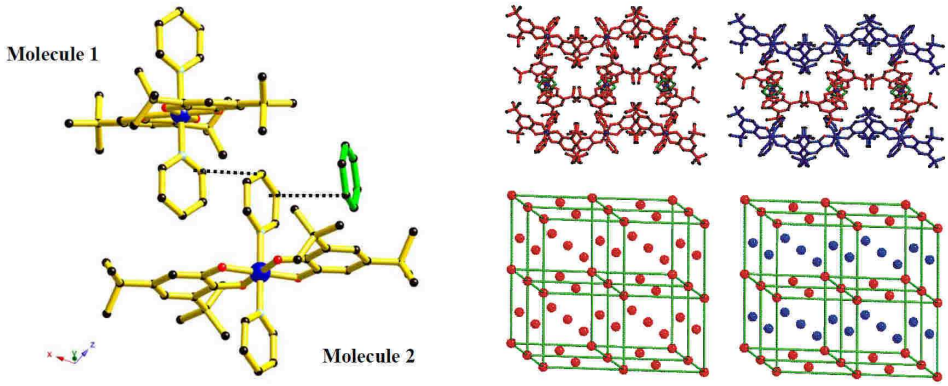

Figure 3.10. *Left*: A structural representation indicating the face-to-face intermolecular π-π stacking interactions in **2**·0.5py via the pyridine molecules of type ligand···ligand (3.42 Å) and ligand···solvate (3.48 Å). *Right*: Packing diagrams for **2**·0.5py at 130 K (left) and 295 K (right) looking down the crystallographic *c* direction; color code: Co^{III}-containing molecules (red), Co^{II}-containing molecules (blue), pyridine solvate (green). The spheres in the lower two figures represent the Co centres only.

The left panel of Figure 3.10 shows the presence of both free and coordinated pyridine in **2**·0.5py, giving rise to two intermolecular face-to-face π-π stacking interactions. One of these occurs between molecule 1 and 2 via the pyridine ligands, with the closest C·C contact between the rings being 3.42 Å. The other π-π interaction is between a pyridine ligand of molecule 2 and the pyridine solvate molecule at a distance of 3.48 Å.

The ligand - solvate π-π stacking interaction that is present only for molecule 2 appears to be the origin of the absence of a VT transition for this molecule. The associated steric crowding of molecule 2 apparently prevents the increase in molecular size that must accompany the VT interconversion.

Recrystallisation of the crude product **2** from acetonitrile affords the solvated compound **2**·2MeCN, which crystallizes in the monoclinic $C_{2/c}$ space group. Half of one complex is evident in the asymmetric unit in Figure 3.11.

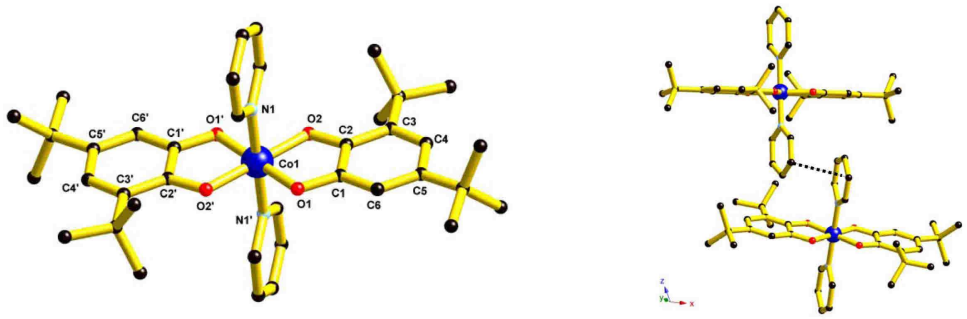

Figure 3.11. *Left*: Structural representation of complex **2**·2MeCN. *Right*: π–π stacking interactions through the pyridine ligands.

The molecule has *Ci* point symmetry. Data collected at 130 K affords Co-O bond lengths in the range 1.879(2)-1.887(2) Å, with a Co-N bond distance of 1.945(3) Å, consistent with a Co^{III} center. The C-O bond distances are between 1.327(4) and 1.335(4) Å, while the ring (O)C-C(O) bond lengths are in the range 1.423(6)-1.425(6) Å. This is again consistent with disorder of the 3,5-$DBCat^{2-}$ and 3,5-$DBSQ^{-}$ ligands over the two *o*-dioxolene sites. Thus complex **2**·2MeCN also has the formulation *ls*-Co^{III}(3,5-DBCat)(3,5-DBSQ)(py)2 at 130 K. Due to the poor diffraction quality, it was not possible to obtain structural information at 295 K and no structural comparison can be presented.

A close inspection of the crystal packing of **2**·2MeCN reveals a face-to-face π-π stacking interaction between the molecules via the pyridine ligands (right panel of Figure 3.11), with the closest C·C contact between the rings of 3.71 Å. This offset ligand·ligand π-π stack gives rise to the formation of a continuous channel that is occupied by acetonitrile molecules.

3.2.3 Magnetometric analysis

The temperature dependence of the entropy driven VT equilibrium in the solid state for **2**·0.5py and **2**·2MeCN has been followed by means of magnetometry.

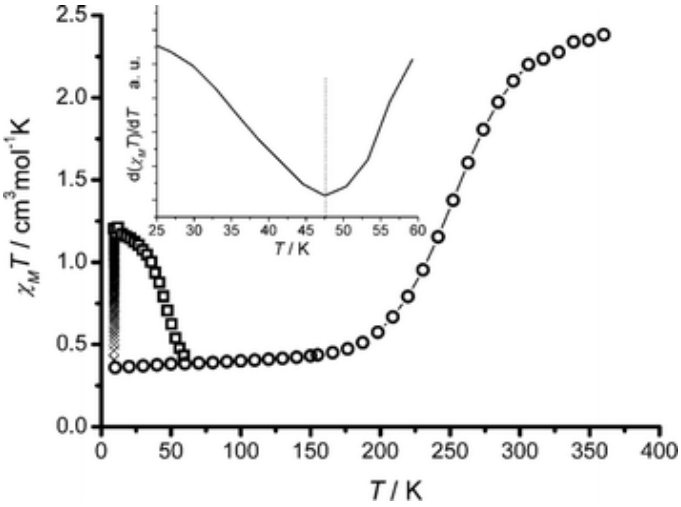

Figure 3.12. Plot of $\chi_M T$ *vs* T for the thermally- (empty circles) and photo-induced (empty squares) VT transition for **2**·0.5py; the crosses indicate the increase in $\chi_M T$ with time upon irradiation of the sample. *Inset.* First derivative of $\chi_M T$ vs T curve, pointing out the TLIESST value.

Magnetic susceptibility data were measured for **2**·0.5py in the temperature range 2.0 to 350 K (Fig. 3.12). This high temperature limit was imposed by the loss of pyridine solvate molecules at higher temperatures as observed by thermogravimetric analysis. The value of $\chi_M T$ increases gradually from 0.38 emu K (mol)$^{-1}$ at 2 K to 0.50 emu K(mol)$^{-1}$ at 200 K before rapidly increasing to 2.10 emu K(mol)$^{-1}$ at 300 K and then more gradually to 2.40 emu K(mol)$^{-1}$ at 350 K. The low temperature value is consistent with a spin-only S = 1/2 system, due to the radical semiquinonate ligand in the *ls*-Co^{III}(3,5-DBCat)(3,5-DBSQ)$_2$(py)$_2$ tautomer. The sigmoidal profile of the thermal variation of $\chi_M T$ indicates the occurrence of a VT transition with $T_{½}$ of about 250 K. However, given the first order orbital contribution to the magnetic susceptibility for high spin octahedral Co^{II} centres, and its large variability,[32] the expected value of $\chi_M T$ for the *hs*-[Co^{II}(3,5-DBSQ)$_2$(py)$_2$] tautomer at the high temperature limit is not obvious.

To overcome this problem we used a reference compound, featuring a similar structure whose magnetisation and conversion dependences on temperature were known. This has been found in the polymeric complex [Co^{III}(3,6-DBCat)(3,6-DBSQ)(pz)]$_n$. Independent spectroscopic studies on this material in the solid state[26] revealed an essentially complete VT transition at 350 K, yielding the *hs*-[Co^{II}(3,6-DBSQ)$_2$(pz)]$_n$ tautomer. A corresponding $\chi_M T$ value of 4.3 emu K(mol)$^{-1}$ was observed at 350 K, which, applied to our case, suggests that the $\chi_M T$ value observed for **2**·0.5py at 350 K can be attributed to a 1:1 mix of the *ls*-[Co(3,5-DBCat)(3,5-DBSQ)(py)] and *hs*-[Co(3,5-DBSQ)$_2$(py)] tautomers at 350 K. This result is consistent with the single

crystal X-Ray diffractometry analysis, which indicated that only one of the two crystallographically independent molecules underwent a thermally-induced VT transition in this temperature range.

Magnetic susceptibility data were obtained for fully solvated wet crystals of **2**·2MeCN and fully desolvated complex **2** from **2**·2MeCN (Fig. 3.13).

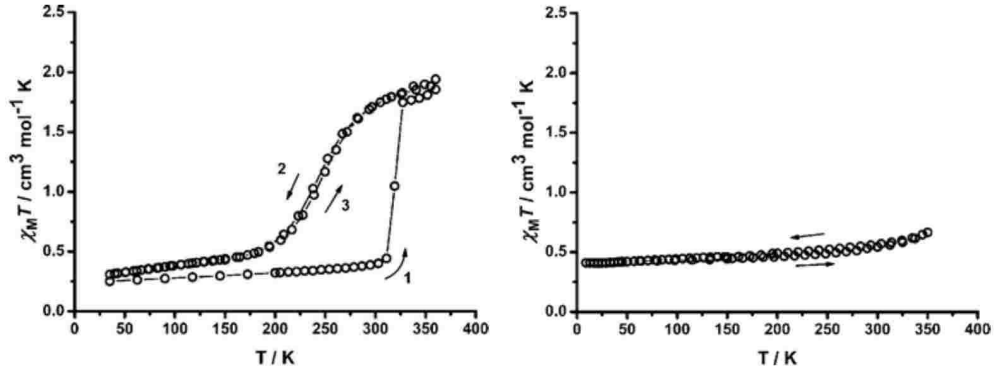

Figure 3.13. Plot of $\chi_M T$ vs T for **2**·2MeCN (*left*) and desolvated **2** from **2**·2MeCN (*right*).

The thermal variation for **2**·2MeCN showed an almost constant $\chi_M T$ value of ca. 0.3 emu K(mol)$^{-1}$ in the range 2-320 K consistent with a *ls*-Co^{III}(3,5-DBCat)(3,5-DBSQ)(py)$_2$ tautomer over this temperature range. After heating the sample above 310 K, the value of $\chi_M T$ increased sharply to 1.8 emu K(mol)$^{-1}$, as reported in the left panel of Figure 3.13, suggesting an abrupt VT transition around this temperature. It is likely that this VT transition has been triggered by rapid loss of solvate molecules above 310 K. This is consistent with the observed ready loss of acetonitrile molecules of crystallization upon standing at room temperature. Steric crowding due to the presence of the acetonitrile molecules in the crystal lattice may prevent the expansion in molecular volume associated with a VT transition. Thus when the solvent molecules have escaped from the lattice, a VT transition may become accessible. Unfortunately, loss of crystallinity associated with rapid solvent loss prevented the crystallographic study of such a VT transition.

Repeated magnetic susceptibility measurements of the same sample down to 25 K (curve labelled 2 in the left side of Fig 3.13) then back to 370 K (curve labelled 3) pointed out a reversible VT transition with a $T_{½}$ value (ca. 250 K) close to that found for **2**·0.5py, although the value of $\chi_M T$ at 350 K is lower than the value observed for **2**·0.5py, suggesting an incomplete VT transition. The original $T_{½}$ value of *ca.* 320 K for the solvated crystals was not obtained on the second and subsequent measurements on the same sample, due to the irreversible loss of solvent molecules from the crystal lattice. The degree of desolvation during this measurement is uncertain, but it appears

to be incomplete, given that a fully desolvated analytically pure sample of **2** (obtained by vacuum drying of **2**·2MeCN) shows a different thermal variation of the magnetic susceptibility (right side of Fig. 3.13). The fully desolvated sample of **2** showed no VT transition in the range 2 to 350 K, remaining as the *ls*-[Co(3,5-DBCat)(3,5-DBSQ)(py)] tautomer. A slight increase in $\chi_M T$ over this temperature range has been attributed to TIP, as is commonly observed for low spin Co(III) compounds.[32,33]

The observed difference in the magnetic behaviour for the solvated, partially desolvated, and fully desolvated samples of compound **2**·2MeCN presumably arises because of the structural effects of the molecules of solvation. In the fully solvated sample, steric crowding by the solvate molecules may inhibit the VT transition, as occurs for molecule 2 in **2**·0.5py. However, upon partial desolvation, this inhibition appears to be reduced and some of the complex molecules can undergo a VT transition. Then, upon complete desolvation, collapse of the structural integrity of the lattice may result in neighbouring molecules of complex 1 packing more closely together, again inhibiting the VT transition.

3.2.4 Photomagnetic properties

Hereafter we report the investigation of photoinduced VT process for **2**·0.5py, followed by means of EPR and inductance based magnetometry. An analogous investigation of the **2**·2MeCN could not have been performed because of the evolution of its content of crystallisation solvent during the measurements, as reported above.

3.2.4.1 EPR investigation

EPR spectroscopy has been scarcely employed in the investigation of 1:1 Co:dioxolene based VT systems since the low temperature species is a diamagnet and in the high temperature one the *hs*-Co^{II} ion features a very short relaxation time, affording only an unstructured broad band in the spectrum.[5] However, the situation is different in the case of 1:2 Co:dioxolene materials, where the high temperature problems remain but the VT interconversion can be followed measuring the signal of the radical low temperature Co^{III}(3,5-DBCat)(3,5-DBSQ)$(py)_2$ tautomer.

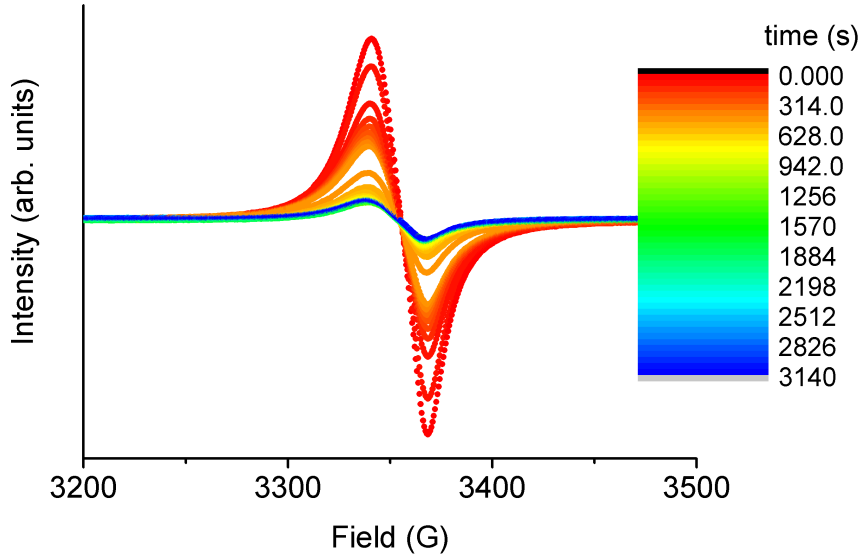

Figure 3.14. EPR spectra of **2**·0.5py during irradiation with 532 nm light at 9 K.

Figure 3.14 shows the effects of irradiation of complex **2**·0.5py at 9 K using 532 nm wavelength light, matching the LMCT band for the 1:2 Co:dioxolene systems.[34] The initial EPR spectrum of the sample after irradiation shows the g = 2.00 signal, which originates from the S = 1/2 3,5-DBSQ^{-} radical ligand of *ls*-CoIII(3,5-DBCat)(3,5-DBSQ)(py)$_2$. As the irradiation continues, the signal disappears due to the formation of the *hs*-Co^{II}(3,5-DBSQ)2(py)$_2$ tautomer, which is EPR silent because of the fast relaxation of Co(II), as stated above. The intensity of the final signal, calculated as the double integral of the resonance line, is less than half of the initial signal, suggesting that one of the independent molecules of **2**·0.5py undergoes complete conversion, with possible partial conversion of the other independent molecule.

The intensity of the signal was recovered by switching off the laser, heating above 70 K and cooling back to 9 K. These results are consistent with the magnetic data for the photo-induced VT transition and with the crystallographic and magnetic susceptibility measurements for the thermally-induced VT transition. It appears that for both the thermally- and photo-induced VT transition, one of the two crystallographically independent molecules undergoes a complete transition, while the other may undergo a partial transition. The somewhat larger (and faster) conversion observed by EPR (compared to the magnetometric investigation reported below)is due to the larger surface to volume ratio of sample exposed to the irradiation in this technique compared to that in the photomagnetic SQUID setup.

3.2.4.2 Magnetometric analysis

The photoinduction of VT, along with the dependence on *T* of the relaxation rate, can be seen in Figure 3.12. Irradiation on the LMCT band resulted in an increase in $\chi_M T$ from 0.38 to 1.20 emu K mol^{-1}, indicative of a photo-induced VT transition from the *ls*-Co^{III}(3,5-DBCat)(3,5-DBSQ)(py)$_2$ tautomer to the *hs*-Co^{II}(3,5-DBSQ)$_2$(py)$_2$ tautomer. Experimentally, it is difficult to determine the percentage of the photo-conversion product as the $\chi_M T$ value at 9 K of *hs*-Co^{II}(3,5-DBSQ)$_2$(py)$_2$ is not known. However, it can be safely assumed that 2.50 emu K(mol)$^{-1}$ is an upper limit for this tautomer at 9 K.[2,11] Using this value, the percentage of photo-conversion is calculated to be a minimum of 40 %, indicating that at least one of the two crystallographically independent molecules in 2·0.5py has undergone almost complete photo-induced conversion to the *hs*-Co^{II}(3,5-DBSQ)$_2$(py)$_2$ tautomer at 9 K. The *T*(LIESST) value has been found to be about 47 K (inset of Fig. 3.12), within the range of 40-80 K at which the photo-induced metastable tautomers of other VT Co complexes have been observed to relax back to the original state.[35-37]

In order to characterise the kinetics of the decays of the photoinduced metastable state at low temperatures, the isothermal time dependence of the photo-induced *hs*-Co^{II}(3,5-DBSQ)$_2$(py)$_2$ tautomer to the *ls*-Co^{III}(3,5-DBCat)(3,5-DBSQ)(py)$_2$ tautomer was monitored by time dependent magnetization measurements at five different temperatures (Fig. 3.15).

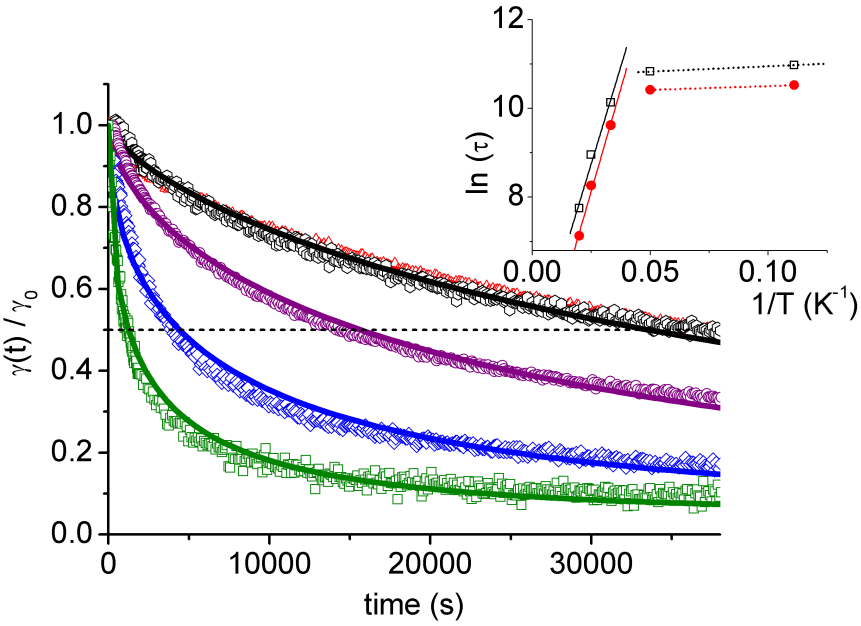

Figure 3.15. Relaxation of the photo-induced metastable form of **2**·0.5py at 10 K (red), 20 K (black), 30 K (purple), 40 K (blue) and 50 K (green), and best fit curves using the stretched exponential model (continuous lines). The dashed horizontal line represents the times at which the same converted fraction (0.5) has relaxed to the ground state. *Inset*: the corresponding Arrhenius plots obtained with the two different methods as described in the text, together with best fit lines in the two different regimes (10-20 K and 30-50 K). Empty squares: relaxation times from stretched exponential method; red circles: relaxation times from constant relaxed fraction.

The photoinduced fraction as a function of time, which is the quantity actually studied, is defined as:

$$M(t)=(M(t)-M_{OFF})/(M(0)-M_{OFF}) \quad (3.2)$$

where $M(t)$ is the magnetization value at time t after illumination, $M(0)$ is the photostationary limit achieved after irradiation at t = 0 (when the laser is switched off and relaxation begins) and M_{OFF} is the magnetization value before illumination. The data presented in Fig. 3.15 clearly show that in the low temperature region the relaxation is almost independent of temperature, whereas a stronger thermal dependence is observed in the higher temperature region. It is also evident that, as has been observed for many other photo-induced VT transitions,[5,6,16,18,38] the relaxation dynamics does not follow a single exponential law. These results resemble the findings coming from the analysis of the metastable lifetimes of **1**·toluene and agree with the

theory of Jortner. However, some differences can be spotted out treating the data with a quantitative basis. In order to do this we performed a fit using a stretched exponential law shown in Eq. 3.1, which is usually adopted in the analysis of photomagnetic data because of the inhomogeneous distribution of the centres undergoing interconversion.[16]

As observed in the case of **1**·toluene, the plot of $\ln(\tau)$ versus $1/T$ reveals that the relaxation rate does not follow a simple Arrhenius law as expected for a single thermally activated process (inset of Fig.3.15). Rather, two distinct relaxation regimes are observed: a low temperature one which is essentially temperature independent (E_a < 10 cm^{-1}), and a higher temperature one (T > 30 K) that can be fitted to an Arrhenius expression, with best fit values of $E_a = 120 \pm 10$ cm^{-1} and $\tau_0 = 80 \pm 10$ s for T < 30 K. Quite interestingly similar results are obtained if one take as τ the time elapsed when the photoinduced fraction has relaxed to 50% of its starting value, thus getting rid of the strong correlations between τ and β which are intrinsic to the stretched exponential model. With this approach the best fit of the Arrhenius plot gave Ea = 130 ± 10 cm^{-1} and $\tau_0 = 35 \pm 5$ s for T > 30 K.

These results are consistent with the behaviour observed for a number of other VT Co complexes and interpreted in terms of a phonon-assisted tunnelling mechanism in the lower temperature range and a thermally assisted relaxation mechanism at higher temperature.[6,16-18,35] The values obtained for the activation energy in the higher temperature range also compare well with previously reported results for other bis(*o*-dioxolene)cobalt complexes, confirming the essentially single molecule nature of the relaxation process. Further, they provide evidence for the remarkable difference between 1:2 and 1:1 Co:dioxolene complexes that undergo photoinduced VT transitions, with the latter generally being characterised by larger activation energies, in agreement with a dominant contribution from the totally symmetric Co–O vibrational breathing mode (300–400 cm^{-1}) in promoting the relaxation process from the metastable state.[5,6,35]

References

[1] Day, P. *Int. Rev. Phys. Chem.* **1981**, *1*, 149-193.

[2] Adams, D. M.; Dei, A.; Rheingold, A. L.; Hendrickson, D. N. *J. Am. Chem. Soc.* **1993**, *115*, 8221-8229.

[3] Cador, O.; Dei, A.; Sangregorio, C. *Chem. Commun.* **2004**, 652-653.

[4] Evangelio, E.; Rodriguez-Blanco, C.; Coppel, Y.; Hendrickson, D. N.; Sutter, J. P.; Campo, J.; Ruiz-Molina, D. *Solid State Sci.* **2009**, *11*, 793-800.

[5] Beni, A.; Dei, A.; Rizzitano, M.; Sorace, L. *Chem. Commun.* **2007**, 2160-2162.

[6] Beni, A.; Dei, A.; Laschi, S.; Rizzitano, M.; Sorace, L. *Chem., Eur. J.* **2008**, *14*, 1804-1813.

[7] Sheldrick, G. M. *SHELX-97* University of Göttingen , 1997.

[8] Altomare, A.; Burla, M. C.; Camalli, M.; Cascarano, G.; Giacovazzo, C.; Guagliardi, A.; Moliterni, A. G. G.; Polidori, G.; Spagna, R. *J. Appl. Cryst.* **1999**, *32*, 115-119.

[9] Varret, F.; Boukheddaden, K.; Chong, C.; Goujon, A.; Gillon, B.; Jeftic, J.; Hauser, A. *Europhys. Lett.* **2007**, *77*, 30007.

[10] Robin, M. B.; Day, P. *Adv. Inorg. Chem. Radiochem.* **1967**, *10*, 247.

[11] Bencini, A.; Beni, A.; Costantino, F.; Dei, A.; Gatteschi, D.; Sorace, L. *Dalton Trans.* **2006**, 722-729.

[12] Slichter, C. P.; Drickamer, H. G. *J. Chem. Phys.* **1972**, *56*, 2142-2160.

[13] Pierpont, C. G. *Coord. Chem. Rev.* **2001**, *219*, 415-433.

[14] Gutlich, P.; Dei, A. *Angew. Chem., Int. Ed. Engl.* **1997**, *33*, 2734-2736.

[15] Beni, A.; Dei, A.; Shultz, D. A.; Sorace, L. *Chem. Phys. Lett.* **2006**, *428*, 400-404.

[16] Carbonera, C.; Dei, A.; Letard, J.-F.; Sangregorio, C.; Sorace, L. *Inorg. Chim. Acta* **2007**, *360*, 3825-3828.

[17] Cui, A.; Takahashi, K.; Fujishima, A.; Sato, O. *J. Photochem. Photobiol., A* **2004**, *167*, 69-73.

[18] Li, B.; Tao, J.; Sun, H. L.; Sato, O.; Huang, R. B.; Zheng, L. S. *Chem. Commun.* **2008**, 2269-2271.

[19] Hauser, A. *Light-Induced Spin Crossover and the High-Spin -> Low-Spin Relaxation* in *Spin Crossover in Transition Metal Compounds II*; Gütlich, P.; Goodwin, H. A., Eds.; Springer: Berlin, 2004; Vol. 234, pp 155-198 .

[20] Gutlich, P.; Garcia, Y.; Goodwin, H. A. *Chem. Soc. Rev.* **2000**, *29*, 419-427.

[21] Buhks, E. ; Navon, G.; Bixon, M.; Jortner, J. *J. Am. Chem. Soc.* **1980**, *102*, 2918–2923.

[22] Hauser, A. *Chem. Phys. Lett.* **1986**, *124*, 543-548.

[23] Sato, O.; Hayami, S.; Gu, Z. Z.; Takahashi, K.; Nakajima, R.; Fujishima, A. *Chem. Phys. Lett.* **2002**, *355*, 169-174.

[24] Liang, H.; Cha, M. S.; Lee, Y. A.; Lee, S. S.; Jung, O. S. *Inorg. Chem. Commun.*

2007, *10* , 71-73.

[25] Kiriya, D.; Chang, H. C.; Kitagawa, S. *J. Am. Chem. Soc.* **2008**, *130*, 5515-5522.

[26] Jung, O. S.; Pierpont, C. G. *J. Am. Chem. Soc.* **1994**, *116*, 2229-2230.

[27] Imaz, I.; Maspoch, D.; Rodriguez-Blanco, C.; Perez-Falcon, J. M.; Campo, J.; Ruiz-Molina, D. *Angew. Chem. Int. Ed.* **2008**, *47*, 1857-1860.

[28] Boone, S. R.; Purser, G. H.; Chang, H. R.; Lowery, M. D.; Hendrickson, D. N.; Pierpont, C. G. *J. Am. Chem. Soc.* **1989**, *111*, 2292-2299.

[29] Ding, Z. R.; Bhattacharya, S.; Mccusker, J. K.; Hagen, P. M.; Hendrickson, D. N.; Pierpont, C. G. *Inorg. Chem.* **1992**, *31*, 870-877.

[30] Boudalis, A. K.; Dahan, F.; Bousseksou, A.; Tuchagues, J. P.; Perlepes, S. P. *Dalton Trans.* **2003**, 3411-3418.

[31] Mulyana, Y.; Nafady, A.; Mukherjee, A.; Bircher, R.; Moubaraki, B.; Murray, K. S.; Bond, A. M.; Abrahams, B. F.; Boskovic, C. *Inorg. Chem.* **2009**, *48*, 7765-7781.

[32] Carlin, R. D. L. *Magnetochemistry*; Springer-Verlag: Berlin, 1986.

[33] Kahn, O. *Molecular Magnetism*; VCH: Weinheim, 1993.

[34] Pierpont, C. G.; Jung, O. S. *Inorg. Chem.* **1995**, *34*, 4281-4283.

[35] Dapporto, P.; Dei, A.; Poneti, G.; Sorace, L. *Chem., Eur. J.* **2008**, *14*, 10915-10918.

[36] Carbonera, C.; Dei, A.; Letard, J. F.; Sangregorio, C.; Sorace, L. *Angew. Chem. Int. Ed.* **2004**, *43*, 3136-3138.

[37] Carbonera, C.; Dei, A.; Sangregorio, C.; Letard, J. F. *Chem. Phys. Lett.* **2004**, *396*, 198-201.

[38] Bodnar, S. H.; Caneschi, A.; Dei, A.; Shultz, D. A.; Sorace, L. *Chem. Commun.* **2001**, 2150-2151.

Chapter IV

Analysis of the relations between entropy and optically driven redox isomerism: The solid solution approach

In the previous chapter we have shown that the replacement of the crystallisation solvent revealed to be a reliable method to change the thermal and photoinduced valence tautomerism in Co:dioxolene systems, affording tuneable transition temperatures and improved light conversion properties. The comparison of the relaxation kinetics for different solvates, however, pointed out the optical metastability at low temperature in the solid state as a phenomenon related to single molecular properties, contrarily to what up to now generally reported in the recent literature. In the present chapter we present a rational approach to investigate the effect of cooperative elastic interactions in the lattice on the entropy and optically driven VT, relying on the solid dissolution of a bistable complex into an inert homologous. This investigation on one side confirmed the thermodynamic character of the thermal transition, being sensitive to lattice pressure and to additional entropy terms introduced by the doping. On the other hand it pointed out that the kinetics of the decay does not depend on the cooperativity in the crystal lattice, thus suggesting a possible application of VT systems in nanostructured materials.

4.1 The role of cooperative interactions in the thermal and light triggered Valence Tautomerism

The possible use of VT systems for applicative purposes has been associated in the past to their possibility of existing, under the same thermodynamic conditions, in at least two states, featuring different physical or chemical properties. This behaviour, called bistability, requires the existence of at least two degenerate minima of the free energy of the system under the same conditions of the external parameters (T, P, H, etc.) and a large free energy barrier between the two minima.[1] However a more appropriate approach to this problem should consider that, for any technological application of these systems, what is actually required is the persistence of the same molecular system in different states for the time required by the technological application. In this sense the existence of a thermodynamic bistability is a sufficient but not necessary condition. It is only necessary that, in addition to the thermodynamic stable species, the system may exist in a metastable state characterized by an appropriate kinetic stability.[2]

These two different approaches are clearly reflected in the different research lines developed in this field. A first one was focused to obtain systems with $T_{½}$ close to room temperature and characterised by large thermal hysteresis, *i.e.* with different $T_{½}$ observed in warming and cooling processes of measure. This is the result of the existence of a large free energy barrier between two possible thermodynamic stable states of the system, arising from a three-dimensional network of elastic interactions in the solid state, which makes possible their physical independent existence according to the historical sequence of perturbations (the so called "memory effect").

The second perspective has been aimed to properly perturb the system to stimulate the conversion between the two states. Once the metastable state is populated, the investigation is focused to understand and to control the factors affecting the kinetics of the decay of the thermodynamic metastable state of the system down to the stable one. In this case it is expected that the time dependence of the relaxation would follow the classic single exponential relationship

$$\gamma(t) = \gamma(0)e^{-\frac{t}{\tau}} \tag{4.1}$$

where $\gamma(t)$ is the molar fraction of the metastable species at time t and $\tau(T)$ is its relaxation time at temperature T.[3] The elucidation of factors affecting the kinetic constant values and the deviation from this law are the main goals of this investigation paradigm. The obvious question is: *are the two approaches providing related answers from the probed physical system?*

The work developed up to now for spin crossover complexes suggests that the answer to this question should be positive. For their application as memory devices, SC complexes should afford low-spin/high-spin transitions with large thermal hysteresis loops. Since hysteresis is a consequence of cooperative effects in condensed phase, *i.e.* of long-range interactions between the metal centres undergoing spin transition, the chemical strategy often adopted was that of increasing the reciprocal interactions within the lattice or pseudolattice, *e. g.* by introducing these centres in a polymeric network.[4] The low-spin/high-spin interconversion occurs with lattice expansion due to the significant increase of the metal-donor bond lengths. It was therefore suggested that cooperativity arises from elastic energy changes due to the expansion of the lattice and vibrational entropy changes due to anharmonicity of vibrations coupled again with expansion of the lattice. Several experimental results have supported the validity of this approach.[5,6]

Similar considerations are believed to hold for complexes undergoing redox isomerism interconversions like manganese and cobalt dioxolene complexes. Again the transitions are associated with lattice expansions according to the difference in metal-donor bond lengths of the two redox isomers and significant photomechanical effects are often observed.[7] Unfortunately the number of molecular systems showing thermal hysteresis is very limited and any further speculation must be avoided. Anyway, the results obtained by using polymeric networks of interconverting moieties support the extension of the same strategies adopted for spin crossover derivatives to VT interconversions.[8] The obtained results therefore suggest that a well defined approach for the control of cooperativity of thermal interconversions is available. It should be mentioned however that factors determining the absolute values of thermal transition temperature $T_{½}$ are far from being quantitatively elucidated, as discussed in Chapter III. In a similar way the same interconversion process may occur in solution and in solid state at very different temperatures. This implies that the limited degree of our knowledge does not allow a prediction of the ratio between the enthalpy and entropy changes involved in the interconversions.

As far as the second approach is concerned, historically and practically the most used tool to induce the transition to a metastable state has been the irradiation of solid bistable compounds at appropriate wavelengths and cryogenic temperatures with the consequent stimulation of the interconversion process. The discovery of LIESST and reverse LIESST effects in a Fe^{II} spin crossover complex by Gütlich, Decurtins and Hauser is a milestone of this topic.[9-11] Relaxation of the metastable species was shown to be nearly independent from temperature down to 20 K and to follow a temperature activated behaviour at higher temperatures. The lifetime of the metastable species therefore is found extremely long at low temperature, and then quickly decreasing being of the order of nanoseconds at room temperature. Again the observed properties have been interpreted in terms of elastic interactions experienced by the

interconverting centres in the lattice. The analysis of several SC complexes in differently diluted materials showed that that lifetime of the metastable species in the tunnelling region (T < 30 K) is inversely proportional to the thermal spin transition temperature $T_{½}$. This relationship is known as the inverse energy gap law, since a large lifetime is related to a small difference of the free energy of the two interconverting species.[12] The intrinsic meaning of this law is that the thermal, entropy driven, spin transition is controlled by the same factors which determine the decay kinetics of the optically induced metastable species.

4.2 The metal dilution approach in the investigation of bistable molecular materials

The results presented in Chapter III about the apparent failure of the IEGL in describing the relaxation times of the photoinduced metastable state's in function of their transition temperatures of different solvates of the same complex left some open questions about the optical bistability in Co:dioxolene VT materials. In particular the point to be addressed concerns the role of the cooperativity, arising from elastic interactions in the solid lattice, on the relaxation time of the metastable *hs*-Co^{II} – SQ state at low temperatures. The IEGL finds its roots in the fundaments of quantomechanics and its validity cannot be challenged. It is rather obvious that its apparent failure in explaining some experimental results arises from the difficulties of its general application to molecular systems where different interactions are operative.[13-15]

The up to now systematic investigations on this problem have been carried out in the field of SC complexes on different molecular systems showing thermal and optical SC bistability. This approach presents the undisputed advantage to cover a very large set of testing grounds for the theory of IEGL, however is keen to compare systems where not only τ and $T_{½}$ are changing, but also the molecular and crystal structural parameters – with consequences on the cooperativity of the interconverting centres. On this regard, in order to assess the role of the interactions present in the solid state on the metastable state's lifetimes in the quantum and thermally activated relaxation regimes, we decided to follow another way: the solid solution approach.[16] The underlying idea is to get a chemically driven control on the structural parameters affecting the entropy and optically induced VT interconversion by changing the degree of solid solution of the system under investigation into an inert crystalline host. This can be achieved considering the host to act a lattice pressure on the molecules of the system, due to a little structural mismatch between them. As we have seen in paragraph

1.3.1.1, the effect of an applied (or reduced) pressure on the energy of the potential wells involved in the VT transition is their relative shift in energy. Also in this case this can be rationalised as a natural consequence of the difference first coordination sphere's volumes of the systems into its two different electronic states. In particular, for bigger (smaller) host molecules a stabilisation of the bigger (smaller) phases of the system is expected. Since these effects are clearly dependent on the doping ion the analysed system is dissolved in, we will hereafter refer to the case of interest in this work: the doping of a Co:dioxolene system in a crystalline host featuring a higher molecular volume. In Figure 4.1 is shown a schematic picture of the effect of increased doping on the relative energies of the electronic wells of a general Co:dioxolene system..

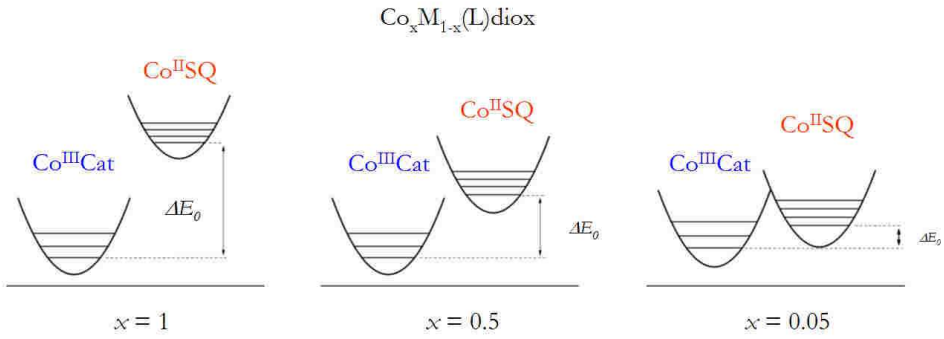

Figure 4.1. Scheme of the effect of increasing solid dilution on the energies of the electronic wells belonging to the two phases of Co:dioxolene materials.

The effects of dilution reported in Figure 4.1 for the reference system Co_xM_{1-x}(L)diox arise from two different causes: the increase in the distances between the system molecules and the smoothing of their strength of interaction. These two factors have been shown to have similar effects on the thermodynamic quantities involved in the VT transition. From an enthalpic point of view the increased volume per molecule, afforded by the enhancement of the lattice volume due to the doping, results in a decrease of the ΔH on decreasing x.[16] A role in the dependence of this quantity on the x is the alteration of the coupling between the vibrational modes of interacting active centres undergoing the VT transition. The same effect is found for the ΔS , where the doping increases the frequency of vibration of the low temperature phase, while the opposite effects is found for the high temperature one, thus leading to a reduction of the entropy change increasing x.

The overall consequence of solid dissolution on the electronic wells can be understood considering the "lattice pressure" on a reference molecule of our system; the effect of an applied pressure has in fact been revealed to be an additive term to the

reduced energy gap ΔE_0 (*cfr.* Figure 4.1) according to Eq. 1.20. In this way is possible to chemically tune the reduced energy gap keeping the others parameters of the systems fixed and thus obtain a proper evaluation of the IEGL for 1:1 Co:dioxolene materials. For these reasons the solid solution approach has been applied previously for the analysis of the thermodynamics of SC materials with different dimensionalities for investigating the mechanisms of transition in the solid state in function of temperature[16,16-20] and light irradiation.[21,22] This technique has been recently employed also for the rationalisation of the structural parameters governing the photomagnetic properties of non molecular systems (PBAs).[23]

To perform this investigation the chosen system has been **1**·toluene. Several reasons suggested this compound, mainly based on its capabilities to ease the experimental side of the investigation: its chemical stability, its transition temperature easily available with commercial ^{4}He cryostats and its record conversion fraction by light irradiation at low temperatures. The latter point is of paramount importance for the analysis of the behaviour of the metastable photoinduced state at high levels of solid dissolution into the inert matrix.

4.2.1 The host matrix

In order to fit into the project, the host matrix should be able to:

- Properly dissolve in the solid state the system under investigation, without undergoing nucleation of the pure phases or phase segregation;
- Be structurally similar to one of the different electronic isomers of the system, in order to selectively stabilise it;
- Possess a well defined electronic and structural state, not depending on time, temperature nor light irradiation.

All of these characteristic can be found for the chosen crystal host: the $[Zn(Me_2tpa)(DBSQ)]PF_6 \cdot C_6H_5CH_3$ complex. Firstly, it shares the molecular structure with **1**·toluene, thus suggesting a great ability to dissolve one into each other in the solid state. The second point of the above scheme is accomplished as well, since the ionic radius of Zn^{II} ion is similar to that of the *hs*-Co^{II} species (0.75 Å *vs* 0.745 Å, respectively) and quite distinct from the one of the *ls*-Co^{III} species (0.545 Å). Finally, it is of course incapable to afford any redox isomerism, since oxidation states for the Zn atom different from two feature energies outside the range of stability of our molecules. The structure of the Zn molecular host, along with its intermolecular interactions in

the solid state, obtained by single crystal X-ray diffractometry at 160 K, is reported in Figure 4.2.

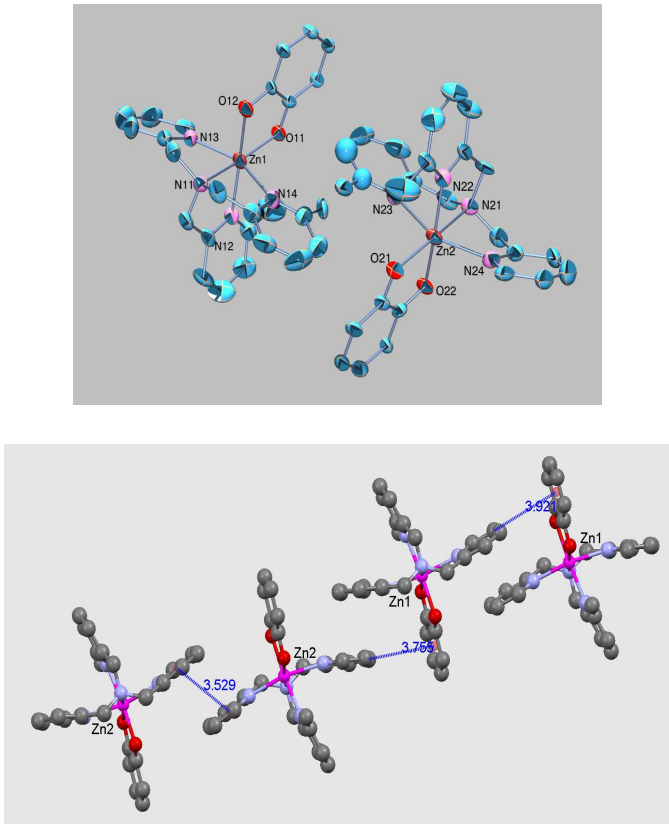

Figure 4.2. *Above*: View of the two molecules in the crystallographic independent cationic moiety of $[Zn(Me_2tpa)(DBSQ)]PF_6 \cdot C_6H_5CH_3$. For clarity sake hydrogen atoms and *tert*-butyl groups are not shown. *Below*: Pattern of the C-H - π and π– π intermolecular interactions among adjacent molecules, along c*.

The structure of the pure Zn derivative obtained by single crystal diffractometry is reported in the upper side of Figure 4.2. The asymmetric unit is composed of two molecular units, as already observed for the 160 K structure of **1**·toluene (*cfr.* Paragraph 3.1.2). Each moiety contains a PF_6 anion, a toluene solvent molecule and a Zn(Me2tpa)DBSQ monocation. In each of these molecules the Zn^{II} ion is in a six-coordinate, distorted octahedral coordination, with two oxygen and four nitrogen donor atoms. The tripodal ligand Me2tpa adopts a folded conformation around the metal ion, with DBSQ acting as a bidentate ligand. This leads to Zn-N bond lengths in the range 2.15-2.31 Å and 2.14-2.28 Å for the two units, while two

types of Zn-O distance are observed (2.00-2.01 Å and 2.10-2.14 Å). For both the units the relevant bond lengths in the dioxolene units are in the expected range for the semiquinonato oxidation state,[24] with C-O ranging from 1.269 to 1.290 Å and C1-C2 being 1.455 and 1.472 for each moiety.

The analysis of the crystal packing and intermolecular contacts also revealed some interesting features. The two molecules constituting the asymmetric unit are interacting through a couple of σ–π interaction between the semiquinonato ligand on one molecule and an orthogonal pyridine on the adjacent one, with C_{py}-SQ centroid distance of 3.7-4.0 Å. Even more relevant is the stacking interaction between the molecule containing a Zn2 centre and the adjacent one, which is reported by symmetry. In this case a π–π interaction between pyridine rings, with distance of 3.5 Å between the respective centroids, is active. The combination of these different interacting paths results in a series of four interacting molecules which repeats along a chain approximately developing in the *ab* plane (Figure 4.2, below).

4.2.2 The solid solutions

Four different solid solutions of formula $[Co_xZn_{(1-x)}(Me_2tpa)(DBSQ)]PF_6 \cdot C_6H_5CH_3$ (x = 0.05; 0.15; 0.25; 0.50) were prepared to investigate the role of the elastic interactions in the entropy- and optically- driven valence tautomeric interconversion of **1**·toluene.[†] The actual Co molar ratio for each dilution has been assessed by magnetometric means, comparing the high temperature magnetisation values with the experimental ones of the pure compound **1**·toluene and the corresponding pure Zn derivative. The ionic radii of Co^{II} and Zn^{II} are very close to each other (0.745 *vs* 0.74 Å), and the host $[Zn(Me_2tpa)(DBSQ)]PF_6 \cdot C_6H_5CH_3$ is isomorphous with the Co derivative, and so it can be considered to be isostructural with the pure Co derivative in its *hs*-Co^{II} - SQ charge distribution, whose structure could not be solved. On its turn, this strongly suggest that the doping of Co^{II} in the Zn analogue occurs with no relevant structural variations of the host molecular structural parameters. This has been anyway checked by recording the X-ray powder diffractogram of the 50% doped Co derivative of **1**·toluene and comparing it with theoretical diffractogram expected for a system isostructural with **1**·toluene, the $[Zn(Me_2tpa)(DBSQ)]PF_6 \cdot C_6H_5CH_3$ taken at 120 K.

[†] The host $[Zn(Me_2tpa)(DBSQ)]PF_6 \cdot C_6H_5CH_3$ complex was synthesized according to the previously reported procedure.[14] Solid solutions of **1**·toluene in the Zn host have been obtained by recrystallisation from toluene of stoichiometric amounts of the complexes.

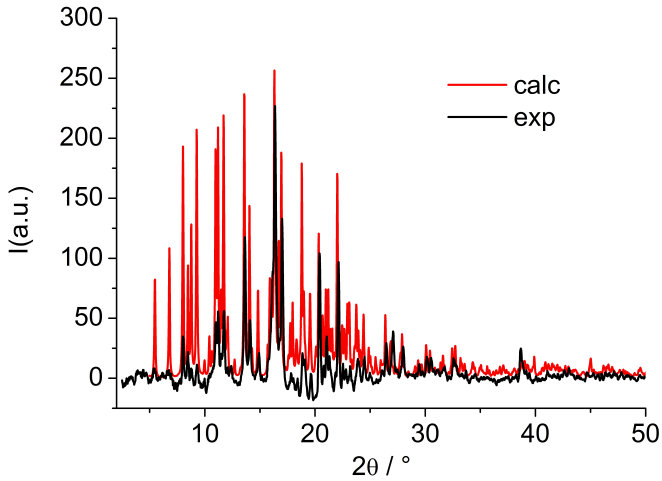

Figure 4.3. X-Ray powder diffractogram of $[Co_{0.5}Zn_{0.5}(Me_2tpa)(DBSQ)]PF_6 \cdot C_6H_5CH_3$ taken at room temperature (black line) compared to the one calculated from the crystal structure of $[Zn(Me_2tpa)(DBSQ)]PF_6 \cdot C_6H_5CH_3$ taken at 120 K.

All the peaks in the theoretical diffractogram are observed in the doped compound indicating that on doping the crystal structure is maintained. Furthermore, since no extra peaks occur, it can be safely concluded that only one, homogeneous, crystalline form is present in the sample, thus confirming the formation of mixed Zn/Co crystals.

4.3 The dependence of the transition temperatures on cooperativity

The transition temperature has been the first parameter to be investigated in function of the degree of dilution. In order to do that the temperature dependence of the valence tautomeric equilibrium for the four solid solutions of **1**·toluene into the homologous Zn based host has been followed by magnetometric means. The results are reported in Figure 4.4.

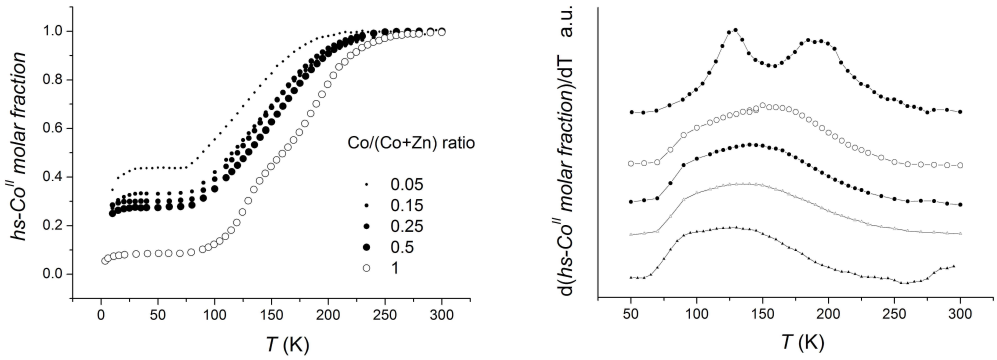

Figure 4.4. *Left*. Thermal evolution of the *hs*-Co^{II} molar fraction with temperature for a series of differently Co/Co+Zn diluted solid solutions of **1**·toluene. *Right*: Rate of variation expressed as *d(hs-Co^{II} molar fraction)/dT vs. T*.

The thermal dependence of the *hs*-Co^{II} – SQ molar fraction is plotted in the left side of Fig. 4.4. This value has been extrapolated from the magnetometric analysis paying attention to remove the contribution arising from the paramagnetic host lattice. This can be accomplished considering the two contributions adding one to each other, affording to the relation

$$\chi_M T_{CoSQ} = \frac{\chi_M T_{meas} - (1-x)\chi_M T_{ZnSQ}}{x} \tag{4.2}$$

where $\chi_M T_{CoSQ}$ is the contribution due to the VT material, while $\chi_M T_{ZnSQ}$ comes from the radical host (thus evaluated as 0.375 emu (K mol)$^{-1}$), $\chi_M T_{meas}$ is the experimentally accessible value and x is the Co molar fraction in the material. Considering the $\chi_M T_{CoCat}$ to be zero, the *hs*-Co^{II} molar fraction can be extrapolated by the data treated according to Eq. 4.2 with a normalisation at 300 K. The reported data highlight several features.

1. the entropy driven transition becomes more gradual with increasing dilution. This behaviour is well documented for solid solutions of spin-crossover complexes,[19,21,22] and it has been usually assigned to the loss of cooperativity of the interconverting centres, since this interaction can be assumed to be proportional to the square of the molar fraction of the interacting species, $\gamma^2_{hs-Co^{II}-SQ}$.[6]

2. the $T_{½}$ for the different solid solutions, shown in the right panel of Figure 4.3 evidences that the thermal interconversion temperature decreases with increasing dilution. This has been highlighted in Figure 4.5.

3. the low temperature $\gamma_{hs-Co^{II}-SQ}$ fraction increases, suggesting that an increased amount of high temperature form is incapable of showing VT.

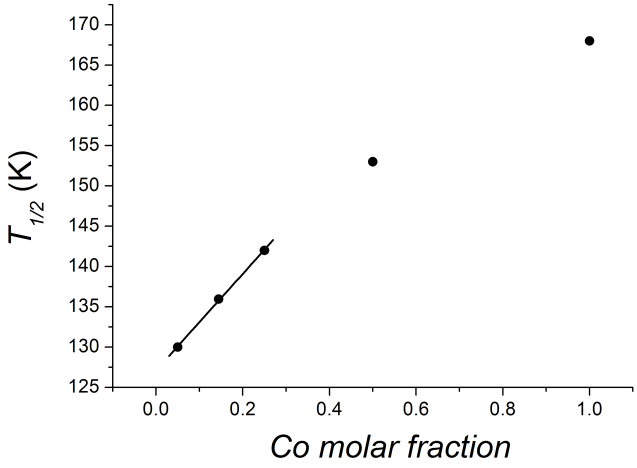

Figure 4.5. The $T_{½}$ dependence of the solid solutions of **1**·toluene on the Co/(Co+Zn) molar ratio.

The observed pattern can be explained in terms of change of internal pressure, determined by the radius of the ions of the host. Indeed, when the host is made up of ions with larger radius than the guest one, it can be considered to exert a "negative pressure" on the guest system, thus favouring the interconversion towards the larger species. The effect of smaller ionic radius for the host compared to the guest is the opposite. Since the ionic radius of the zinc(II) ion is very similar to that of the *hs*-cobalt(II) ion and much larger than the *ls*-cobalt(III), the induced negative pressure stabilises the cobalt(II)-semiquinonato species, leading to a decrease of $T_{½}$ with increasing dilution.

At low Co molar fractions we found an roughly linear dependence of the $T_{½}$ on the Co concentration in the sample, with a rate of $T_{½}$ variation of 69(2) K / Co molar fraction in the solid solution, and an estimated conversion temperature at infinite dilution of 126.6(6) K. This value can be assumed to be the transition temperature of **1**·toluene free from cooperative interactions in the solid state.

Finally, an enhancement of the residual cobalt(II)-semiquinonato species is observed with increasing dilution. Again this can be explained by taking into account the negative pressure of the host lattice. All of the observed data compare well with the

similar ones reported for spin crossover complexes.[19,21,22] For these systems both the enthalpy and entropy changes associated with the spin conversion decrease with dilution if a negative pressure is operative; in particular the determining role of vibrational entropy change with dilution has been recently stressed by Real and coworkers.[20]

4.4 Lattice interactions' effects on the optically induced valence tautomerism

In the following we present the second part of our investigation about the role of elastic interactions on the transition features of optically triggered VT materials. We have followed the dependence of the metastable state lifetime at low temperature, in a pure quantum activated relaxation regime, and at high temperature, where a crossover in the relaxation process takes place, and the VT system relaxes to the electronic ground state with a classic thermally activated barrier overcoming mechanism.

4.4.1 The tunnelling relaxation regime

In order to investigate the dynamics of relaxation of the photoinduced metastable state in function of solid dilution, the four solid solutions were irradiated at 904 nm and 9 K to induce the interconversion of cobalt(III)-catecholato to cobalt(II)-semiquinonato moieties. The kinetic decay of the photoinduced metastable state to the ground state has been measured at the same temperature by recording the time dependent magnetization of the samples 35 s after having switched off the light source at the photostationary limit of each sample, in order to get insight into the low-temperature tunneling relaxation regime of **1**·toluene. The normalised converted paramagnetic molar fraction γ *vs* time patterns are shown in Figure 4.6.

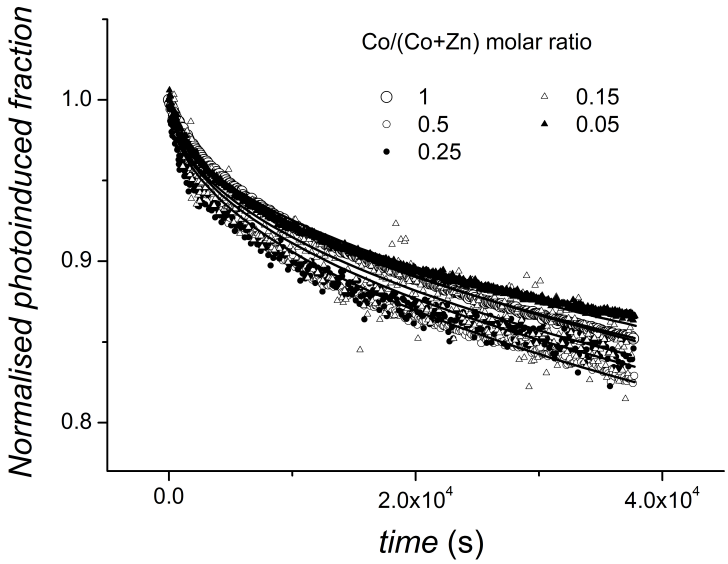

Figure 4.6. Normalised converted fraction $\gamma(t)$ decay after laser irradiation at 904 nm at 9 K for differently diluted solid solutions of **1**·toluene in its zinc analogue. The full lines are the fitting curves whose equations are described in the text.

The relaxation times at 9 K obtained for the pure compound as well as its four solutions are almost independent of the degree of metal dilution. This has been confirmed by fitting each curve using the stretched exponential function described in Eq. 3.1.

The relaxation times obtained fitting the time evolution of the *hs*-Co^{II}SQ molar fraction shown in Fig. 4.6 are shown in Table 4.1. In order to reduce the correlation between the τ and β parameters the τ values have been extrapolated keeping the β parameter fixed at 0.5 value.

Co molar ratio	1	0.5	0.25	0.15	0.05
r[1]	1.481 ± 0.004	1.021 ± 0.003	1.158 ± 0.008	1.264 ± 0.011	1.665 ± 0.004

[1] Relaxation times, measured at 9 K, as expressed in Ms.

Table 4.1. Relaxation times of **1**·toluene along with its four solid solutions as extrapolated using the stretched exponential fitting function described in the text.

Again the best fitting parameters τ shown in Table 4.1 fully agree with a decay process independent of the concentration of the metastable species. It must be noted

that only a fraction of molecules have relaxed to the ground state during the time window employed in these experiment. An accurate determination of τ would have required much longer experiments, not affordable for experiments at cryogenic temperatures.

4.4.2 The thermal activated relaxation regime

We extended our investigation of the role of cooperativity on the metastable state's lifetimes for the thermally activated relaxation regime. This relaxation behaviour has been analysed using the *T*(LIESST) approach described in Chapter I. On this regard, Létard and coworkers proposed a linear relationship (T(LIESST) = $T_0 - 0.3T_{½}$, where T_0 is a constant related to the symmetry of the first coordination sphere of each complex[25] for a family a closely structurally related complexes, but the results they have recently reported on a series of solid solutions of a spin crossover iron(II) complex in diamagnetic zinc analogues seem to contradict their paradigm and more in general the inverse gap energy law.[21,21,22] Indeed, the observed pattern of $T_{½}$, values follows the thermodynamic general expectation, but surprisingly the *T*(LIESST) values is found to be independent of the concentration of the paramagnetic iron(II) complex in the diamagnetic lattice.

With this in mind, we have analysed the relaxation features of **1**·toluene in the thermally assisted relaxation regimes measuring the *T*(LIESST) values of the different solid solutions. The results are shown in Figure 4.7, reporting the temperature dependence of the normalized photoinduced *hs*-Co^{II}SQ molar fraction. It is rather evident that the *T*(LIESST) values for the solid solutions at different Co concentrations are the same, within our experimental error.

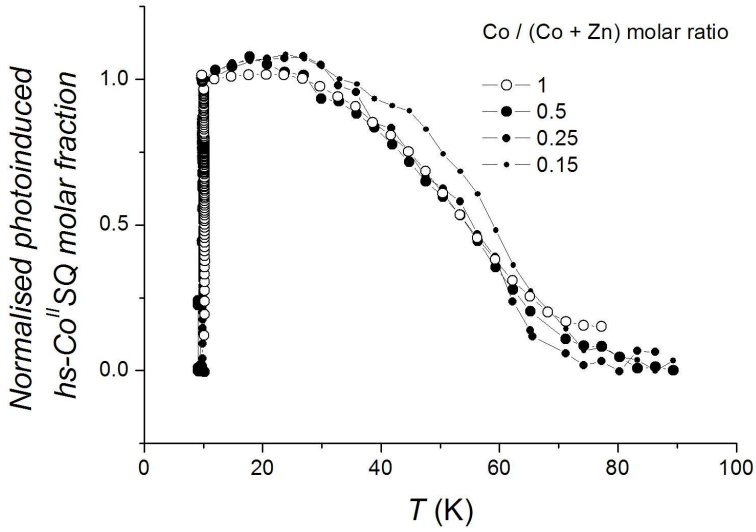

Figure 4.7. *T*(LIESST) pattern for **1**·toluene and its different diluted solid solutions.

The observed results have been rationalised on the basis of a nonadiabatic process within the framework of the Jortner radiationless multiphonon relaxation,[26,27] predicting a thermally activated behaviour of the relaxation decay as well as a temperature independent relaxation rate at cryogenic temperatures. The latter phenomenon is explained in terms of tunnel effect between the vibronic levels belonging to different electronic states.

In a simplified view the phenomenon is usually described by means of the energy potential diagram where the two redox isomers Co^{III}-Cat and Co^{II}-SQ are represented by the two harmonic potential energy curves. In the present case the Co^{III}-Cat redox isomer lies at lower energy than Co^{II}-SQ and therefore constitutes the ground state species. In classic kinetics, the relaxation rate from one state to the other is controlled by the thermal energy necessary to overcome the free energy barrier between the two potential curves. In a quantum mechanic approach, the tunneling probability for a non radiative process is determined by both intramolecular and intermolecular vibrations. Since the latter are significantly smaller with respect to the former, it is usually assumed that they could be simply expressed by an appropriate parameter. As a matter of fact we have found for several 1:1 Co:dioxolene systems that the temperature dependence of the tunneling rate in the low temperature region follows a thermally activated pseudo-Arrhenius behavior with a pseudo-activation energy of 5-15 cm^{-1} which is attributed to a process promoted by low-energy phonons.[8,13-15] This supports the hypothesis that the intermolecular vibrations do not play a significant role, though in principle they cannot be neglected since the phonon bath provides the continuum of states required for the non adiabatic process. However,

when the relaxation decay follows a thermally activated behaviour, the observed activation energies lie close to 300 cm^{-1}, *i.e.* the one associated to the symmetric breathing mode. Therefore in practice the non radiative process is determined by the overlap of a given vibrational level *k* of the symmetric breathing mode of the Co^{II}-SQ state and a vibrational level $i + n$ of the analogous mode of Co^{III}-Cat one. Following this treatment, the relaxation from the metastable state is expected to slow down as the difference in bond lengths between the two isomers increases and the electronic coupling and the zero point energy difference decrease.

The lifetimes reported in Table 4.1 are related to the temperature independent relaxation regime. Since the electronic coupling and the difference in bond lengths can be reasonably expected not to vary with dilution, the above mentioned theoretical expectations that the lifetimes of the metastable species would increase with dilution were based on the expectation of a decrease of the reduced energy gap ΔG^0, as a result of the stabilization of the metastable Co^{II}-SQ species by the zinc host pictorially described in Figure 4.1. However, the similarities of the observed lifetimes suggest that reduced energy gap does not significantly vary upon dilution. On the other hand, the clear decrease of the critical temperature for the entropy driven transition on decreasing the Co:Zn ratio can be attributed to the gain in mixing entropy. Thus, as far as this chemical approach is used to test the cooperativity effects onto the kinetics of relaxation in tunnelling conditions, we can state that optical bistability in this class of compounds is related to single molecular properties and not to a three dimensional network of interactions able to stabilize in time the photoinduced metastable state.

In this framework, also the observed independence of *T*(LIESST) value from the doping level can be easily explained. Indeed, *T*(LIESST) is intrinsically associated to a temperature range where the rate of decay of the metastable state is temperature dependent. Therefore since the energies of the involved vibrational levels do not appear to vary with the dilution, it is expected that the relaxation kinetics should be characterised by similar Franck-Condon factors. If this consideration holds, it is highly reasonable to observe similar *T*(LIESST) for solid solutions at different concentrations.

References

[1] Gatteschi, D.; Sessoli, R. *Angew. Chem. Int. Ed.* **2003**, *42*, 268-297.

[2] Wernsdorfer, W. *Nature Mater.* **2007**, *6*, 174-176.

[3] Hauser, A. *Light-Induced Spin Crossover and the High-Spin -> Low-Spin Relaxation* in *Spin Crossover in Transition Metal Compounds II*; Gütlich, P.; Goodwin, H. A., Eds.; Springer: Berlin, 2004; Vol. 234, pp 155-198 .

[4] Krober, J.; Codjovi, E.; Kahn, O.; Groliere, F.; Jay, C. *J. Am. Chem. Soc.* **1993**, *115*, 9810-9811.

[5] Garcia, Y.; Niel, V.; Munoz, M. C.; Real, J. A. *Spin Crossover in 1d, 2d and 3d Polymeric Fe(II) Networks* in *Spin Crossover in Transition Metal Compounds I*; Gütlich, P.; Goodwin, H. A., Eds.; Springer: Berlin, 2004; Vol. 233, pp 229-257.

[6] Spiering, H. *Elastic Interaction in Spin Crossover Compounds* in *Spin Crossover in Transition Metal Compounds III*; Gütlich, P.; Goodwin, H. A., Eds.; Springer: Berlin, 2004; Vol. 235, pp 171-195.

[7] Jung, O. S.; Pierpont, C. G. *J. Am. Chem. Soc.* **1994**, *116*, 2229-2230.

[8] Beni, A.; Dei, A.; Shultz, D. A.; Sorace, L. *Chem. Phys. Lett.* **2006**, *428*, 400-404.

[9] Decurtins, S.; Gütlich, P.; Köhler, C. P.; Spiering, H.; Hauser, A. *Chem. Phys. Lett.* **1984**, *105*, 1-4.

[10] Decurtins, S.; Gutlich, P.; Hasselbach, K. M.; Hauser, A.; Spiering, H. *Inorg. Chem.* **1985**, *24*, 2174-2178.

[11] Hauser, A. *J. Chem. Phys.* **1991**, *94*, 2741-2748.

[12] Hauser, A.; Vef, A.; Adler, P. *J. Chem. Phys.* **1991**, *95*, 8710-8717.

[13] Beni, A.; Dei, A.; Rizzitano, M.; Sorace, L. *Chem. Commun.* **2007**, 2160-2162.

[14] Beni, A.; Dei, A.; Laschi, S.; Rizzitano, M.; Sorace, L. *Chem., Eur. J.* **2008**, *14*, 1804-1813.

[15] Dapporto, P.; Dei, A.; Poneti, G.; Sorace, L. *Chem., Eur. J.* **2008**, *14*, 10915-10918.

[16] Martin, J. P.; Zarembowitch, J.; Bousseksou, A.; Dworkin, A.; Haasnoot, J. G.; Varret, F. *Inorg. Chem.* **1994**, *33*, 6325-6333.

[17] Haddad, M. S.; Federer, W. D.; Lynch, M. W.; Hendrickson, D. N. *J. Am. Chem. Soc.* **1980**, *102*, 1468-1470.

[18] Haddad, M. S.; Federer, W. D.; Lynch, M. W.; Hendrickson, D. N. *Inorg. Chem.* **1981**, *20*, 131-139.

[19] Constantmachado, H.; Linares, J.; Varret, F.; Haasnoot, J. G.; Martin, J. P.; Zarembowitch, J.; Dworkin, A.; Bousseksou, A. *J. Phys. I* **1996**, *6*, 1203-1216.

[20] Tayagaki, T.; Galet, A.; Molnar, G.; Munoz, M. C.; Zwick, A.; Tanaka, K.; Real, J. A.; Bousseksou, A. *J. Phys. Chem. B* **2005**, *109*, 14859-14867.

[21] Balde, C.; Desplanches, C.; Wattiaux, A.; Guionneau, P.; Gutlich, P.; Letard, J. F. *Dalton Trans.* **2008**, 2702-2707.

[22] Balde, C.; Desplanches, C.; Gutlich, P.; Freysz, E.; Letard, J. F. *Inorg. Chim. Acta* **2008**, *361*, 3529-3533.

[23] Cafun, J. D.; Londiniere, L.; Riviere, E.; Bleuzen, A. *Inorg. Chim. Acta* **2008**, *361*, 3555-3563.

[24] Pierpont, C. G.; Buchanan, R. M. *Coord. Chem. Rev.* **1981**, *38*, 45.

[25] Letard, J. F. *J. Mater. Chem.* **2006**, *16*, 2550-2559.

[26] Adams, D. M.; Hendrickson, D. N. *J. Am. Chem. Soc.* **1996**, *118*, 11515.

[27] Buhks, E. ; Navon, G.; Bixon, M.; Jortner, J. *J. Am. Chem. Soc.* **1980**, *102*, 2918–2923.

Chapter V

X-Ray Absorption Spectroscopy for the investigation of Co-dioxolene valence tautomeric materials

The magnetometric analysis presented in the previous chapters let us reveal the conversion features of the entropy and optically driven valence tautomeric interconversion for different Co:dioxolene systems, but was unable to provide a detailed description of the electronic states characterising the two redox isomers. In the following we present an X-Ray Absorption Spectroscopy investigation of the redox bistability of 1:1 Co:dioxolene materials, able to elucidate the electronic structure of the species involved in the entropy and optically driven process. The fine structure of the spectra gave as well information about the structural features of both transitions. By tuning the energy of the X-photons it was possible to control their role in the investigations presented, shifting from probe of the electronic states to pump of the photoinduced population of the metastable state at low temperature.

5.1 Synchrotron radiation

With the advent of easily accessible II generation synchrotron radiation sources in the 80's, like the AT&T Bell Laboratories' Dragon at the National Synchrotron Light Source in New Jersey or such as the Photon Factory in Japan, the research activity on bistable molecular materials faced a new set of spectroscopic tools to elucidate the structural and electronic features of the systems. This electromagnetic radiation is generated by the deviation of a beam of electrons accelerated at relativistic energies by means of a magnetic field: the energy loss involved in this process is released radiatively and gives rise to a very wide, continuous, spectrum. In a synchrotron electrons are produced by means of an electron gun and accelerated by a linear accelerator up to relativistic energies of the order of several tens of MeV. They are then moved into the so called "booster ring", where their energy is increased up to the GeV range, and then pass into the "storage ring", a twelve side polygon featuring straight and curved sections. In the latter some magnets (bending magnets and insertion devices) apply a centripetal force to the electron beam with the consequent emission of electromagnetic radiation.
This radiation has a set of unique features:

- **High brightness**: the X-ray beam is extremely intense (hundreds of thousands of times more than conventional X-ray tubes) and collimated.

- **Wide frequency spectrum**: the mechanism of light generation affords a continuous frequency spectrum ranging from IR (10^{-6} eV) to the Hard X-rays (10^{4} eV).

- **High degree of polarisation**: the light emitted in the plane of electrons' motion is linearly polarised, while in the upper and lower regions is circularly polarised. The latest generation of monochromatizing units (undulators and wigglers) afford pure polarisation states.

In the following sections we present a brief experimental overview of synchrotron radiation, considering the different parts of a synchrotron responsible for the production of this particular electromagnetic radiation (bending magnets and insertion devices) and the available detection systems for the measurement of XAS, which can afford information related to different zones of the samples in analysis.

5.1.1 Bending magnets

Bending magnets (BMs) are the parts of the storage ring that alter the linear motion of electrons by giving them a transverse acceleration that introduces the beam into the next straight section of the ring. Such centripetal acceleration results in a loss of kinetic energy, released as emitted photons. The electromagnetic radiation is emitted in a cone propagating in a direction that is tangent to the trajectory of the electrons and the photon energy range depends on several parameters, but typically spreads from the infrared to hard x-rays, highest intensity being reached in the x-ray region (*cfr.* upper part of Figure 5.1).

A parameter that is often used to characterize radiation sources is brightness, which is defined as:

$$\text{Brightness} = \frac{\text{Photons}}{\text{Time} \cdot \text{Beam collimation} \cdot \text{Source area} \cdot \text{Spectral distribution}}$$

where beam collimation is expressed in mrad^2 and relates to the degree of divergence of the photon beam as it propagates, while the source area corresponds to the electron beam size in units of mm^2. Spectral distribution refers to the photon energy range accepted for the experiment and a bandwidth of 0.1% is taken by convention.

The electric component of electromagnetic radiation is parallel to the acceleration vector and therefore the light emitted by a bending magnet is linearly polarized in the plane of the storage ring. This is not true for the radiation emitted above or below the plane of the storage ring, which is elliptically polarized.

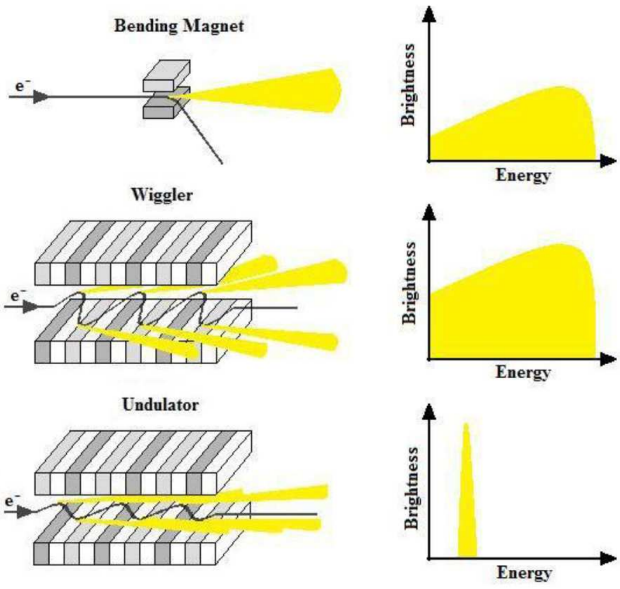

Figure 5.1. *Left*: Schematic representation of a bending magnet, a wiggler and an undulator. *Right*: Diagram of typical brightness profile produced by these radiation sources.

5.1.2 Insertion devices

Working with bending magnets, brightness can be increased either by using higher magnetic fields or increasing the kinetic energy of the electron beam. None of the two solutions, however, is convenient from an experimental as well as an economical point of view. To overcome this limit and obtained higher brightness beams, insertion devices (IDs) were designed. In addition to this advantage, IDs yield photons with greater coherence over a wider energy range. IDs are made up of periodic arrays of magnets placed above and below the electron pathway in straight section of the storage ring (middle part of Figure 5.1). The array is formed by contiguous sections in which magnetization direction is opposite from one another, so electrons travelling through the ID are continuously deviated into a wiggling motion. At each change of trajectory, photons are emitted. IDs are divided into two categories: wigglers and undulators, and are able to produce linearly or elliptically polarized light.

Wigglers are composed of magnetic sections cause a large oscillation amplitude of the electrons, due to high static magnetic fields. The larger number of deviations to which the electrons undergo with respect to the ones occurring in BMs

leads to an overall higher energy (10-20KeV) and brightness comparably to that emitted from BMs, but to a poorer are poorly collimation.

In **undulators** on the other hand, the magnetic sections are weaker, so electrons are deviated less significantly oscillate with reduced amplitude. This results in a narrower radiation cone and a smaller spectral width. By changing the distance between the upper and lower rows of magnets, thus the field intensity in the gap, the energy interval can be tuned into the appropriate range. Radiation produced by undulators is horizontally polarized light, similar to that produced by wigglers; however, by using four sets of magnet arrays, two above and two below the electron pathway, it is possible to control polarization of the photons in any desired way by changing the relative positions of the four sets. More precisely, translation of the four quadrants changes the phase between the vertical and horizontal components of the magnetic field (B_x and B_y). When B_x and B_y are dephased by a $\pi/2$ factor circularly polarized x-rays are generated, while for a π phase shift, vertically polarized X-rays are obtained.

5.1.3 Detection methods

5.1.3.1 Transmission

The measurement of X-ray absorption in transmission mode follows a typical layout where the sample is placed between a source of X-rays and a detector (typically a gas ion chamber), which measures the transmitted photon flux. The signal recorded is referred to as sample transmission spectrum (I) and its measurement as a function of energy leads to an absorption spectrum. The transmitted intensity is them compared to the incident photon flux (I_0) to obtain the optical density (OD) as a function of photon energy:

$$OD = -\ln\frac{I}{I_0} \tag{5.1}$$

OD can be related to sample of thickness t (cm) and to the elements it contains:

$$OD = \mu(E)\rho t \tag{5.2}$$

where μ, the mass absorption coefficient ($cm^2 \cdot g^{-1}$) and ρ, the sample density ($g \cdot cm^{-3}$) are element specific with μ being related to the atomic absorption cross section σ_x by

$$\mu = \frac{N_A}{MW} \sum_i n_i \sigma_{xi} \tag{5.3}$$

where N_A is Avogadro's number, σ_{xi} the absorption cross section for the n_i atoms of each element i and MW is the molecular weight of the compound. In the case of molecular compounds this detection mode samples the whole depth of the investigated material.

5.1.3.2 Total electron yield

The formation of a core-hole due to photo-excitation of a core electron upon x-ray absorption creates short lived core excited states and leads to a series of relaxation processes. The deexcitation pathways foresee the emission of fluorescence photons and Auger electrons, schematically reported in Figure 5.2. The relative probability of each process is related to the atomic number Z of the elements: for absorption edges below 2000 eV, Auger electron emission dominates the relaxation processes. As represented in Figure 5.2, Auger electrons are created when a valence electron decays in order to refill the core-hole vacancy. During the decay process the excess of energy released by the valence electron is transferred to another valance electron, the Auger electron, which is then emitted.

Total electron yield (TEY) detection is achieved by measuring the drain current from the sample, which is proportional to the number of Auger electrons and photoelectrons leaving the sample. The incident photon flux I_0 is monitored by measuring the drain current from a mesh located upstream from the sample and is used to normalize the sample current I according to:

$$TEY = \frac{I}{I_o} \tag{5.4}$$

TEY is experimentally simple to measure and extremely surface sensitive, since only the first ~2 nm of the sample surface are probed, since for longer paths of the electron travelling in the solid sample self-absorption phenomena occur.

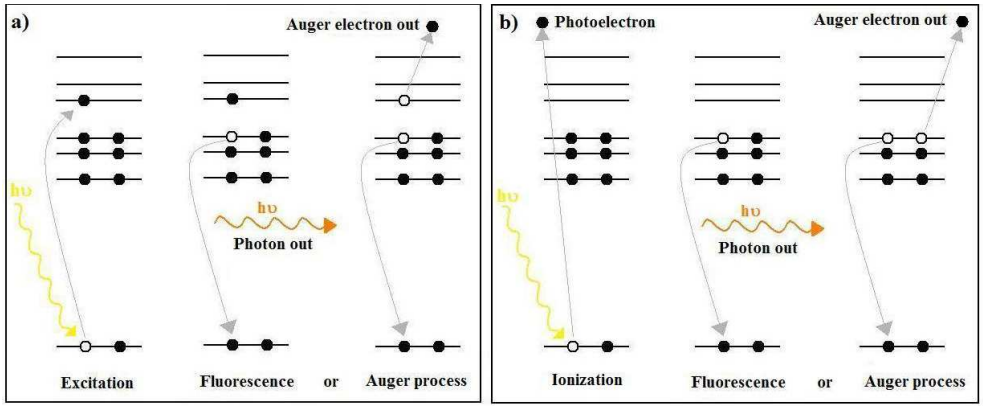

Figure 5.2. Schematic description of the phenomena occurring during the X-rays absorption and subsequent relaxation, in the case of bound (*left*) and continuum states (*right*) excitations.

5.1.3.3 Fluorescence

A third detection method commonly used is the measurement of photons emitted by radiative decay. This relaxation channel is most efficient for high energy excitations (>2000 eV), yet it can be used also for lower photon energy. Emitted photons can be detected with a gas proportional chamber or a diode. As for electron yield, fluorescence is proportional to the number of absorbed photons but, differently from TEY it is able to probe deeper portions of the sample, down to a few tens of nm.

5.2 The phenomenology of X-Ray Absorption spectroscopy

X-ray Absorption Spectroscopy (XAS) is a very powerful tool for the analysis of electronic and structural features of metallo-organic systems. The phenomenon of X-ray light absorption features peculiarity of striking interest for the investigation of bistable compounds:

- **Atomic selectivity**: the absorption process involves inner cores of atoms and thus the peak's energy is a fingerprint of the atomic species;

- **Sensitivity to charge**: XAS is related to transitions from inner core level to first empty orbitals, whose energy relies on the oxidation state of the absorbing atom;

- **Sensitivity to spin state**: Using circularly polarised light is possible to selectively trigger transitions between spin sublevels and to gain insight into the local magnetism of the absorber (XMCD);

- **Access to the coordination sphere**: Constructive diffraction patterns of photoelectrons afford direct access to the coordination environment around the atom even in absence of structural long range order (EXAFS).

In order to understand the phenomenology of XAS, we discuss briefly in the following from a quanto-mechanical point of view the basis of X-ray absorption.

5.2.1 The one electron approximation

A simplified view of the physical processes involved in the absorption of X-rays by matter can be gained using the so called "one electron approximation" or also "active electron approximation".[1] In this picture the energy levels involved in the transition are thought independent of electronic correlation and act as a "inert landscape" where the electrons roam free after the excitation by X-ray light. This treatment is of course an oversimplification of the physics underlying the phenomenon of X-ray absorption and can not be invoked to treat on a quantitative basis the spectra of d^n transition metal ions ($n \neq 1, 9$, for which we address the reader to paragraph 5.3.3), but indeed they assure us an easier exposure of the physical phenomena triggered by X-ray absorption. When X-rays travel through matter in the solid state, two phenomena take place: absorption and scattering. The latter, consisting in light emission from matter excited by X-rays, can be elastic or anelastic and gives rise to a wide set of spectroscopies. On this theme excellent reviews can be found in literature.[2] Figure 5.3 points out the electronic states of an atom absorbing X-ray with different energies, introducing the reader to the terminology used throughout the text.

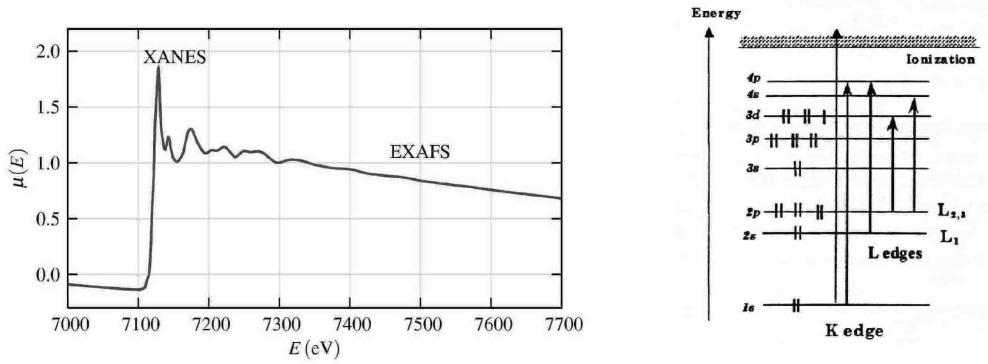

Figure 5.3. *Left*: The Fe K-edge of FeO as paradigm of XAS spectrum, pointing out the XANES and the EXAFS regions. *Right*: Different absorption processes of X-ray radiation by matter.

Figure 5.3 helps also in clarifying what happens in a standard XAS experiment. In this case the X-rays absorption coefficient $\mu(E)$, defined as

$$I(x) = I(0)e^{-\mu x} \tag{5.5}$$

is measured in function of the energy of the X-ray beam. Two main regions can be highlighted in the spectrum reported in the left side of Figure 5.3: the XANES (X-Ray Absorption Near Edge Spectroscopy) at lower energies, and the EXAFS (Extended X-Ray Absorption Fine Structure). On the right side of the figure are reported the corresponding transitions classified according to the one electron approximation.

XANES region: this region concerns transitions to bound states of the excited system. When the photon energy $\hbar\omega$ is lower than the binding energy E_b of the core level considered, the corresponding electron cannot be excited. This "pre-edge" region contains essentially contributions from the excitation of less energetic core levels (the tails of the corresponding absorption edges) if any or, for ions for instance, it corresponds to the excitation of the core electron to empty states of lower binding energy. The "edge", or white line, so called for the white dot impressed on the film tapes of the old X-rays detectors, corresponds to the situation where $\hbar\omega = E_b$. In this case the photon energy matches exactly the energy difference of the levels involved in the absorption process and a peak in the absorbance profile appears. This part of the spectrum reports the peaks corresponding to transitions from the inner core levels to empty bound atomic states; the spectrum gives hints about the higher levels of the system. For non correlated materials, this is essentially the density of empty states while for correlated systems, the multiplet structure dominates the spectra. The "name" of the edge depends upon the core electron which is excited: the principal

quantum numbers n=1, 2, and 3, correspond to the K-, L-, and M-edges, respectively. Due to the quantum mechanical selection rules for electric-dipole allowed transitions ($\Delta l = \pm 1$, *cfr.* paragraph 5.2.3) the $1s \rightarrow 4p$ and to the $2p \rightarrow 3d$ transitions are the most relevant for the K-edge and L-edge, respectively (*cfr.* right side of Figure 5.3). In this range of energies it is possible to extract information about the electronic structure of the absorber atom.

EXAFS region: Increasing the energy of the incoming photon, we face the EXAFS region, ranging from 50 eV up to over 1000 eV after the main resonance peak. At these energies electrons are removed from the atoms and move in the crystal, being scattered one or several times by the surrounding atoms. Analysing the phase of the wave vector of the back-scattered electron in function of its energy is possible to take out structural information of the absorber.

5.2.2 The X-ray absorption theoretical description

The phenomenon of X-ray absorption by matter can be rationalised as a time dependent perturbation (the electromagnetic field of the propagating radiation) of the atomic levels (described by the stationary Hamiltonian containing electron/nucleus and electron/electron interactions). In a non relativistic approach, the transition probability T_{if} for this process can thus be expressed using the formalism developed by Kramers and Heisenberg[3] and by Dirac[4] as

$$T_{if} = \frac{2\pi}{\hbar}\left|\langle f|\mathcal{H}_{int}|i\rangle + \sum_n \frac{\langle f|\mathcal{H}_{int}|n\rangle\langle n|\mathcal{H}_{int}|i\rangle}{\varepsilon_i - \varepsilon_n}\right|^2 \rho(\varepsilon_f) d(\varepsilon_i - \varepsilon_f) \tag{5.6}$$

where

$$\mathcal{H}_{\text{int}} = \frac{e}{m_c}\vec{p}\cdot\vec{A} \tag{5.7}$$

is the Hamiltonian related to the interaction between the excited electron of rest mass m_e, charge e and momentum p and the electromagnetic field of the radiation, of potential vector A (we remind that the electric field of the radiation can be obtained from A according to $\vec{E} = \frac{\delta\vec{A}}{\delta t}$).

This expression provides some information about the physical actual process going on. In particular it states that the effect of the light/matter interaction to the

atomic electronic levels obtained by the atomic unperturbed Hamiltonian is a perturbation to the first (left term of the sum in Eq. 5.6) and second (right term) orders. Let us stress this point.

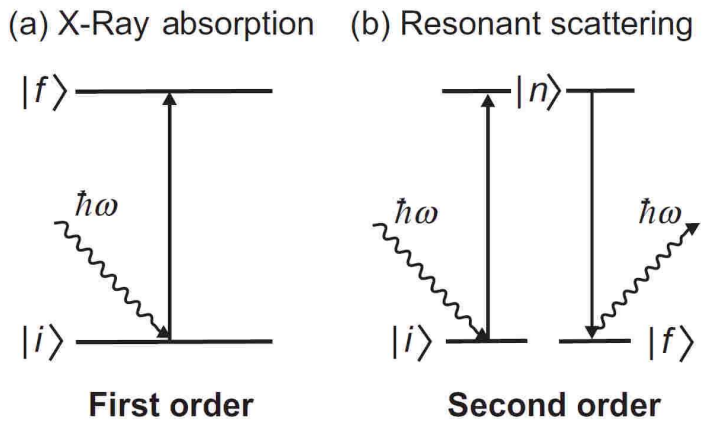

Figure 5.4. Scheme of the first and second order states transitions triggered by X-rays absorption.

- $\langle f|\mathcal{H}_{int}|i\rangle$ This term describes a first order correction to the energies of the levels resulting from the atomic Hamiltonian and provides a direct connection between the initial and final states of the system afforded by the light-matter interaction. In a classic view it corresponds to the allowed transition between the initial and final state induced by X-ray absorption.

- $\sum_n \frac{\langle f|\mathcal{H}_{int}|n\rangle\langle n|\mathcal{H}_{int}|i\rangle}{\varepsilon_i - \varepsilon_n}$ The second order correction to the Hamiltonian of non irradiated atom involves three states and is related to the scattering of light from the absorbing species. For a review *cfr.* 5.

An appropriate rearrangement of the terms present in Eq. 5.6 lets us calculate the intensities of the transitions. It has been shown[6] that it is possible to separate Eq. 5.6 in an electronic and a photonic part, evaluate the photon part, and obtain the matrix elements in terms of transitions between two electronic states. The matrix equation thus describing the photoinduced electronic transition assumes the form

$$\mathcal{M} = \langle b | \vec{p} \cdot \varepsilon \cdot e^{i\vec{k}\cdot\vec{r}} | a \rangle \tag{5.8}$$

where *a* and *b* are the initial and final electronic states of the system, *p* is the electron momentum, ε the unit photon polarization vector and *k* the photon wave vector.

Eq. 5.8 can be simplified on the basis of a simple structural consideration, usually referred to as the "electric dipole approximation". This approximation considers that the wavelength of the X-radiation is much longer (λ > 0.5 Å) than the radial linear extension of an atomic core orbital (0.02 Å for a *2p* orbital), and thus the electromagnetic field of the incident radiation can be thought as constant over the whole absorber and independent from their relative distance. In this case we can safely assume that

$$\mathcal{M} = \langle b | \vec{p} \cdot \varepsilon \cdot e^{i\vec{k}\cdot\vec{r}} | a \rangle = \langle b | \vec{p} \cdot \varepsilon \cdot (1 + i\vec{k} \cdot \vec{r}) | a \rangle \approx \langle b | \vec{p} \cdot \vec{\varepsilon} | a \rangle = i m_e \omega \langle b | \vec{r} \cdot \vec{\varepsilon} | a \rangle \tag{5.9}$$

where ω is the frequency of the photon triggering the transition. From Eq. 5.9 can be appreciated the removal of the *k* dependence of the transition matrix.
We are now able to write the explicit equation describing the X-ray absorption cross section, which, after an integration in the domain of energies, will provide us the intensities of the transitions.

$$\sigma = \frac{T_{if}}{\Phi_0} = 4\pi^2 \alpha \left| \langle b | \vec{r} \cdot \vec{\varepsilon} | a \rangle \right|^2 \partial[\hbar\omega - (E_b - E_a)] \rho(E_b) \tag{5.10}$$

where

$$\alpha = \frac{e^2}{4\pi\varepsilon_0 \hbar c} \approx \frac{1}{137} \tag{5.11}$$

is the fine structure constant. The calculation of the transition matrix element depends on the wavefunctions $|a\rangle$ and $|b\rangle$. In a one-electron picture, the initial state is given by the core electron wavefunction. The final state consists of the valence electron wavefunctions.

Integrating Eq. 5.10 in the resonance conditions, where the energy of the incoming X-photon matches the energy difference between the initial and final electronic state ($\hbar\omega = E_b - E_a$) and considering the electronic wavefunctions normalised, the intensity of the transition becomes

$$I_{res} = 4\pi^2 \alpha \hbar \omega \left| \langle b | \vec{r} \cdot \vec{\varepsilon} | a \rangle \right|^2 \tag{5.12}$$

5.2.3 The selection rules of X-ray absorption

In order to closer describing the set of information available from a XAS experiment we will show in this section the selection rules of absorption of polarised X-rays. In a general way we can state that photons are bosons with angular momentum quantum number L = 1 (in units of $\hbar$). We refer to their angular momentum as expectation value of the angular momentum operator along their direction of propagation, *e.g.* the z axis. This quantity can assume three different values:

- $l_z = 0$ for linearly polarised light;
- $l_z = 1$ for right circularly polarised light;
- $l_z = -1$ for left circularly polarised light. §

In the phenomenon of light absorption the photon momentum is transferred to the excited electron, thus triggering a change in orbital configuration. This picture can be explained taking in consideration the form of the transition operator and the initial and final states of the system appearing in Eq. 5.6.

The *r* vector, describing the excited electron position, can be written as

$$\vec{r} = x\vec{u}_x + y\vec{u}_y + z\vec{u}_z \tag{5.13}$$

where u_i are the space versors. Considering the k vector of the electromagnetic wave aligned along the z direction, the polarisation vector on the other hand can be expressed:

- for a linearly polarised wave: $\vec{\varepsilon} = \varepsilon_z$
- for circularly polarised wave: $\varepsilon_z^{\pm} = \pm \frac{1}{\sqrt{2}} (\varepsilon_x \pm \varepsilon_y)$

§ The sense of polarisation is referred to the sense of rotation of the electric field of the wave in its plane of propagation. This can be evaluated pointing the thumb in the direction of the k vector: for a right (left) polarised wave the rotation in time of the electric field follows the right (left) hand rule.

In a more general case, it is useful to express the polarisation vector according to Racah's spherical tensor operators,[7] defined as

$$C_m^{(l)} = \sqrt{\frac{4\pi}{2l+1}} Y_{l,m}(\theta,\phi) \tag{5.14}$$

and whose explicit description is given in ref 1. These formalism concerns a more general description of the transition operator for linearly and circularly polarised light propagating in each spatial direction. In this case the transition operator $P_\alpha^q = \vec{r} \cdot \vec{e}_\alpha^q$ may be written as a linear combination of these operators according to

$$P_\alpha^q / r = \sum_{p=0,\pm1} e_{\alpha,p}^q C_p^{(1)} = e_{\alpha,1}^q C_1^{(1)} + e_{\alpha,0}^q C_0^{(1)} + e_{\alpha,-1}^q C_{-1}^{(1)} \tag{5.15}$$

where the e_α^q may be imaginary and normalised to unity.

Concerning the general description of the wavefunctions of the initial and final electronic states of the system undergoing X-ray light absorption, the simplest way to express them is

$$\Psi(r) = R_{n,l}(r) \cdot Y_{l,m_l} \cdot \chi_{s,m_s} = \left| R_{n,l}(r); l, m_l, s, m_s \right\rangle \tag{5.16}$$

as the product of an orbital (made out of a radial, $R_{n,l}(r)$, depending on the first and second quantum numbers and on the electrons – nucleus distance r, and a angular part, Y, relying on the quantum numbers l and m_l) and spin functions. This form is the usual one for electrons moving in a central electrostatic field afforded by the nucleus and experiencing a mean repulsion from the other electrons.[8]

This expression is particularly fruitful for the understanding of the effect of the transition dipole operator P_α^q on the wavefunctions. It is possible in fact to factorise several elements of the transition matrix reported in Eq. 5.12, thus leading to a simple description of the selection rules for the X-ray absorption process.

$$\begin{aligned} &\left\langle b \left| \vec{P}_\alpha^q \right| a \right\rangle = \left\langle R_{n',l}(r); l, m_l, s, m'_s \left| \vec{P}_\alpha^q \right| R_{n,l}(r); l, m_l, s, m_s \right\rangle = \\ &\delta(m_s', m_s) \left\langle R_{n',l'}(r) \left| r \right| R_{n,l}(r) \right\rangle \sum_{m_s, m_l, p} e_{\alpha,p}^q \left\langle l', m_l' \left| C_p^{(1)} \right| l, m_l \right\rangle \end{aligned} \tag{5.17}$$

Some consideration can be extrapolated analysing each factor of Eq. 5.17.

$\left\langle R_{n',l'}(r)\middle|r\middle|R_{n,l}(r)\right\rangle$: Even if the radial part of the wavefunctions involved in the transition does not show dependence on the polarisation, it provides us some information about XAS. It is in fact possible to plot the matrix element corresponding to the radial part of the transition integral in function of the distance from the nucleus under excitation, as reported in Figure 5.5.

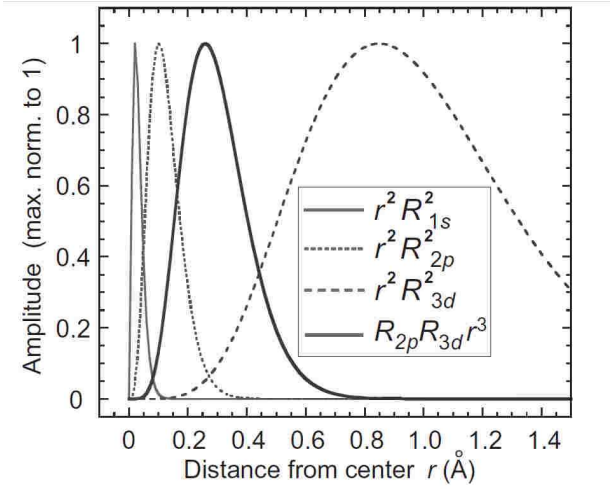

Figure 5.5: Dependence of the radial matrix element involved in X-ray absorption on the electron – nucleus distance for different energies of excitation.

The plot points out the strong atomic localisation of the excited orbital in the X-ray photon absorption process, since the maxima of the $r^2R_{1s}^2$ and $r^2R_{2p}^2$ functions are related to the spatial probability of finding the electron. In strikingly contrast with the standard UV-Vis optical spectroscopy, which is a probe essentially of molecular states, involving transitions in the eV range, thus between the HOMO and LUMO states of molecules, which are usually related to molecular orbitals with significant participation of the distinct molecular centres, XAS appears as an atomic states probe, at least for what concerns the initial state. From this feature arises the atomic and charge selectivity of XAS. It must be stressed, however, that this spectroscopy is able to detect also changes in the coordination environment parameters, like the strength of the ligand field, because of the sensitivity to the coordination of the final, excited, state.

$\sum_{m_s,m_l,p} e^q_{\alpha,p} \left\langle l', m_l' \middle| C^{(1)}_p \middle| l, m_l \right\rangle$: From this expression it is easy to highlight the effects of the application of the dipole moment operator on the initial wavefunction: it does not act on the spin part of the wavefunction, while it does on the angular part, which depends on the polarisation of the incident photon. In Table 5.1 are presented the nonzero matrix elements corresponding to the angular part of the wavefunctions.

$\langle l+1, m \vert C^{(1)}_0 \vert l, m \rangle$	$=$	$\sqrt{\frac{(l+1)^2 - m^2}{(2l+3)(2l+1)}}$
$\langle l-1, m \vert C^{(1)}_0 \vert l, m \rangle$	$=$	$\sqrt{\frac{l^2 - m^2}{(2l-1)(2l+1)}}$
$\langle l+1, m+1 \vert C^{(1)}_1 \vert l, m \rangle$	$=$	$\sqrt{\frac{(l+m+2)(l+m+1)}{2(2l+3)(2l+1)}}$
$\langle l-1, m+1 \vert C^{(1)}_1 \vert l, m \rangle$	$=$	$-\sqrt{\frac{(l-m)(l-m-1)}{2(2l-1)(2l+1)}}$
$\langle l+1, m-1 \vert C^{(1)}_{-1} \vert l, m \rangle$	$=$	$\sqrt{\frac{(l-m+2)(l-m+1)}{2(2l+3)(2l+1)}}$
$\langle l-1, m-1 \vert C^{(1)}_{-1} \vert l, m \rangle$	$=$	$-\sqrt{\frac{(l+m)(l+m-1)}{2(2l-1)(2l+1)}}$

Table 5.1: Non vanishing matrix elements of the angular part of Eq. 5.17 calculated for linear (*above*), right (*middle*) and left (*below*) polarisations of incident beam.

From the analysis of the nonzero matrix elements and considering also Eq. 5.17 we can lay down the *selection rules* for XAS:

- $\Delta l = l' - l = \pm 1$
- $\Delta m_l = m_l' - m_l = q = 0; \pm 1$
- $\Delta s = s' - s = 0$
- $\Delta m_s = m_s' - m_s = 0$

5.2.4 X-Ray Absorption spectroscopy on bistable molecular materials

The unique properties of the radiation summarised above boosted the research field of bistable molecular materials, allowing the investigations of structural features of the interconverting species. Pioneering work of Verdaguer *et al.* showed the possibility to address the spin state of different Ni^{II} complexes with a combined experimental and theoretical approach, based on XAS spectroscopy and subsequent simulation of the spectra, and dates back to 1987.[9] The ability of XAS to "look" into non crystalline environments was subsequently used by the group of Sato in 1998 to obtain structural information about the polycianometallate Prussian Blue analogues,[10] known to afford a light-triggered network of magnetic interactions in the solid state at cryogenic temperatures; one year later the same group succeeded in the first XAS characterisation of the metastable light induced state.[11] The studies laid the basis for the subsequent investigation carried out by the group of Verdaguer in 2000, which, analysing the spectra of the ground and metastable state of a series of differently composed PBA, revealed the role of the coordination network flexibility governing the possibility of photoinducing a metastable state at low temperature in these non molecular nor crystalline systems, an issue impossible to be addressed by the standard X-ray crystallographic methods.[12,13]

The first observation of entropy driven bistability in a molecular context dates back to 1992, when Cartier dit Moulin *et al.* reported the SC behaviour of a Fe^{II} complex followed by $L_{2,3}$ XAS.[14] The same compound has been later on investigated by the group of Wang revealing, also for molecular systems, the possibility to detect light-induced metastable states by means of Hard and Soft X-ray absorption spectroscopy. [15] Another interesting example of the unique capabilities in addressing spin states of XAS has been provided by the group of Chergui, who solved the long-standing issue of the mechanism of photoinduction of Fe^{II} complexes in solution at room temperature using a femtosecond XAS setup and thus revealing the three steps process so far taken into account theoretically to explain the light induced SC in Fe^{II} compounds.[16]

Coming back to the compounds investigated in this work, the possibility to investigate both electron transfer and spin bistable materials stimulated the attention of the VT scientific community, which did not delay the employment of the XAS in the analysis of ground and metastable states in Co:dioxolene based VT materials. Hendrickson and Verdaguer in 1996 showed the first proof of VT equilibrium investigated by means of XAS, measuring for the first time the onset of pressure driven VT in a Co:dioxolene 1:2 complex from the analysis of the pressure evolution of the XANES spectra and EXAFS oscillations.[17] The XAS evidence of a metastable state for this class of materials came out one year later, afforded by the Japanese group of Sato.[18] Particular relevance in the Fe^{II} SC community resides in the ability to follow

the electronic details of the light induced process in solution by means of time resolved XANES spectra in the femtosecond time domain.[19]

The reported examples point out the possibilities afforded by the XAS technique for the investigation of bistable molecular materials, in particular exploiting the wide energy spectrum typical of synchrotron radiation. However, as above exposed, this is not the only interesting feature of this probe. In particular, synchrotron radiation absorption spectroscopy is now showing its full potentialities for the analysis of physical properties of systems in nanostructured environments due to its high brilliance, beam stability and the possibility to employ a particular surface selective detection mode (Total Electron Yield, TEY). On this regard worth of being noted are the results obtained by Sessoli *et al.* about the detection of magnetic hysteresis at cryogenic temperatures[20] and by Gambardella *et al.* for the analysis of ultrathin magnetic films. [21]

5.2.5 Open issues for the XAS investigation of stable and metastable electronic states

In the previous paragraph we have shown how XAS may be considered a powerful investigation tool in the characterization of bistable systems, highlighting its outstanding capabilities to investigate matter to the core, and reviewing the striking results it afforded in the case of several classes of bistable materials such as spin crossover,[15,22,23] Prussian blue analogues[11,24] and 1 : 2 Co : dioxolene valence tautomers.[17,18] In the latter case, which is clearly closer to the subject here exposed, the experiments allowed to address the role of the Co ion in the interconversion process as well as following the change of the first coordination sphere during the VT transition. Notably, not only the entropy driven, thermodynamic, VT equilibrium has been followed by means of XAS, but also the metastable state photoinduced at low temperature may be addressed with a high energy optical probe like X-rays.

At the beginning of this thesis' work this investigation for 1:1 Co:dioxolene based VT was lacking. Such an analysis may answer several open questions for this class of compounds:

- **A complete characterisation of electronic picture of the metastable state**. Is this state the same as the high temperature stable one? Are just two the states involved in the VT optically driven transition at cryogenic temperature? This atomic selective probe may answer these questions combined with a theoretical analysis of the spectra.

- **A detailed analysis of the structural features of the metastable state**. The determination of the electronic and structural parameters of the photoinduced phase, up to now unavailable, would be important for the rationalisation of the physical parameters affecting the metastable state lifetime.

- **The surface effects on the VT properties**. We have shown in Chapter III how matrix effects may strongly affect the entropy driven behaviour. Particular setups for XAS allow the measurements of just the first layers of solid samples and could reveal how a low crystalline pressure acts on the VT properties.

- **The role of the X-radiation on the analysis of bistable systems**. Is really synchrotron radiation an innocent probe of electronic bistable systems? Or will it act on the system, damaging or promoting electronic transition – *i.e.* will the excited final state of the system after the X-ray absorption relax in the same electronic potential well before the absorption?

These issues are still open in our field of research, and some of them do not concern our investigated area only. We will present our results for the electronic and structural analysis of $Co(Me_2tpa)(DBdiox)PF_6 \cdot C_6H_5CH_3$ (**1**·toluene) through Co K and L edge XANES and Co K-edge EXAFS. This compound has been chosen because is representative of the 1:1 Co:dioxolene class of VT materials, it has a experimentally accessible $T_{½}$ and it features the highest optically driven interconversion at low temperature among the other 1:1 systems.

5.3. Hard X-Rays as probe of VT equilibrium

In this section an analysis of the temperature dependence of the spectra for the **1**·toluene complex is reported, with the aim of defining the electronic structures of the phases involved in the entropy and optically driven VT conversion. Particular efforts have been spent in the determination of the optimal experimental condition, allowing a non destructive and fully reproducible XAS analysis of these class of electronically labile systems.

5.3.1. Looking for best experimental conditions

The first rule of researcher working on photomagnetism is the control of the reversibility of the photoinduced process. This behaviour is of paramount importance both from applicative and fundamental point of view: it is clear that a physical process funding a device is expected to be repeated several times, and an irreversible change in the state of the system is not called photoinduction, but damaging. The same problem is faced by every scientist working in a synchrotron: very often, in fact, sample undergo damaging under the exposure to the X-ray beam and long running measurements fail. With this in mind, we have firstly checked the effect of Hard X-ray absorption on the electronic features of **1**·toluene.

Figure 5.6 reports the time dependence of four different spectra acquired with a photon flux on the sample of 10^{14} photons s^{-1} and with a 200-fold reduced one, at 300 K, on different areas of the sample in order to irradiate fresh, undamaged, compound. On this regard the sample was mounted as a pure 2 tons pressed pellet in a sample-holder attached to the cold finger of the cryostat that was in turn inserted into a specific chamber optimised for standard XAS experiments. All XAS spectra have been recorded in total X-ray fluorescence yield detection mode using Si photodiodes as detectors.

The upper part of Fig. 5.6 shows a time evolution of the acquired spectra. In particular, all the spectral features (three of whose have been highlighted in the insets) evolve in a coherent direction: the peaks increase in energy, meaning that an overall X-ray triggered oxidation of Co^{II} to Co^{III} is taking place.

In order to overcome this problem we tried measuring the same acquisition pattern but on a new area of sample and with a 200-fold reduced photon flux. This can be achieved by switching from the first to the second operating harmonic of the undulator of the ID12 beamline[25,26] at ESRF. The results, reported on the lower part of Figure 5.6, indicate that in this time scale, corresponding to about 1 hour, the sample is no more damaged by the X-ray beam. Several temperature cycles showed that the thermal transition measured in these conditions is highly reversible.

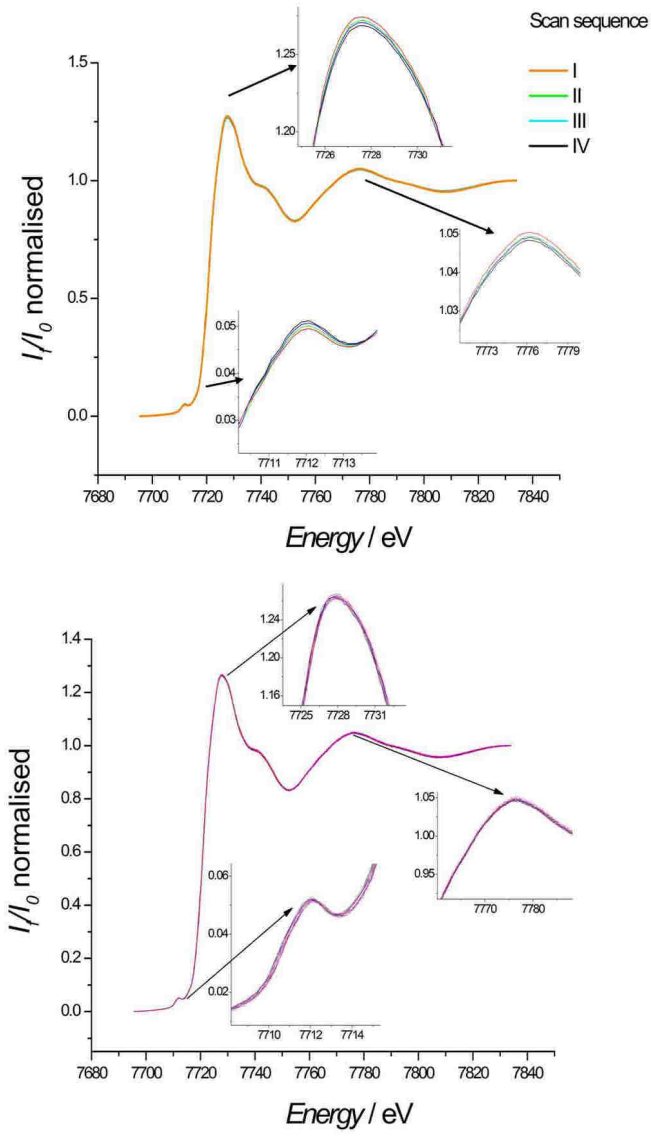

Figure 5.6. *Top*: Set of four consecutive spectra of **1**·toluene acquired with high photon flux on the sample at 300 K. *Bottom*: The same acquisition pattern but with 200-fold reduced photon flux on a new area of the sample at 300 K.

Using an appropriate experimental set-up (reduced X-ray density and fast XAS acquisition), the XAS technique is revealed as a suitable and innocent analytical tool for the investigation of these photomagnetic compounds. This achievement allowed an excellent sensitivity and reproducibility of the X-ray absorption measurements curve without the need to scan different areas of the sample, a previously unreported features of the XAS measurements of bistable molecular materials.

5.3.2. Temperature dependence of XAS spectra

In order to characterise the electronic states of the Co ion in the entropy driven VT equilibrium in 1:1 Co:dioxolene complexes we performed a temperature dependent analysis of the absorption profile of **1**·toluene working with energies matching the K-edge of cobalt. Figure 5.7 shows the normalised K edge XAS spectra of 1 in the 6 – 325 K range.

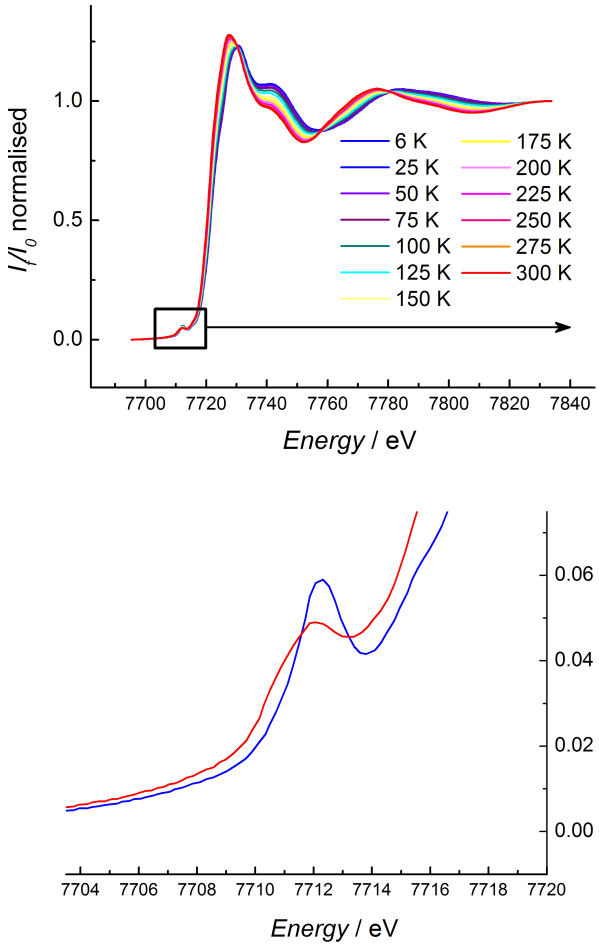

Figure 5.7. *Top:* Temperature dependence of the normalised K edge XANES spectra of a pelleted sample of **1**·toluene. *Bottom*: Pre-edge region of the 300 K (red line) and 6 K (blue line) spectra in a magnified view.

The recorded spectra exhibit marked differences with decreasing temperature. An overall shift of all the spectral features to higher energies (2.8 eV at the maximum of absorption) is observed, as expected for the increased ligand field strength

associated with the contraction of the coordination lengths passing from high-spin Co^{II} to low-spin Co^{III}.[17] Besides, in the pre-edge region an overall rise in intensity occurred, which can be assigned to the depopulation of the e_g based *3d* atomic monoelectronic orbitals. It has recently been shown that the isotropic pre-edge features could be rationalized within a simplified monoelectronic description.[27] The theoretical interpretation of this spectral feature is presented in the next paragraph.

From this fingerprint approach, the Co pre-edge features in Figure 5.7 can be understood as follow. At high temperature (300 K), the pre-edge presents two structures at 7710.5 eV and 7712 eV (bottom of Fig. 5.7) typical for high-spin Co^{II}. They correspond respectively to transitions towards t_{2g} and e_g levels with minority spin orientation. At lower temperature the Co^{II} to Co^{III} transition accompanied by the high-spin to low-spin conversion leaves only one doubly degenerate e_g level empty with no distinction between minority or majority spins for this singlet Co^{III} ground state. Thus the feature observed at 7712 eV corresponds to a transition towards this unoccupied e_g level.

Furthermore a quantitative analysis of the thermal induced VT process has been performed. On the basis of the previously reported magnetic characterization we can consider that, within ± 5% error, the highest (325 K) and lowest (6 K) temperature represent respectively the *hs*-Co^{II} and *ls*-Co^{III} limit composition cases. Linear combinations of these data have then been used to fit the thermal behaviour of the XAS of **1**·toluene at the intermediate temperatures:

$$I(E,T) = x_{Co^{III}}(T) I_{Co^{III}}(E) + x_{Co^{II}}(T) I_{Co^{II}}(E) \qquad (5.18)$$

where $x_i(T)$ and $I_i(E)$ represent respectively the molar fraction and the X-ray absorption spectra for the two oxidation states. The obtained thermal dependence of the *hs*-Co^{II} and the *ls*-Co^{III} fractions of the sample are reported in Figure 5.8.

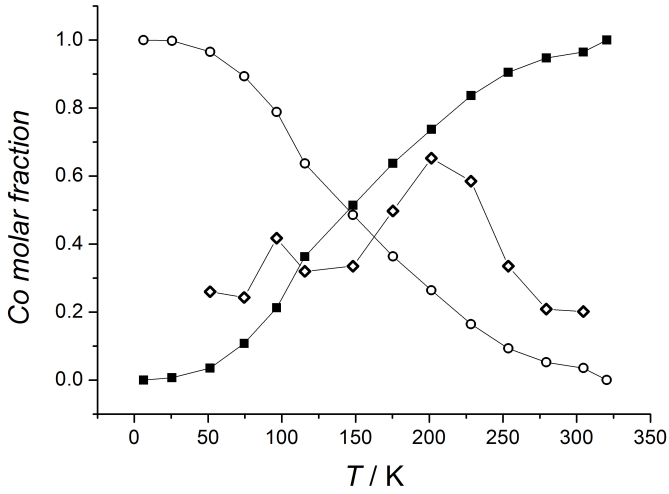

Figure 5.8. Thermal transition curves obtained from the line shape analysis of the XAS spectra as described in the text. These correspond respectively to *hs*-Co^{II} (black squares) and *ls*-Co^{III} (empty circles) molar fraction dependence on the temperature. A 250 times magnified view of the standard deviation of the fit for each temperature is represented by open squares.

This plot allows to address the change of oxidation state of the Cobalt ion during the VT process, being in qualitatively good agreement with the previous reported standard magnetic susceptibility investigation, even if is not capable of revealing remnant *hs*-Co^{II} fraction at low temperature. [28] In line with those results no thermal hysteresis phenomena could be observed. On the other hand, due to the broadness of the transition, we could not unambiguously detect the double stepped behaviour reported by magnetic measurements: however, the observed transition temperature (155 K) is in very good agreement with the average of those reported in literature. The observed differences between the two techniques are tentatively assigned to the operational differences between them (different rate of temperature variation, different sample preparation and crystallinity and different operational conditions).

Additional information can be gained by representing the standard deviation yielded by the fitting procedure *vs* the temperature variation, as shown in Figure 5.8 (with a 250 times magnification). This plot shows two maxima at about 100 K and 200 K respectively, indicating the occurrence of the transition in two steps, corresponding to the internal ET process taking place in the two crystallographically independent molecules in the crystal lattice of **1**·toluene. The most reasonable explanation for this behaviour is that the VT process involves a nucleation-like phenomenon with formation of phase boundaries characterized by slightly different structural and electronic parameters, during the transition.[29] This would confirm the hypothesis,

reported in Chapter III, made on the basis of single crystal x-rays diffraction experiments at different temperatures, which suggested the presence of a phase nucleation at low temperatures but were however unable to give satisfying insights in the process.[28]

5.3.3. The Ligand Field Multiplet approach for the interpretation of XAS spectra

As previously shown, the XAS spectra by themselves are not sufficient to safely describe an electronic transition of an absorbing atom, but have to be interpreted. Historically, this task has been underwent following two distinct approaches. The first one relies on the calculation of the cross sections in function of the energy of the beam with *ab initio* methods.[30] Several methods allow indeed the calculation of the final state density of states of the system through the band structure calculations, carried out in reciprocal space. The second tool for the rationalisation of the XAS absorption profiles is based on the Ligand Field Multiplet analysis (LFM) of the cross section of the absorbing atoms.[2,27,32-34] This method is particularly useful for the calculations of the intensity of transitions involving, as initial or final state, an electronic configuration with strong correlation, *i.e.* the situation encountered working with transition metal ions. In this case the active electron approximation, previously used for the qualitative description of the X-ray absorption process, breaks down and several states have to be taken into account in the transition. The approach foresees the calculation of the transition matrix elements of the kind of Eq. 5.12 for all the different electronic states arising from the $3d^{n+1}$ charge configuration of the absorber.

The transition involving *d* orbitals in K-edge spectra are the symmetry-forbidden $1s \rightarrow 3d$, found in the pre-edge region of the spectrum. This spectral feature is found at lower energies and intensities with respect to the resonance white line absorption. The lower energy of the peak is due to the fact that *3d* orbitals in the first row transition metal ions are more stable than the *4p*, responsible of the white line. The lower intensity can be understood considering that the $1s \rightarrow 3d$ transition involve a $\Delta l = 2$, which is forbidden by the selection rules of X-ray absorption spectroscopy treated with a pure dipolar transition operator. The pre-edge region of the transition-metal *1s* edges has thus led to a number of debates regarding the quadrupole and/or dipole nature and possible excitonic effects. Both direct $1s \rightarrow 3d$ quadrupole transitions and dipole transitions to *4p* character hybridized with the *3d* band are possible. For the quadrupole transitions, the matrix elements are only about 1% of the dipole transition, but on the other hand, the amount of *3d* character is by far larger than the *p* character. This can make, depending on the particular system, the contributions of quadrupole and dipole transitions equivalent in intensity.

In order to completely clarify the role of the Co ion in the VT process of 1 : 1 Co : dioxolene based valence tautomers we have characterized the two electronic states using a LFM theory approach; figure 5.9 reports the results obtained for the simulation of the pre-edge spectral features of **1**·toluene.

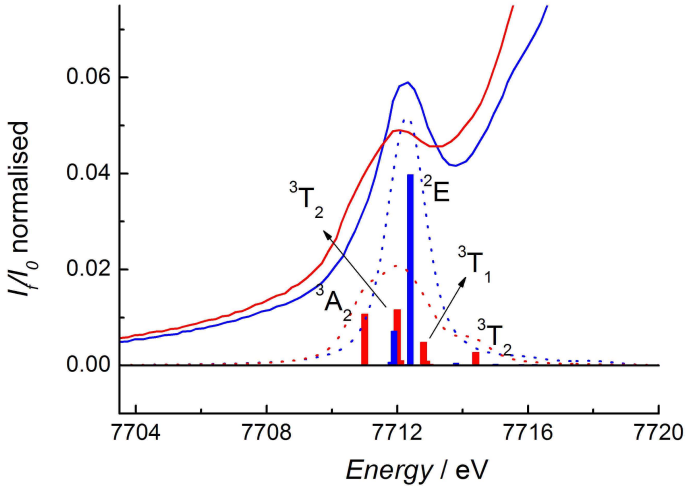

Figure 5.9. Pre-edge features at 6 K (solid blue line) and 325 K (solid red line) and the corresponding calculated pre-edge features (dotted blue line for Co^{III} and dotted red line for Co^{II}). The sticks underneath the theoretical dotted lines correspond to the intensity of the discrete transitions to the labelled state.

The pre-edge absorption bands at the K-edge of *3d* transition metals is attributed to an electric quadrupole *1s* → *3d* transition with some admixture of electric dipole *1s* → *4p* transition.[2,32,33,35,36] When the *3d* transition metal ion is isolated and its environment has a centre of inversion, the electric dipole transitions are negligible.[27] In the Co valence tautomeric complexes, we are left with the calculation of the electric quadrupole transition between a $1s^2 3d^n 4p^0$ multielectronic ground state and all the $1s^1 3d^{n+1} 4p^0$ multielectronic excited states. The calculations were performed taking into account the crystal field of appropriate symmetry acting on the metal centre. For both Co oxidation states, the Slater integrals simulating the multielectronic Coulomb repulsion are scaled down by 20% compared to the isolated ion values and the 3d spin-orbit integrals are equal to isolated ion values, according to the nephelauxetic effect.

With this approach, the experimental pre-edge features were nicely reproduced considering an octahedral environment around the metal ion and assuming a Co^{III} phase for the low temperature data (with crystal field parameter given by $10Dq(Co^{3+})$ = 2.2 eV) and a Co^{II} phase for the high temperature data ($10Dq(Co^{2+})$= 1.0 eV). The intensities of the theoretical electric quadrupole transitions, shown in Figure 5.8 as

sticks, whose height is proportional to the intensity of the transition, are normalized to the theoretical *1s* to *4p* edge jump calculated with the resources made available by the Center of X-Ray Optic X-ray.[37] Thus both experimental and theoretical intensities can be compared without extra scaling coefficient. The temperature dependence of these spectral features has been taken as fingerprint of the Valence Tautomerism transition, in agreement with the results observed for polycyanometallato and spin crossover systems.[12,17,38] This confirms the effectiveness of the XAS technique as element and valence sensitive tool in monitoring this process, which implies a reversible interconversion between a low spin, S=0, Co^{III} based species at low temperature and a high-spin, S=3/2, Co^{II} one at high temperature.

When all parameters of LFM are included, the agreement with the experiment is quite fair but the interpretation is cumbersome because spin-orbit coupling, and multielectronic *3d-3d* and *1s-3d* Coulomb interactions are present.[27] In the LFM approach, the pre-edge structures are described as electric quadrupole transitions from Co $1s^2 3d^n$ ground state to Co $1s^1 3d^{(n+1)}$ excited states. The *1s-3d* Coulomb exchange interaction is almost negligible because the Slater integrals are $G(1s,3d) = 0.065$ eV for Co^{II} and 0.072 eV for Co^{III}. Moreover spin-orbit coupling acting on the *3d* shell is small and can be switched to zero for interpretation's sake. In this simplified picture, the *1s* core-hole (S=1/2) does not play any orbital role, and the "allowed" excited states are then mainly determined by the $1s^1 3d^{(n+1)}$ excited configuration for which the total spin is identical to the one of the ground state $3d^n$ configuration. The $3d^{(n+1)}$ spectroscopic terms and their energies are found by solving Tanabe-Sugano matrices with appropriate values for the ligand field parameters (*10Dq*, and the Racah parameters *B*). [39,40]

- For *hs*-Co^{II} ($3d^7$) the total spin is S=3/2 so that the allowed $3d^8$ configurations are S=1 and S=2. There are no quintuplet (S=2) states with $3d^8$, so that the only possible configurations are $3d^8$ triplet (S=1) states. In octahedral (O_h) symmetry, the pre-edge features are then the transitions from the $^4T_{1g}$ $3d^7$ *hs*-Co^{II} ground state to the Co^{II} $(1s)^1(3d)^8$ excited states. Since the *hs*-Co^{II} ground state is $^4T_{1g}$, the only reachable states are $(3d)^8$ triplet final states yielding $(1s)^1(3d)^8$ quadruplet final states, corresponding to spin-allowed transitions. The triplet spectroscopic terms for O_h d^8 ion are $^3A_{2g}$ ($(t_2)^6(e)^2$ configuration), $^3T_{2g}$ ($(t_2)^5(e)^3$ configuration), $^3T_{1g}$ ($(t_2)^5(e)^3$ configuration) (the three previous terms derive from the ^3F free ion term) and $^3T_{2g}$ (derived form the ^3P free ion term). The *hs*-Co^{II} K pre-edge presents indeed four main transitions. The relative energies between the four $3d^8$ terms are given in ref. 39,40. It must be stressed that the energy difference between the first two transitions gives the crystal field strength *10Dq* in this simplified model, a quantity of paramount importance in determining the spin flip induce by the change in charge

configuration of the molecule, which has been shown in Chapter I to be at the origin of the thermodynamic as well as optical bistability of VT systems.

- In the case of *ls*-Co^{III}, the ground state is $^1A_{1g}$ ($(t_{2g})^6(e_g)^0$ configuration) so that the electric quadrupole allowed excited states are $3d^7$ doublet (S=1/2) states. This gives mainly the ^2E_g spectroscopic term ($(t_2)^6(e)^1$ configuration) with other doublet states at higher energies: several $^2T_{1g}$, $^2T_{2g}$ terms deriving from intermediate and high-spin configurations. Thus the *ls*-Co^{III} K pre-edge is mainly built from one transition. Within the present simplified interpretation the main discrete transitions have been labelled as reported in Figure 5.8. The other non-labelled transitions have smaller intensities and they derive from the non-zero spin-orbit coupling and non-zero *1s-3d* Coulomb repulsion.

5.3.4. Hard X-rays as probe of metastable states in 1:1 Co:dioxolene systems

As already mentioned in Chapter III, **1**·toluene was found to undergo valence tautomeric interconversion between diamagnetic *ls*-Co^{III}Cat and paramagnetic *hs*-Co^{II}SQ species both entropy and optically driven, by irradiation on the LMCT band, located at 904 nm. In particular **1**·toluene showed the up to now highest percentage of photoinduction (85 %, *cfr.* Chapter III) and thus is a natural candidate to investigate light induced modifications of electronic structure with a probe like Hard X-ray absorption spectroscopy. To perform the analysis the sample holder was specifically designed to allow the irradiation of the sample with both the X-ray probe and the IR light of the CW laser diode (mounted externally to the cryostat, working at 904 nm with a 10 mW cm^{-2} power on the sample). The results obtained after 20 hours of irradiation of the VT system on the LMCT band at 6 K are reported in Figure 5.10.

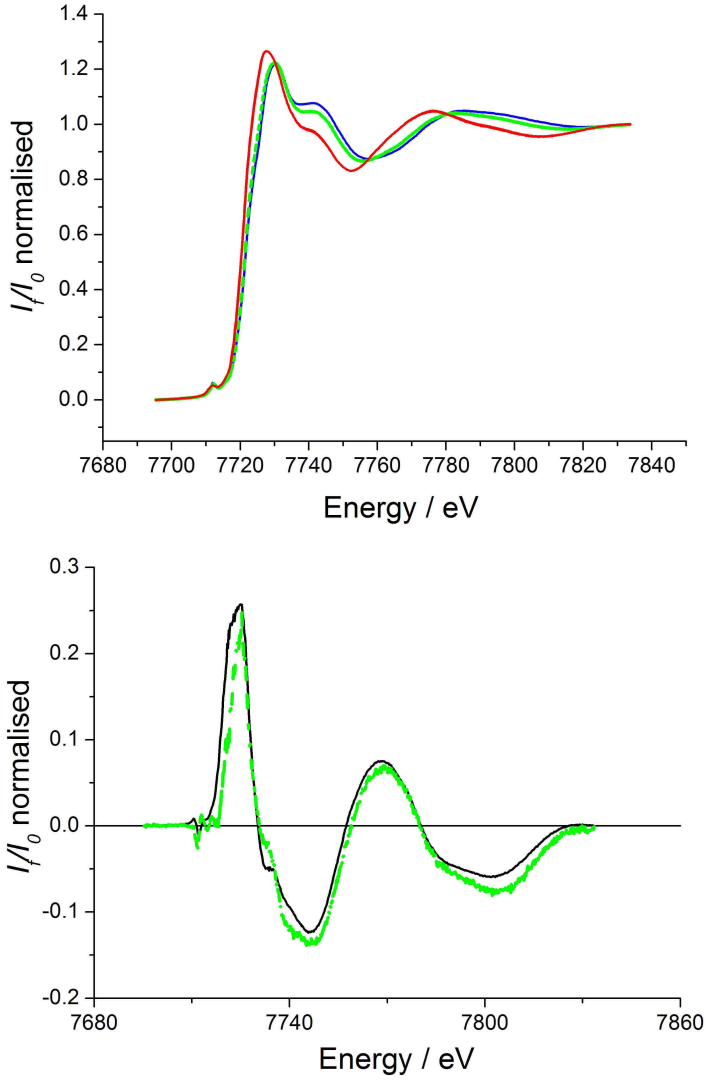

Figure 5.10. *Top*: Effect of 904 nm laser irradiation on the 6 K XAS spectrum (dotted green line) compared to the 6 K (solid blue line) and 325 K spectra (solid red line). The solid black line with empty circles evidences the reversibility of the optically induced VT process. *Bottom*: Comparison of the difference of the normalised XAS spectra of **1** between 325 K and 6 K in the dark (black line) and at 6 K after and before irradiation at 904 nm, multiplied by a factor 4 (dotted green line).

The upper part of Fig. 5.10 shows the different spectra obtained before and after the irradiation on the LMCT of **1**·toluene. This plot provides us an at a glance

description of the metastable state spectrum, which in fact lies in between the low (solid blue line) and high (solid red line) temperature ones. On the other side it reveals the complete reversibility of the optical induction, being completely superimposable the 300 K spectra obtained before and after the low temperature irradiation. The lower part of Fig. 5.10 presents the difference in the XAS normalised absorption spectra of the 325 K and 6 K spectra in the dark (solid black line) is compared to the one between the 6 K spectra acquired after and before laser diode irradiation, multiplied by a factor 4 (dotted green light). From the data treatment, with particular attention to energy shifts due to the monochromator, we can rule out spurious derivative effects to be the reason for the signal of the photoinduced metastable phase. This plot lets us draw out two conclusions:

- The percentage of photoinduction is 25 %. This value is much lower than the one found with magnetometric techniques, and this difference in conversion efficiency should be ascribed to the different sample preparation procedure and slightly different conditions of visible light irradiation.

- The electronic features of the metastable phase are the same of the high temperature phase, being the difference spectra with respect to the low temperature phase identical.

Finally, a key point for this kind of characterisation is the complete reversibility of the detected process both via the thermal variation and via the light irradiation processes.

In Figure 5.11 we report the summary of the Co^{II} and Co^{III} composition of the sample as monitored by varying the temperature and by irradiating the sample at low temperatures, obtained by multiple regression of the different spectra according to Eq. 5.13. We emphasize that this reversibility has been monitored for the first time using the hard X-rays as probe, in the operational condition of working on the same spot on the sample for the whole experimental set of measurements.

Thanks to this XANES analysis at the Co K-edge of a thermal and light induced Valence Tautomeric transition of a 1:1 Co:dioxolene system it has been possible to show the temperature dependence of the XAS spectra. This allowed us to unambiguously address the role of the metal ion in the magnetism of the two isomers, and suggested the formation of distorted phase boundaries during the VT process, in analogy with what previously argued from temperature dependent X-ray crystallographic analysis.

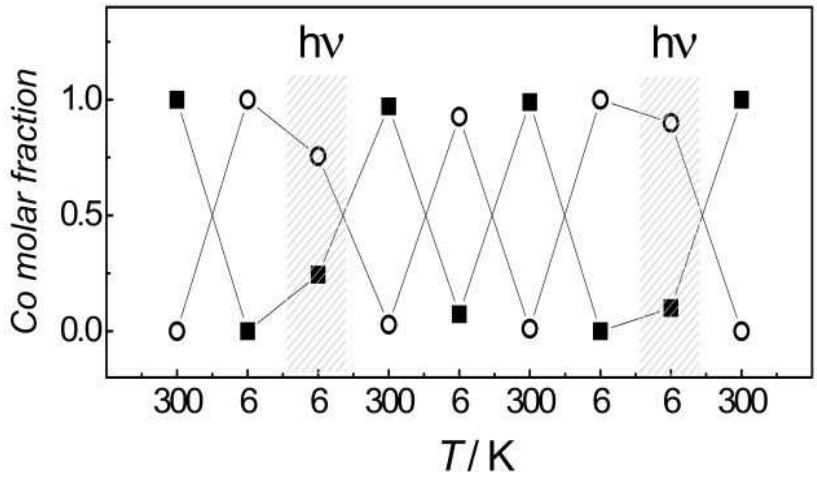

Figure 5.11. Sequence of the Co^{II} (*full squares*) and Co^{III} (*empty circles*) molar fractions monitored varying the temperature and irradiating the sample with 904 nm laser light. Shaded points correspond to the measurements carried out after irradiation with the laser for on 20 h (*left*) and 2 h (*right*).

The MLF approach employed, on the other side, clarified the electronic states involved in the transition, suggesting that the perfect equivalence between the electronic structure of the photoinduced metastable state and the high temperature redox isomer. It must be stressed that all of these results have been taken working on the same spot of the sample, showing 1·toluene as an ideal candidate for the investigation of VT conversion features in 1:1 Co:dioxolene systems and for the development of molecular based devices. On this respect, the high sensitivity afforded by the use of the synchrotron radiation opens new perspectives for the investigations of valence tautomeric complexes in nanostructured materials. These results nicely confirm that the XAS is a well suited probe for the investigation of the electronic structure and the transformation processes of this photoswitchable materials.

5.4 Structural analysis of metastable states using EXAFS

After the addressing of the electronic features of the Co ion in the VT process for a system representative of the 1:1 class of Co:dioxolene materials through XANES spectroscopy, we will present in the following the structural analysis of the same system based on EXAFS spectroscopy.

5.4.1 The fine structure of X-ray absorption

The EXAFS region of the more general XAS spectrum starts from 50 eV after the white line and usually is considered to extend 1 keV or more above it. In this case the photoelectron, after the excitation due to the X-ray absorption, possesses an energy greater than its binding one to the atomic nucleus, and thus leaves the atom going in the continuum, unbound, state. This is the so called "photoelectric effect".[41] This phenomenon gives rise to a series of peaks in the XAS spectrum.

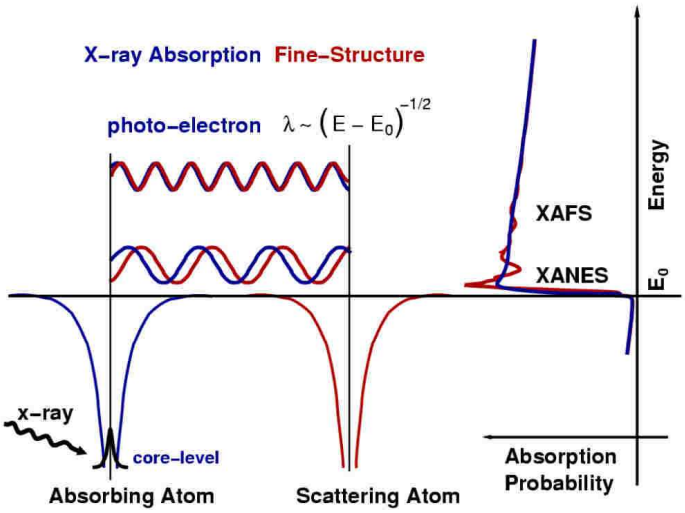

Figure 5.12. The schematic picture of the EXAFS working principle. The absorber, on the left side of the picture, emits a photoelectron which, scattered by a surrounding atom, travels back to the absorber, thus modulating the amplitude its absorption coefficient μ.

The origin of these can be understood looking at the right side of Figure 5.12. In absence of scattering centres near the absorber (gas phase) the absorption profile is represented by the blue line. In the solid phase, however, the photoelectron undergoes processes of single or multiple scattering by the surrounding atoms. For the sake of

simplicity, we can consider a single scattering event for the photoelectron, which in these conditions leaves the absorber atom and comes back after the scattering process (this is a very rough approximation – especially near the white line, where multiscattering processes are frequent). The oscillations are caused by the interference between the photoelectron wave function and the parts of it backscattered by the neighbouring atoms towards the absorber. Since the latter depend on the position and the atomic number of the scattering centres, information about the local structure around the absorber can be extracted from the EXAFS spectrum, and especially their radial distribution around it. The theory of the process will be described in more detail in paragraphs 5.3.2.

Actually, the EXAFS oscillations observed are essentially due to the nearest neighbours shell with the other neighbours contributing as a more or less weak perturbation, depending on their backscattering properties and their distance from the absorber. This can be seen very clearly from Figure 5.13.

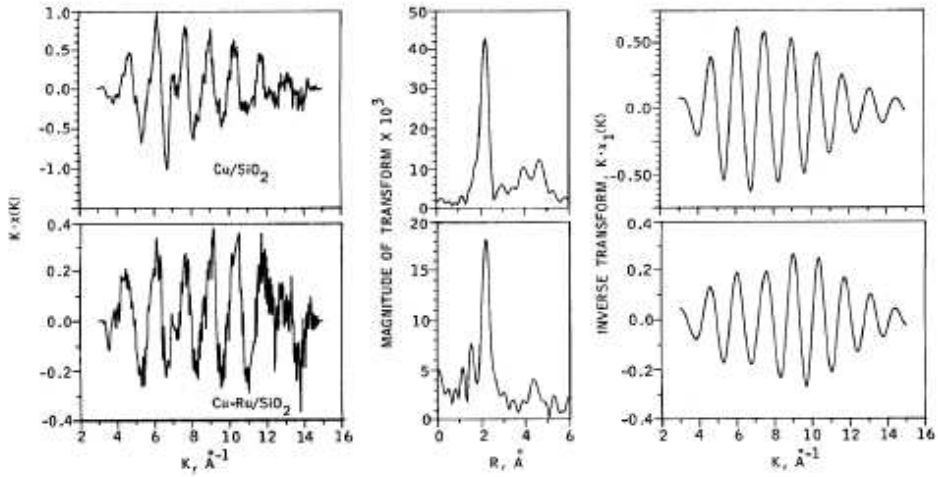

Figure 5.13. Normalized EXAFS data at 100K, with associated Fourier transforms and inverse transforms, for silica supported copper and ruthenium-copper clusters. The inverse transforms correspond to nearest neighbours only.

Here, the Cu K edge EXAFS spectra at 100K of Cu and Cu-Ru clusters on SiO_2 are shown together with their Fourier transform (which gives the radial distribution) and the inverse transform of the contribution of the first coordination shell. The similarity between the true EXAFS spectrum and the one resulting from the first shell of neighbors is striking.[5]

5.4.2 The EXAFS equation

For a quantitative description of the EXAFS phenomenology it is useful to refer to the EXAFS fine-structure function $\chi(E)$, defined as

$$\chi(E) = \frac{\mu(E) - \mu_0(E)}{\Delta\mu_0(E)} \tag{5.19}$$

where $\mu(E)$ is the absorption coefficient, $\mu_0(E)$ is a smooth background function representing the absorption of an isolated atom, and $\Delta\mu_0$ is the measured jump in the absorption $\mu(E)$ at the white line energy E_0. This function can be more properly written as explicitly dependent on the wave-number k of the outgoing photoelectron

$$k = \sqrt{\frac{2m(E - E_0)}{\hbar^2}} \tag{5.20}$$

where m is the electron mass, E its energy and E_0 is the white line energy. Within these considerations, we can describe the EXAFS oscillations in function of the energy of the back-scattered photoelectron using the EXAFS equation,

$$\chi(k) = \sum_j \frac{N_j f_j(k) e^{-2k^2 s_j^2} e^{-\frac{2R_j}{\lambda(k)}}}{kR_j^2} \sin(2kR_j + \Phi_j(k)) \tag{5.21}$$

This relation is of paramount importance in the quantitative interpretation of the EXAFS signal. It will not be demonstrated here for brevity purposes, we remind the interested reader to ref. 41. Eq. 5.21 consists in a sum of damped sinusoids, corresponding to the different scattering paths for the photoelectron by means of the surrounding atoms and the damping effect is related to the loss of energy of the photoelectron travelling in the solid. Several factors take part into Eq. 5.21:

Electronic factors:
- f_j: scattering amplitude of the j-back-scatterer;
- $\Phi_j(k)$ total phase shift of the back-scattered electron with respect to the outgoing one;

Structural factors: R_j distance between the absorber and the j-back-scatterer;

$e^{-\frac{2R_j}{\lambda(k)}}$ damping factor related to the loss of energy in case of anelastic scattering. The $\lambda(k)$ parameter is the electron's mean free path in the solid;

$e^{-2k^2s_j^2}$ damping factor related to the static disorder along with the thermal vibrations, expressed by the Debye-Waller factor σ_j.

By the knowledge of the electronic parameters of the system under investigation (usually calculated or tabulated) Eq. 5.21 affords a set of structural information about the absorbing atom: the number of neighbours, their distance from the absorber (if less than usually 5 Å from the absorber, according to the R^{-2} and the f_j terms), the degree of lattice vibrations and the kind of the surrounding atoms (since the electronic factors depend on Z). All of these information, of course, can be extracted even in the absence of a three dimensional lattice order or for systems with a very low degree of crystallinity (as in the present case).

5.4.3 Sample preparation

In order to obtain EXAFS spectra of good quality it is mandatory a correct balance in the absolute intensity jump in the white line absorption. This balance is due to the required meeting of two opposite conditions: the presence of a fairly intense absorption edge (featuring a $\Delta\mu_0$ of about 1), assuring a good evaluation of the background $\mu_0(E)$ signal, and the correct transparency of the sample, able to let detect the small absorption jumps called EXAFS, in the standard conditions: transmission detection mode with a ionisation chamber detector. For these reasons the sample has been finely grounded to reduce inhomogeneities and mixed with BN in order to enhance its thermal conductivity. Then a calculation has been made to evaluate the correct thickness of the resulting pellet in function of the desired absorption jump at the white line, according to Eqs. 5.1, 5.2 and 5.3.

These are not however the only points to be satisfied. We found in fact that, in the case of EXAFS investigation of photoinduced states, a dependence of the photoinduced fraction on the active compound : BN ratio is present as well.

5.4.4 XAS of ground state and light induced metastable state species

We investigated the valence tautomeric transition in function of temperature and light irradiation for **1**·toluene, in order to gain structural information on the photoinduced metastable state at cryogenic temperature. First of all we have measured the temperature dependence of the XAS spectrum at the K edge of cobalt, working at 300 K and 5 K and paying particular attention to the reproducibility of the signal without damaging the samples in function of the time of exposure to the X-ray beam. The results obtained are reported in Figure 5.13, corrected for the background absorption.

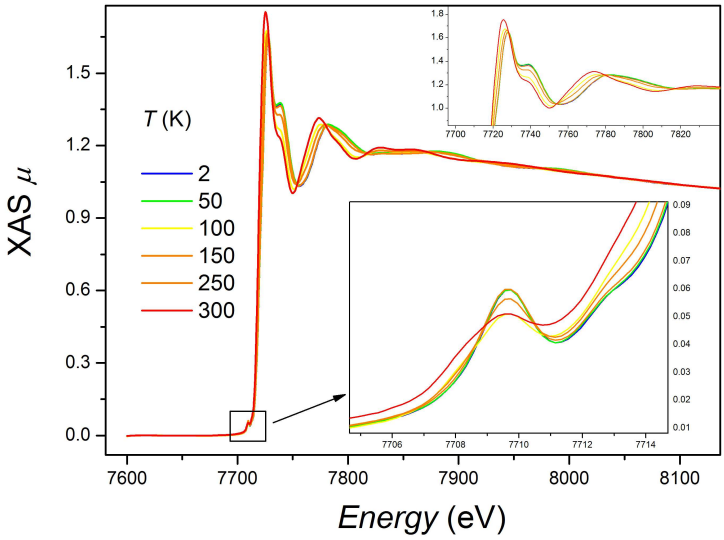

Figure 5.13. Temperature dependence of the XAS spectra of **1**·toluene.

Figure 5.13 points out the VT entropy driven equilibrium occurring for the system in analysis, showing an increase of the edge energy along with an enhancement of the intensity of the pre-edge features on lowering the temperature, thus confirming the *hs*-Co^{II} to *ls*-Co^{III} transition, in line with what previously seen with magnetometric and with the data taken from the XANES analysis of the same compound.

We checked also the possibility of detection of the light induced metastable state with this particular setup. After 1 h of irradiation of **1**·toluene with 904 nm laser light with a radiant power on the
sample of 5 mW cm^{-2}, we found significant changes in the XAS spectra, reported in Figure 5.14.

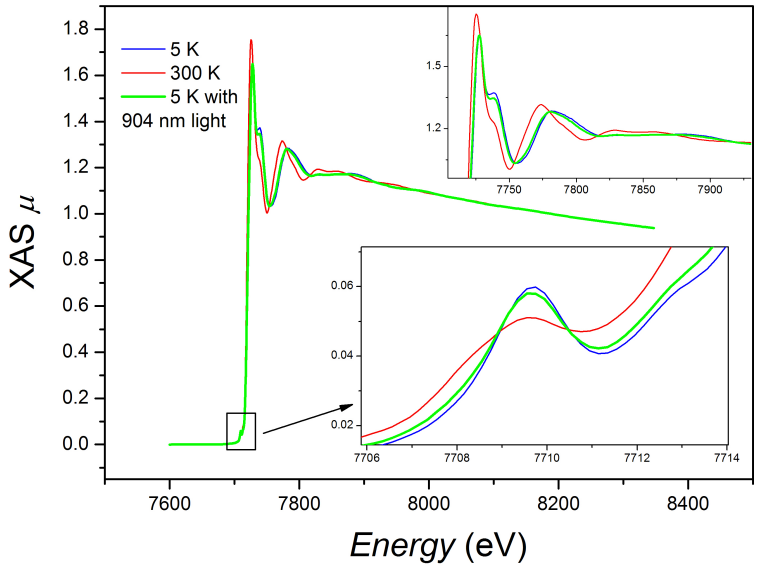

Figure 5.14. Temperature dependence of the XAS spectra of **1**·toluene after 1 h of irradiation on the LMCT band.

From a multiple regression using as references the low and high temperature spectra for the *hs*-Co^{II} and *ls*-Co^{III} compositional situations, we found an overall 18% of photoconverted molar fraction, value that can be explained taking into account a non complete penetration of the IR light into the whole pellet's thickness.

5.4.5 EXAFS analysis

Thanks to the high sensitivity setup afforded by the BM29 beamline at ESRF we were able to characterize the structural modifications of the first coordination sphere of the Co ion during the VT conversion following the EXAFS oscillations in function of temperature and light irradiation.

The extraction of the EXAFS signal from the XAS spectrum is based on the application of Eq. 5.19. In this case particular importance resides in the correct evaluation of the background absorption $\mu_0(E)$, which in our case has been estimated using a polynomial function afforded by the Viper software.[42] The resulting EXAFS oscillations have been reported in Figure 5.15 as $k^*\chi(k)$ product to highlight the oscillations occurring at high k values.

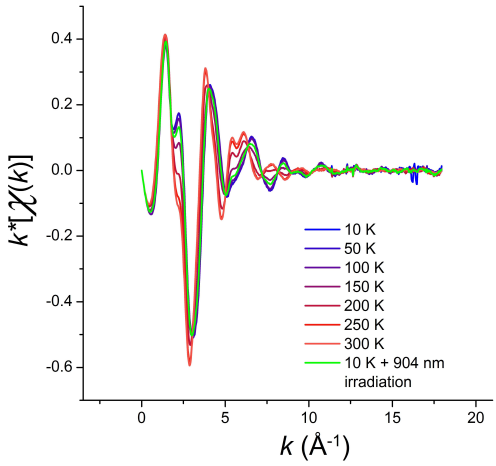

Figure 5.15. Co K-edge EXAFS $k^*\chi(k)$ spectra measured in function of temperature and light irradiation.

In order to apply Eq. 5.21 for the determination of the structural parameters the EXAFS signal must be analyzed. The extracted real part component obtained by the Fourier Transformation treatement of the $\chi(k)$ at 10K is reported in the left side of Figure 5.16.

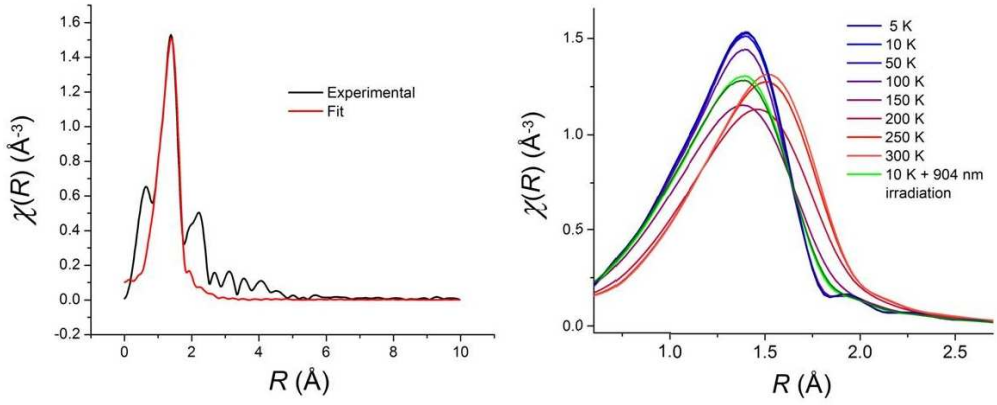

Figure 5.16. *Left*: Result of the calculation fitting of the Fourier transform as described in the text (red curve = simulated; black curve = experimental).*Right*: Real part of the Fourier transform of the EXAFS signals measured in function of temperature and light irradiation.

This directly evidences a huge peak originated from the first shell of neighbours, corresponding to the oxygen and nitrogen atoms of the first coordination sphere of **1**·toluene. For a first preliminary analysis of these data however we

considered a single scattering path for the photoelectron, exerted by a first coordination sphere made out by six oxygen atoms and we fitted the experimental data using the Artemis software, an interactive graphical utility for fitting EXAFS data based on the FEFF package.[43] The result for the 10K spectrum is reported in the left side of Figure 5.16. This analysis has been obtained by filtering a kaiser-bessel window of the real space between 0.8 – 2.5 Å range, pointing out the contribution of the first shell of neighbours of the absorber Co ion on the oscillations.

The right side of Figure 5.16 shows the results of the fitting for the EXAFS spectra at different temperatures and before and after 904 nm light irradiation. Despite the strong approximation we used in the analysis we afforded a nice example of conversion profile followed by means of structural investigation, as reported in Figure 5.17.

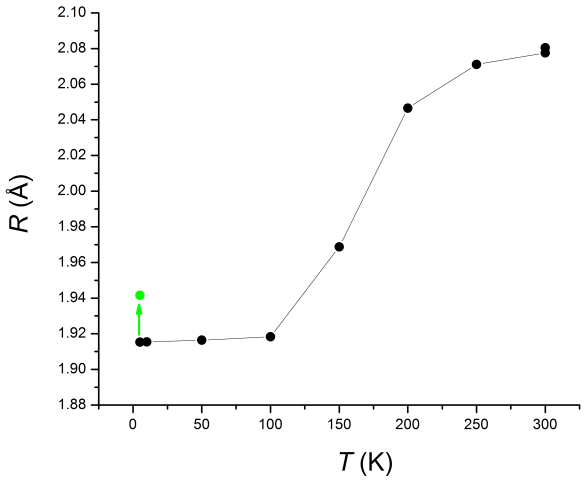

Figure 5.17. Temperature and light irradiation (green point) dependence of the average Co-L distance extracted from the analysis of the EXAFS spectra.

During the VT process, in fact, the average distances between Co and neighbouring atoms increase, acting as a fingerprint of the conversion. The diagram, shown in figure 5.15 for **1**·toluene, for the first time for this class of compounds gives evidence of the structural features of the photoinduced metastable state at low temperature, pointing out the structural changes in the first coordination sphere of the Co ion during the thermal and light induced processes.

5.5 Soft X-Rays investigation of stable and metastable electronic states

We have previously shown the role of probe of different electronic states played by Hard X-rays for a 1:1 Co:dioxolene VT system (**1**·toluene). In the following we will present the results obtained on the same system about the investigation of ground and excited electronic states using a probe of lower energy, the Soft X-rays.

Soft X-rays absorption spectroscopy (XAS) is an element sensitive synchrotron based technique and provides a powerful tool to study the electronic and chemical structure of a specific atom and its coordination environment. It is particularly powerful in magnetic study of *3d* metal complexes.[18,22,36,44,45] With the additional asset of very high detection sensitivity, XAS has been effectively used in the characterization of systems with multiple quasi degenerated electronic states,[11,15,24,27] including very diluted and nanostructured systems.[20,21,46] The X-rays absorption spectra measured at the $L_{2,3}$ edges of transition metal ions involve the electronic transitions from a spin-orbit split core *2p* ($2p_{3/2}$ for L_2 and $2p_{1/2}$ for L_3) orbital to a *3d* one. The structures of the $L_{2,3}$-edges depend on several electronic factors: the crystal field acting on the final state, the electronic correlations (of coulombian, exchange and spin-orbit coupling origin) taking place among the *2p* and *3d* sets of orbitals involved in the absorption process, and on spin-orbit interaction on the *2p* and *3d* shells. So, $L_{2,3}$-edges directly probe the *3d* levels of each ion involved in the proposed electron transfer. We have found that for **1**·toluene this technique not only yields these important information, but also intrinsically provides the perturbation for inducing interconversion between the two redox isomers.

Moreover, the presented set of experiments on the entropy and optically induced VT transition deserve attention because of the particular setup used for this XAS analysis, able to investigate the first layers of the samples analysed, and thus reveal environmental effects on the VT features for this class of systems, related to the reduce lattice pressure acting on surface molecules with respect to the ones placed in the bulk material.

5.5.1 Soft X-rays as probe of ground electronic states

As in the previously shown XAS analysis of the VT behaviour of **1**·toluene we have firstly measured the temperature dependence of the $L_{2,3}$ spectra without light irradiation. The experimental setup used for the measurement of $L_{2,3}$ spectra resembles the ones previously shown, where the sample is put in contact with the cold finger of a cryostat able to shift the temperature in the 6 - 320 K range. However, in the present

case, the sample consists in a toluene solution of **1**·toluene drop cast on the sample holder, and no more in a solid pellet. Moreover, in this case the spectra were recorded in total electron yield detection mode. The complete $L_{2,3}$ spectra at 10 K and 300 K are reported in Figure 5.16 and show dramatic differences, as expected for the occurrence of an entropy driven VT equilibrium.

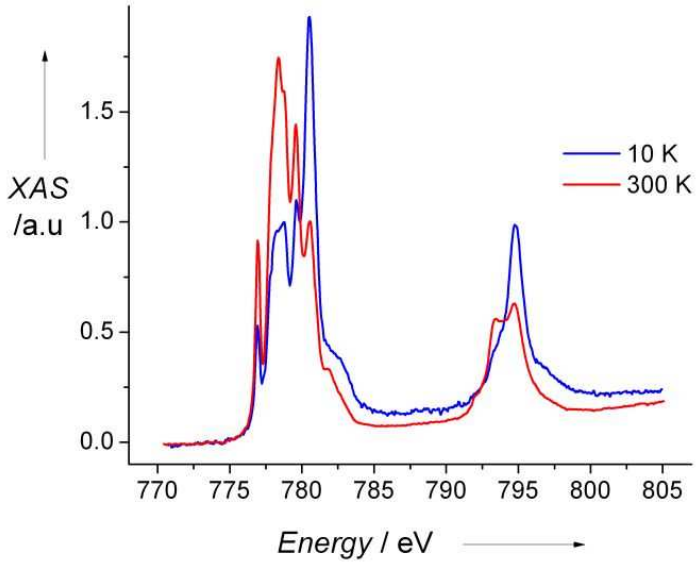

Figure 5.16. Complete Co $L_{2,3}$ edge spectra of complex **1**·toluene at 10 K and 300 K, showing the characteristic features of Co^{III} and Co^{II} respectively. Note the large L_2 edge at 10K, indicating the dominant presence of *ls*-Co^{III} ion.

In order to obtain a detailed description of the electronic structure of the isomers involved in VT equilibrium, we focused our attention on the L_3 edge of the spectra, reported in Figure 5.17.

The spectra clearly show the features of the entropy driven interconversion involving two different redox species, as evidenced by the presence of a single isosbestic point. In order to address the role of the Co ion in the VT equilibrium, we followed the coupled experimental and theoretical approach describe for the Co K-edge investigation, using again a Ligand Field Multiplet (LFM) calculation approach.[2,47]

The calculation of the spectra has been performed using the electronic parameters obtained from the K-preedge analysis of the same system.[48] The results of the simulation for the *ls*-Co^{III} and *hs*-Co^{II} ions are shown in Figure 5.17 as dark and light grey lines, respectively, and allow the attribution of the different features of the experimental spectra to the two contributions. The deconvolution of the acquired

signal with the ones related to the pure phases, according to Eq. 5.17, affords two interesting hints about the entropy driven VT equilibrium.

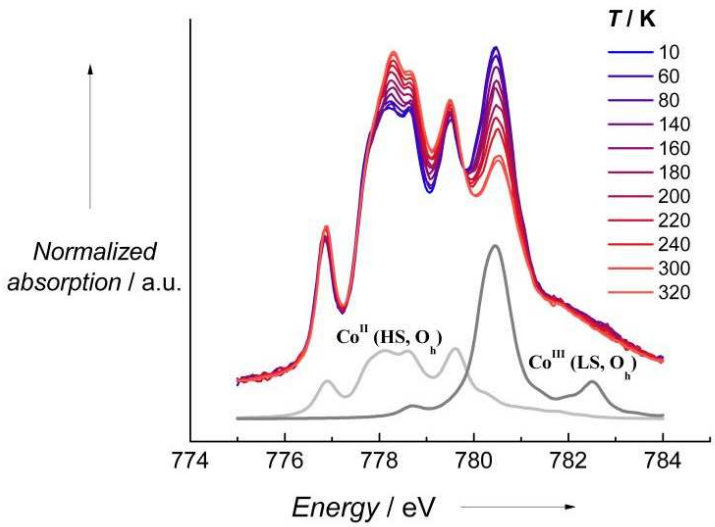

Figure 5.17. Temperature dependence of the normalized L_3 edge X-rays Absorption spectra of **1**·toluene. The underlying light grey and dark grey curves show the theoretical spectra expected for pure *hs*-Co^{II} and *ls*-Co^{III} states, respectively.

At low temperatures, a high percentage (65 %) of the high temperature phase is present. This effect has already been found in the bistable systems' literature and is related to two different physical situations. In the first case the rapid thermal quench (with rate of temperature variation of about 30 K min^{-1}) of systems showing strong cooperativity in the solid state,[16,49] which have no enough energy (in terms of molecular vibrations) to afford the structural rearrangement accompanying the transition. In this case the high temperature phase frozen in cryogenic conditions is not the system's ground state and exhibits a time dependence typically found for the decay of low temperature photoinduced metastable states. In the second case, previously encountered in Chapter IV, the increase of the remnant high temperature phase is due to an increase of the entropy change occurring in the VT equilibrium; in this situation the VT transion smooths and appears usually to be uncompleted at low temperature.[50,51] Since in our case the low temperature *hs*-Co^{II} percentage appears to be independent on time, we attribute its presence to surface effects affecting the thermodynamics of VT equilibrium. As we have previously shown, TEY detection system is sensitive only to the first layers of the solid compound. In this confined environment, surface molecules do not feel the same coordination than the ones placed in the bulk material. In particular, surface molecules are supposed to feature a

reduced lattice pressure on them, the same effect chemically induced by the solid solution approach described in Chapter IV. In the same way we claim this to be the origin of the presence of the high temperature phase at low temperature.

The second conclusion we are able to draw out by the interpolation of the 300 K spectrum with the calculated ones is the presence of a significant percentage of *ls*-Co^{III} containing redox isomer at high temperature. Even if this can be due to a smoothing of the transition profile due to an increase of the entropy of the transition, an analysis of the transition profile by means of standard magnetometry, reported in Figure 5.18 as normalised *hs*-Co^{II} molar fraction *vs.* T, revealed that this effect is more likely to be related to the sample preparation than to entropy effects on the VT equilibrium of **1**·toluene.

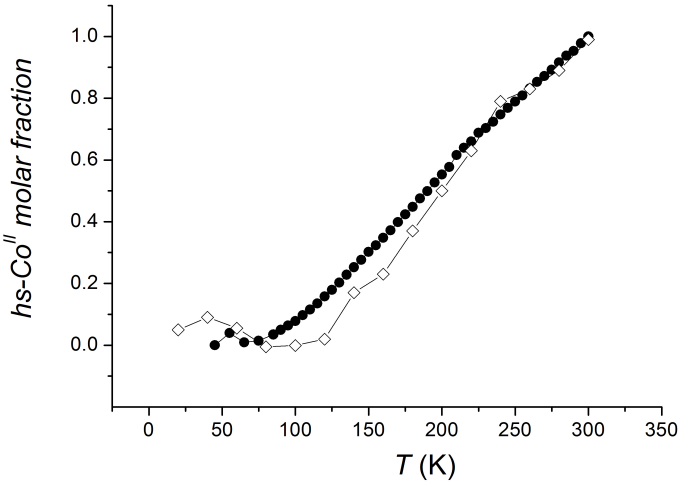

Figure 5.18. Temperature dependence of the normalised *hs*-Co^{II} molar fraction extrapolated from standard magnetometric analysis (full black points) and from XAS, pointing out the incompleteness of the VT transition in the T range investigated.

It must be stressed that, in the present case, the spectra used for the interpolation and affording the transition profile are not the calculated ones by means of LFM approach, but the 80 and 300 K experimental ones. At these temperatures, in fact, the system is in its limit compositional cases, and thus these spectra can be used as a standard internal reference to follow the active centres taking part into the VT transition.

A close inspection of the low temperature range of Figure 5.18 reveals the presence of a little increase of the *hs*-Co^{II} fraction, which is relaxing back at 80 K. This behaviour suggests the possibility to induce the VT interconversion at low temperature with the only Soft X-rays irradiation, and its detailed investigation is presented in paragraph 5.4.3.

5.5.2 Soft X-rays as probe of photoinduced metastable electronic states

In analogy to the investigation carried out for the Hard X-ray case, we attempted the investigation of the metastable state, induced by laser irradiation on the LMCT band, by means of L_3 XAS. To perform this experiment the soft-X-ray based setup can be adapted using a similar setup respect to the one previously shown about the Hard X-ray study to allow the *in-situ* irradiation of the sample with the 904 laser light promoting the LMCT transition, shone by a diode like laser. The power on the sample has been tuned to 10 mW cm^{-2}. The obtained results are reported in Figure 5.15.

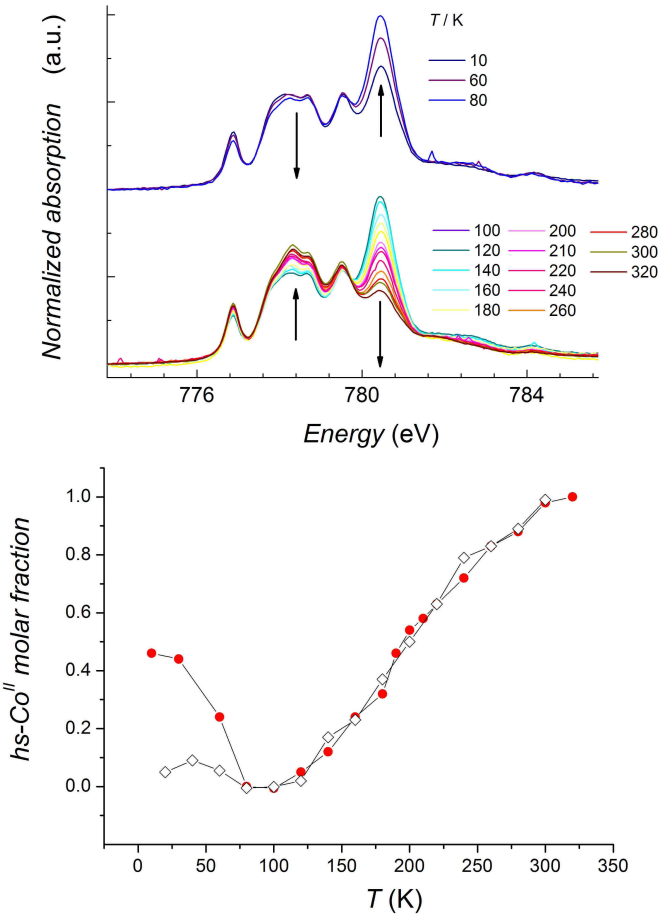

Figure 5.19. *Top*: Temperature dependence of the normalized X-Ray Absorption spectra of **1**·toluene, acquired after 1 hour of 904 nm laser light irradiation. *Bottom:* Temperature dependence of the normalised *hs*-Co^{II} molar fraction taken from dark (open black points) and with laser irradiation measurements (full red points).

The upper part of Figure 5.19 highlights the different rates of variation of the spectral features in the 10 – 80 K and in the 100 – 320 K ranges of temperature. The non monotonic behaviour of variation of the spectra is in agreement with the presence of a metastable state featuring an activation barrier to the relaxation to the ground state. In fact, raising up the temperature in the range 10-80 K the amount of the optically induced *hs*-Co^{II} metastable phase decreases because of thermally activated relaxation to the electronic *ls*-Co^{III} ground state; however, heating the sample above 100 K, the *hs*-Co^{II} concentration increases because of the occurrence of the entropy driven interconversion process. The comparison between the temperature dependence of the normalised *hs*-Co^{II} molar fraction estimated from the spectral deconvolution using, as shown in the upper paragraph, the 80 and 320 K spectra as limiting compositional cases, shows an overall 46 % of optically induced metastable electronic state, featuring a temperature of relaxation to the ground state (T(LIESST), *cfr.* Chapter I, paragraph 1.4.2.3) roughly estimated to be about 60 K. The entropy driven VT equilibria are perfectly superimposable for the two cases, confirming the excellent stability of **1**·toluene under the X-rays irradiation.

5.5.3 Soft X-rays as pump of metastable electronic states

As highlighted by Figure 5.18, a long exposure to the X-Ray beam evidences that at low temperature a weak but detectable interconversion from Co^{III}-catecholato species to Co^{II}-semiquinonato may occur even in the absence of laser light irradiation. For this reason, once excluded any radiation damaging processes, we investigated the effect of an increase of the Soft X-ray photon flux on the electronic structure of **1**·toluene. By selecting the opening of the slits downstream of the Apple II undulator of ID08, the X-ray density of the irradiating beam was brought from 10^8 up to 10^{10} photons/s, yielding the temperature dependent XAS spectra shown in Figure 5.20.
The temperature dependence of the spectra recorded on the sample without 904 nm light irradiation but in high X-ray photon density regime is qualitatively identical to that observed after the 904 nm laser light irradiation with lower X-ray photon density. Again we face a non monotonic trend of variation of the spectral features related to the different metal ion's electronic configurations.

The close similarity observed between the two patterns holds also at a quantitative level, as it is clear by comparing the temperature dependence of the *hs*-Co^{II} fraction undergoing VT equilibrium in the two cases (lower part of Figure 5.20). Again, to exclude the contribution of the redox inactive *hs*-Co^{II} we assumed that at each temperature the XAS spectrum is the result of a linear combination of the spectra taken at 300 K and 80 K (considered as the limiting compositional cases, 100 % and 0 % respectively, of the *hs*-Co^{II} -semiquinonato phase). The photoinduced fraction at

low temperature is the same when using 904 nm irradiation with low X-Ray flux and with high X-Ray flux irradiation only. On the other hand, the temperature at which the *hs*-Co^{II} -semiquinonato charge distribution completely relaxes to the *ls*-Co^{III}-catecholato one is somewhat higher for the spectra measured under high X-ray flux, confirming the efficiency of Soft X-rays in promoting the VT interconversion. The reversibility of the X-Ray triggered conversion is confirmed by the comparison of the thermal distribution of the *hs*-Co^{II} molar fraction obtained in different experimental conditions.

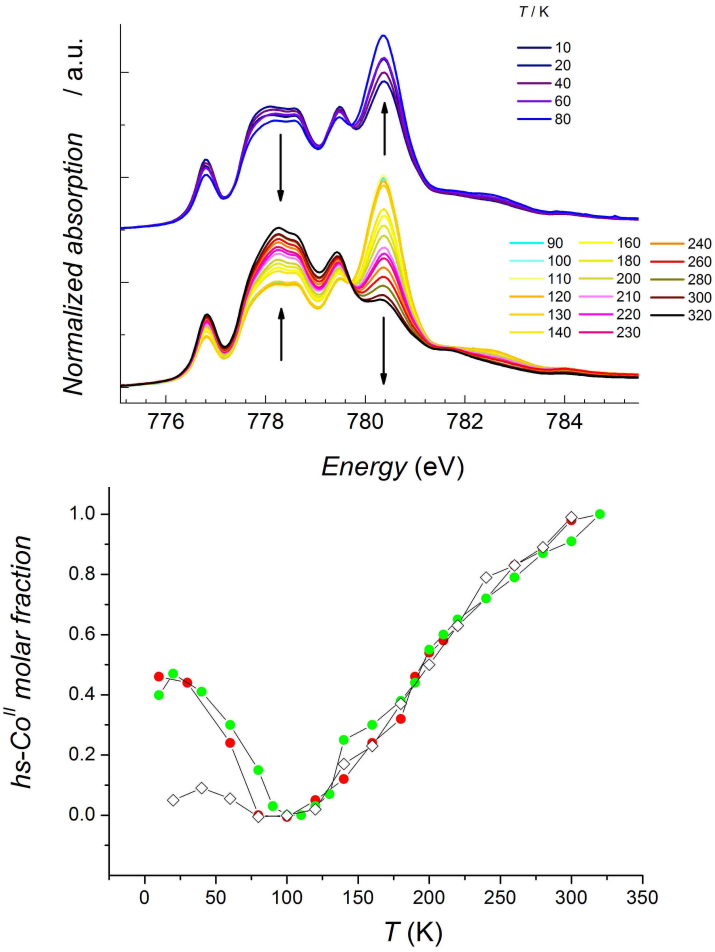

Figure 5.20. *Top*: Temperature dependence of the normalized X-Ray Absorption spectra of **1**·toluene, acquired with high photon flux (10^{10} photons s^{-1}) on the sample. *Bottom*: Temperature dependence of the normalised *hs*-Co^{II} molar fraction taken from dark (open black points), with 904 nm laser irradiation measurements (full red points) and high photon flux measurements (full green points).

The present results clearly demonstrate that soft X-rays trigger the same process as 904 nm laser light, *i.e.* they are capable of inducing an intramolecular electron transfer. Figure 5.21 points out the complete reversibility of the process, as pointed out by the comparison among the spectra recorded at 10 K before and after a complete thermal cycle up to 300 K.

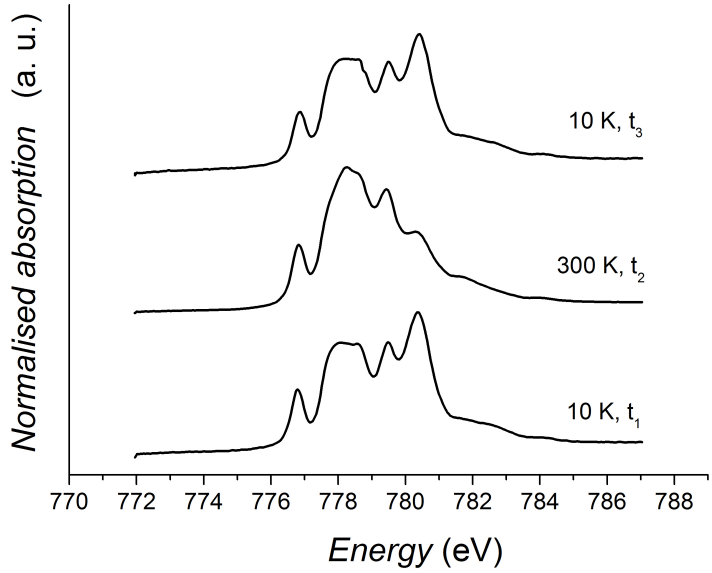

Figure 5.21. Evidence of the reversibility of the Soft X-ray induced Valence tautomeric interconversion: L_3 edge XAS spectra of complex **1**·toluene at 10 K before (t_1) and after (t_3) a complete thermal cycle up to 300 K (t_2) (time scale $t_1<t_2<t_3$).

The sample began showing photoinduced degradation only after 600 spectra (corresponding to more than 24 h) have been recorded on the same spot of the sample.

Even though the detailed mechanism by which Soft X-rays promote the VT interconversion in **1**·toluene is not clear yet, we attribute it to the presence of secondary electrons having energy in the range of the LMCT transition, emitted by the relaxing systems after the excitation by the absorption of the X-ray radiation, with consequent formation of the core-hole vacancy,[52-54] in line with the interconversions induced by Hard X-rays reported up to date, including photoreduction of manganites,[55] spin state switching in iron spin crossover[56] and electron transfer in polycyanometallates.[57-60] In these cases the switching process triggered by the X-ray absorption phenomenon haa been attributed to the scattering of secondary electrons produced by a remote ionization.[18,22,36,44,45,56] A similar mechanism is known in the SC

literature with the name of NIESST (Nuclear Induced Excited Spin State Trapping), where a cascade-like electronic de-excitation process triggers the spin crossover phenomenon.[61] The phenomenology of this phenomenon foresees the radioactive ^{57}Co nucleus decay by capture of a K-electron or, to a lesser extent, an L-electron and the subsequent emission of a neutrino of 0.7 eV, thereby populating the 136.5 keV excited state of ^{57}Fe. The consequent electronic de-excitation of the nucleogenic ^{57}Fe species feature radiative processes (X-rays of up to several keV) or non-radiative Auger-processes (Auger electrons of several keV) and give thus rise to the phenomenon of SC. Such a mechanism has been also taken into account for the rationalisation of the Hard X-rays triggered SC process in an Fe^{II} complex, found by Vankò *et al.*. The order of magnitude of the energies coming into play in the process is indeed the same considered in the present study and corroborates the attribution of energy release by secondary electrons to be the cause of the VT triggering.

In the case of Soft X-rays photo-absorption the non-radiative decay via Auger and Coster–Kronig electrons is expected to be higher with respect to the Hard X-rays case,[54] resulting in a higher efficiency of the secondary electrons produced by inelastic scattering compared to Hard X-rays. In principle, this makes Soft X-rays more efficient in promoting the redox isomerism. However, the larger number of secondary electrons can easily induce irreversible damage of the system, making the X-ray induced transitions harder to be detected. In this framework, the observed behaviour of **1**·toluene points out a large robustness of this molecular complex, which allowed us to monitor the occurrence of Soft X-rays induced VT without undergoing irreversible radiation damage.

The result reported here constitutes in fact, to the best of our knowledge, the first example of a completely reversible Soft X-ray induced electron transfer in a molecular complex. During the writing of this thesis' work a conference communication concerning a Soft X-Ray induced electron transfer in a Prussian Blue analogue, *i.e.* a non-molecular system, has been reported.[62] An earlier reported Soft X-ray induced spin crossover transition in a molecular complex is unfortunately associated with a significant sample damage caused by the photon beam and it is rather unclear if the latter process could be associated with the observed spin transition.[63] The authors found that such an effect was in fact in competition with a significant photoreduction of the sample, limiting the repeatability of the experiments without changing the position of investigation on the sample, and tentatively attributed these phenomena to an energy transfer from secondary electrons, emitted by the molecules in the lattice after the absorption of the X-ray light, to the iron centres of the switchable molecules. Such explanation was indeed capable of rationalize the time-dependent damaging of the sample under X-light exposure as well as the temperature dependence of the process of relaxation to the diamagnetic low spin state, in analogy with the previously encountered LIESST and NIESST effects.[16,61]

In conclusion, these results show that Soft X-rays are a useful tool for obtaining information about the electronic properties of 3d metal ions, but also provide a powerful external stimulating perturbation like temperature, pressure, magnetic field and optical photons. As a matter of fact in the interaction with matter they play the role of a pump of metastable electronic states. In fact, the increased interest about molecules in the bistable materials' science community is due to their peculiarity to be switched among their different physical states by means of more than just one stimulus. For VT systems several physical means have been revealed to act on the electronic states, like temperature, light irradiation, pressure and high magnetic fields. Fe/Co based polycyanometallates have been shown to be sensitive to the application of an electric field as well, even if only a one way switching process may be set on, whose effect could only be erased by means of temperature variation of the system.[64,65] The quest for new active physical means to reversibly change the electronic structure of a bistable system is very active field of research which straddles the way among the different classes of bistable materials. At the moment complete rationalization of the results reported up to now seem to be lacking, as some of the aforementioned authors already pointed out, due to the need of more experimental evidences and comparisons of X-ray absorption experiments. From this point of view our investigation is worth of consideration from two points of view: a fundamental one, providing the only up to date available source of coupled Hard / Soft X-ray absorption study of the switch of the electronic distribution in a molecular VT complex; second, from an applicative view, it affords a new stimulus to trigger the VT transition in a very robust molecular material.

References

[1] Stohr, J.; Siegmann, H. C. *Magnetism - From Fundamentals to Nanoscale Dynamics*; Springer: 2006.

[2] De Groot, F.; Kotani, A. *Core Level Spectroscopy of Solids*; CRC Press: 2008.

[3] Kramers, H. A. *Z. Phys.* **1926**, *39*, 826-840.

[4] Dirac, P. A. M. *Proc. Roy. Soc* **1929**, *A123*, 714.

[5] Sebilleau, D. *X-ray and Electron Spectroscopies: An Introduction* in *Magnetism: a Synchrotron Radiation Approach*; Beaurepaire, E.; Bulou, H.; Scheurer, F.; Kappler, J.-P., Eds.; Springer-Verlag: Berlin Heidelberg, 2006; Vol. 697, pp 15-57.

[6] Loudon, R. *The Quantum Theory of Light*; Clarendon: Oxford, 1973.

[7] Shore, B. W.; Menzel, D. H. *Principles of Atomic Spectra*; Wiley: New York, 1968.

[8] Spiering, H. *Elastic Interaction in Spin Crossover Compounds* in *Spin Crossover in Transition Metal Compounds III*; Gütlich, P.; Goodwin, H. A., Eds.; Springer: Berlin, 2004; Vol. 235, pp 171-195.

[9] van der Laan, G.; Thole, B. T.; Sawatzky, G. A.; Verdaguer, M. *Phys. Rev. B* **1988**, *37*, 6587-6589.

[10] Yokoyama, T.; Ohta, T.; Sato, O.; Hashimoto, K. *Phys. Rev. B* **1998**, *58*, 8257-8266.

[11] Yokoyama, T.; Kiguchi, M.; Ohta, T.; Sato, O.; Einaga, Y.; Hashimoto, K. *Phys. Rev. B* **1999**, *60*, 9340-9346.

[12] Bleuzen, A.; Lomenech, C.; Escax, V.; Villain, F.; Varret, F.; Moulin, C. C. D.; Verdaguer, M. *J. Am. Chem. Soc.* **2000**, *122*, 6648-6652.

[13] Moulin, C. C. D.; Villain, F.; Bleuzen, A.; Arrio, M. A.; Sainctavit, P.; Lomenech, C.; Escax, V.; Baudelet, F.; Dartyge, E.; Gallet, J. J.; Verdaguer, M. *J. Am. Chem. Soc.* **2000**, *122*, 6653-6658.

[14] Cartier-dit-Moulin, C.; Rudolf, P.; Flank, A.; Chen, C. *J. Phys. Chem.* **1992**, *96*, 6196-6198.

[15] Lee, J. J.; Sheu, H. S.; Lee, C. R.; Chen, J. M.; Lee, J. F.; Wang, C. C.; Huang, C. H.; Wang, Y. *J. Am. Chem. Soc.* **2000**, *122*, 5742-5747.

[16] Hauser, A. *Spin Crossover in Transition Metal Compounds II*; Gütlich, P.; Goodwin, H. A., Eds.; Springer: Berlin, 2004; Vol. 234, pp 155-198.

[17] Roux, C.; Adams, D. M.; Itie, J. P.; Polian, A.; Hendrickson, D. N.; Verdaguer, M. *Inorg. Chem.* **1996**, *35*, 2846-2852.

[18] Yokoyama, T.; Okamoto, K.; Nagai, K.; Ohta, T.; Hayami, S.; Gu, Z. Z.; Nakajima, R.; Sato, O. *Chem. Phys. Lett.* **2001**, *345*, 272-276.

[19] Bressler, C.; Milne, C.; Pham, V. T.; Elnahhas, A.; Van Der Veen, R. M.; Gawelda, W.; Johnson, S.; Beaud, P.; Grolimund, D.; Kaiser, M.; Borca, C. N.; Ingold, G.; Abela, R.; Chergui, M. *Science* **2009**, *323*, 489-492.

[20] Mannini, M.; Pineider, F.; Sainctavit, P.; Danieli, C.; Otero, E.; Sciancalepore, C.; Talarico, A. M.; Arrio, M. A.; Cornia, A.; Gatteschi, D.; Sessoli, R. *Nature Mater.* **2009**, *8*, 194-197.

[21] Gambardella, D.; Dallmeyer H.; Maiti, K.; Malagoli, M. C.; Eberhardt, W.; Kern, K.; Carbone, C. *Nature* **2002**, *416*, 301-304.

[22] Blundell, S. J. *Molecular Magnetism* in *Magnetism: a Synchrotron Radiation Approach*; Beaurepaire, E.; Bulou, H.; Scheurer, F.; Kappler, J.-P., Eds.; Springer-Verlag: Berlin Heidelberg, 2006; Vol. 697, pp 345-373.

[23] Briois, V.; Moulin, C. C. D.; Sainctavit, P.; Brouder, C.; Flank, A. M. *J. Am. Chem. Soc.* **1995**, *117*, 1019-1026.

[24] Escax, V.; Bleuzen, A.; Moulin, C. C. D.; Villain, F.; Goujon, A.; Varret, F.; Verdaguer, M. *J. Am. Chem. Soc.* **2001**, *123*, 12536-12543.

[25] Rogalev, A.; Goulon, J.; Goulon-Ginet, C.; Malgrange, C. *Instrumentation Developments for Polarization Dependent X-ray Spectroscopies* in *Magnetism: a Synchrotron Radiation Approach*; Beaurepaire, E. ; Scheurer, F.; Krill, G.; Kappler, J.-P., Eds.; Springer: Berlin, 2001; Vol. 14, pp 60-86.

[26] http://www.esrf.eu/UsersAndScience/Experiments/ElectStructMagn/ID12/old1996Handobook

[27] Juhin, A.; Brouder, C.; Arrio, M. A.; Cabaret, D.; Sainctavit, P.; Balan, E.; Bordage, A.; Seitsonen, A. P.; Calas, G.; Eeckhout, S. G.; Glatzel, P. *Phys. Rev. B* **2008**, *78*, 195103.

[28] Dapporto, P.; Dei, A.; Poneti, G.; Sorace, L. *Chem., Eur. J.* **2008**, *14*, 10915-10918.

[29] Varret, F.; Boukheddaden, K.; Chong, C.; Goujon, A.; Gillon, B.; Jeftic, J.; Hauser, A. *Europhys. Lett.* **2007**, *77*, 30007.

[30] Zeller, R. in *Unoccupied Electronic States*; Fuggle, J. C.; Ingsfield, J. E., Eds.; Springer-Verlag: Berlin, 1992.

[31] Thole, B. T.; van der Laan, G.; Butler, P. H. *Chem. Phys. Lett.* **1988**, *14*, 9295.

[32] de Groot, F. M. F. *J. Electron Spectrosc. Relat. Phenom.* **1994**, *67*, 529-622.

[33] de Groot, F. M. F. *Chem. Rev.* **2001**, *101*, 1779-1808.

[34] Thole, B. T.; van der Laan, G.; Fabrizio, M. *Phys. Rev. B* **1994**, *50*, 11466.

[35] Arrio, M.-A.; Rossano, S.; Brouder, C.; Galoisy, L.; Calas, G. *Europhys. Lett.* **200**, *51*, 454-460.

[36] Westre, T. E.; Kennepohl, P.; Dewitt, J. G.; Hedman, B.; Hodgson, K. O.; Solomon, E. I. *J. Am. Chem. Soc.* **1997**, *119*, 6297-6314.

[37] http://www-cxro.lbl.gov/index.php?content=/tools.html

[38] Briois, V.; Cartier, Ch.; Momenteau, M.; Maillaro, P.; Zarembowitch, J.; Fontaine, A.; Tourillon, G.; Thuery, P.; Verdaguer, M. *J. Chim. Phys.* **1989**, *86*, 1623-1634.

[39] Lever, A. B. P. *Inorganic Electronic Spectroscopy*; Elsevier: Amsterdam, 1984.

[40] http://wwwchem.uwimona.edu.jm/courses/Tanabe-Sugano/TSintro.html

[41] Koningsberger, D. C.; Prins, R. e. *X-Ray Absorption. Principles and Applications: Techniques of EXAFS, SEXAFS and XANES*; Wiley: New York, 1988.

[42] www.esrf.eu/computing/scientific/exafs/viper.html

[43] http://cars9.uchicago.edu/~ravel/software/Welcome.html

[44] Roux, C.; Adams, D. M.; Itie, J. P.; Polian, A.; Hendrickson, D. N.; Verdaguer, M. *Inorg. Chem.* **1996**, *35*, 2846-2852.

[45] Wasinger, E. C.; De Groot, F. M. F.; Hedman, B.; Hodgson, K. O.; Solomon, E. I. *J. Am. Chem. Soc.* **2003**, *125*, 12894-12906.

[46] Wende, H. ; Bernien, M.; Luo, J.; Sorg, C.; Ponpandian, N.; Kurde, J.; Miguel, J.; Piantek, M.; Xu, X.; Eckhold, Ph.; Kuch, W.; Baberschke, K.; Panchmatia, P. M.; Sanyal, B.; Oppeneer, P. M.; Eriksson, O. *Nature Mater.* **2007**, *6*, 516-520.

[47] Thole, B. T.; Cowan, R. D.; Sawatzky, G. A.; Fink, J.; Fuggle, J. C. *Phys. Rev. B* **1985**, *31*, 6856-6858.

[48] Poneti, G.; Mannini, M.; Sorace, L.; Sainctavit, P.; Arrio, M. A.; Rogalev, A.; Wilhelm, F.; Dei, A. *Chemphyschem* **2009**, *10*, 2090-2095.

[49] Li, D.; Clérac, R.; Roubeau, O.; Harté, E.; Mathoničre, C.; Le Bris, R.; Holmes, S. M. *J. Am. Chem. Soc.* **2008**, *130*, 252-258.

[50] Martin, J. P.; Zarembowitch, J.; Bousseksou, A.; Dworkin, A.; Haasnoot, J. G.; Varret, F. *Inorg. Chem.* **1994**, *33*, 6325-6333.

[51] Tayagaki, T.; Galet, A.; Molnar, G.; Munoz, M. C.; Zwick, A.; Tanaka, K.; Real, J. A.; Bousseksou, A. *J. Phys. Chem. B* **2005**, *109*, 14859-14867.

[52] Henke, B. L.; Liesegang, J.; Smith, S. D. *Phys. Rev. B* **1979**, *19*, 3004-3021.

[53] Henke, B. L.; Knauer, J. P.; Premaratne K. *J. Appl. Phys.* **1981**, *51*, 1509-1520.

[54] Henneken, H.; Scholze, F.; Ulm, G. *J. Appl. Phys.* **2000**, *87*, 257-268.

[55] Kiryukhin, V.; Casa, D.; Hill, J. P.; Keimer, B.; Vigliante, A.; Tomioka, Y.;

Tokura, Y. *Nature* **1997**, *386*, 813-815.

[56] Vanko, G.; Renz, F.; Molnar, G.; Neisius, T.; Karpati, S. *Angew. Chem. Int. Ed.* **2007**, *46* , 5306-5309.

[57] Escax, V.; Bleuzen, A.; Itie, J. P.; Munsch, P.; Varret, F.; Verdaguer, M. *J. Phys. Chem. B* **2003**, *107*, 4763-4767.

[58] Bleuzen, A.; Marvaud, V.; Mathoniere, C.; Sieklucka, B.; Verdaguer, M. *Inorg. Chem.* **2009**, *48*, 3453-3466.

[59] Margadonna, S.; Prassides, K.; Fitch, A. N. *Angew. Chem. Int. Ed.* **2004**, *43*, 6316-6319.

[60] Papanikolaou, D.; Margadonna, S.; Kosaka, W.; Ohkoshi, S.; Brunelli, M.; Prassides, K. *J. Am. Chem. Soc.* **2006**, *128*, 8358-8363.

[61] Gütlich, P. *Nuclear Decay Induced Excited Spin State Trapping (NIESST)* in *Spin Crossover in Transition Metal Compounds II* ; Gütlich, P.; Goodwin, H. A., Eds.; Springer: Berlin, 2004; Vol. 234.

[62] Kitajima, Y.; Ishiji, K.; Matsuda, T.; Tokoro, H.; Ohkoshi, S.; Iwazumi, T. *LXIII Yamada Conference on Photo-Induced Phase Transition and Cooperative Phenomena (Pipt3)* **2009**, *148*, 12032.

[63] Collison, D.; Garner, C. D.; Mcgrath, C. M.; Mosselmans, J. F. W.; Roper, M. D.; Seddon, J. M. W.; Sinn, E.; Young, N. A. *Dalton Trans.* **1997**, 4371-4376.

[64] Sato, O.; Kawakami, T.; Kimura, K.; Hishiya, S.; Kubo, S.; Einaga, Y. *J. Am. Chem. Soc.* **2004**, *126*, 13176-13177.

[65] Mahfoud , T.; Molnar, G.; Bonhommeau, S.; Cobo, S.; Salmon, L.; Demont, P.; Tokoro, H.; Ohkoshi, S.-I.; Boukheddaden, K.; Bousseksou, A. *J. Am. Chem. Soc.* **2009**, *131*, 15049-15054.

Conclusions

This work sets into the scientific field of valence tautomerism of molecular systems, a topic featuring the Laboratory of Molecular Magnetism in Florence as a pioneering research group, where this subject has always found a prolific soil to grow on. At the beginning of this thesis, the research lines of the group, lead by Professor Andrea Dei, foresaw the development of new Co:dioxolene based valence tautomers along with the rationalisation of the structural and electronic parameters governing their properties of photoinduction.

This PhD work started with the development of a rational approach for the control of the transition properties of valence tautomeric materials, relying on the chemical tuning of the redox potentials of the electronically active building blocks of the systems. This lead to the successful synthesis of a new molecular entity capable of undergoing intramolecular electron transfer in solution and in the solid state ([Co(Me_3TPA)TCdiox]PF_6). The system belongs to the simplest class of Co:dioxolene systems, where the metal ion and the redox active organic ligand occur in an equimolar amount. The investigation of the effect of the donor ability of a set of solvents on the stabilisation of different charge distributions in solutions allowed the choice of the proper solvent to follow the temperature dependence of the valence tautomeric equilibrium in solution. This analysis, unprecedented in the literature of 1:1 Co:dioxolene molecules, pointed out entropy to be the driver of the redox equilibrium for this class of materials, featuring enthalpy and entropy changes in the process comparable to the ones known in literature for 1:2 systems.

We moved then towards the tuning of the conversion features in the solid state studying the effect of vibrational coupling with the crystalline environment on the thermal and photoinduced interconversion processes. This has been performed inducing a change in the lattice structures keeping the molecular cores intact, by changing the crystallisation solvent, for two different species, a 1:1 and a 1:2 Co:dioxolene systems ([Co(Me_ntpa)(diox)](PF_6) and [Co(3,5-DBdiox)$_2$(2,2'-bpy)], respectively), the latter being the result of a fruitful collaboration with the group of Dr. Colette Boskovic from the University of Melbourne in Australia. This investigation highlighted several issues about the mechanism of temperature or light induced interconversion. In the first case the control of the interaction present in the solid state revealed to be of paramount importance in determining the relative stability of the two redox isomers. Interesting effects came out also in the case of photoswitchable properties. In particular the ([Co(Me_ntpa)(diox)](PF_6) system underwent an increase in

the molecular volume after the replacement of the solvent of crystallisation from ethanol to toluene, resulting in the highest response to light irradiation at low temperature up to now reported in the field of molecular redox isomerism. This finding, besides the fundamental interest of the chemical community working towards a rational strategy of improvement of the conversion features of these class of molecular materials, turned out to be strikingly important for the investigation of this compound in highly diluted environments.

This was indeed the further step of this research project, aimed to clarify the role of elastic interactions in the solid state in determining the thermal and optical conversion features of 1:1 Co:dioxolene materials, among which $[Co(Me_ntpa)(diox)](PF_6)$ stands out as an ideal testing ground for theories. The previously mentioned analysis suggested that the optical bistability of these materials is independent from cooperative effects in the solid state, in contrast with up to now reported by the literature of valence tautomeric and spin crossover materials. To clarify this issue, we undertook an analysis of the transition temperatures as well as the lifetimes of the low temperature photoinduced metastable state as a function of the degree of solid dilution of the system in an inert crystalline lattice. In this way we have been able to chemically finely tune the interactions in the crystal lattice and, thanks to the outstanding conversion features of $[Co(Me_ntpa)(diox)](PF_6)$, to reveal their role in both thermally and optically activated valence tautomeric processes up to high degrees of dilution. The study suggested that, while the thermal bistability of valence tautomeric materials strongly depends on the crystal lattice, the optical one is a single molecule property, opening the way for the application of these systems in nanostructured environments.

Keeping an eye on this issue, the next step of my research has been the employ of a high energy probe like synchrotron radiation for the detailed analysis of the electronic and structural parameters of the ground and photoinduced metastable states for $[Co(Me_ntpa)(diox)](PF_6)$. The study revealed the perfect equivalence of the low temperature photoinduced and the high temperature stable phases, and pointed out the non innocence of synchrotron radiation in the investigation of valence tautomeric materials. We found in fact, for the first time for this class of molecular compounds, that Soft X-rays are able to promote the transition usually pumped by a diode laser emitting IR light.

Acknowledgment

The realisation of this work has not been, of course, a one man project. First and foremost, I am glad to say thanks to the people who more closely take care of me, not only from a professional side. I wish to deeply thank Professor Andrea Dei for sharing with me his knowledge about chemistry and for turning his scientific ideas into a common research line. His suggestions, encouragements, ideas and human touch have been an invaluable source of learning for me, which I will hardly forget. On the other side, the passion, preparation and humanity of Roberta Sessoli had a very huge impact on me, and I'm honoured to have worked with such a person. I extend my acknowledgment to the rest of the LAMM group in Florence: Lorenzo Sorace for closely taking care of me and of my preparation in magnetism and Italian history, Matteo Mannini for having introduced me to the magic world of Synchrotron radiation (and the night shifts too!), Andrea Caneschi for being always present in the moment of laboratory chaos in lifting up every sort of stuff I could have made fall into the cryostat, Claudio Sangregorio for easing my everyday worries, and all the other old timers of the group: Claudia Innocenti, Maria Fittipaldi, Cesar de Julien Fernandez for giving me a smile every time I crossed the door of the laboratory. I am very glad to say thank also to two former members of the group, Lapo Bogani and Kevin Bernot, for introducing me to the secrets of the molecular magnetism with special patience and care. I say thanks to the people I had collaborated with, in particular Alessandro Feis, Andrea Cornia and Colette Boskovic for their enthusiasm.

I wish to thank of course the great number of young guys who shared with me the life of the young scientist: Pine, Claudina, Lore, la Dani, Angelo, Lapino, Mael, Rafa, Ludovica, Alessandra for teaching me how to carry out helium transfers, you made me aware that importance of the coordination environment is huge not only for molecular bistable system.

Infine ringrazio i miei genitori e la mia intera famiglia per avermi supportato in questi anni di studi con grande amore e cura.

My last thought is for Giulia, for being always on my side, even in the writing of this work.

Florence, January 2010